JMENTATION PAGE

Form Approved
OMB No. 0704-0188

AD-A238 426

2. REPORT DATE	3. REPORT TYPE AND DATES COVERED
20 June 1991	Final. 1 March 86 - 31 March 1990

4. TITLE AND SUBTITLE
The Coastal Transition Zone: Nutrient Distributions and Transformations Associated with Cool Filaments off Northern California.

5. FUNDING NUMBERS
N 00014-86-K-0314 (C)

6. AUTHOR(S)
Burton H. Jones

7. PERFORMING ORGANIZATION NAME(S) AND ADDRESS(ES)
Hancock Institute for Marine Studies
University of Southern California
University Park
Los Angeles, CA 90089-0371

8. PERFORMING ORGANIZATION REPORT NUMBER

9. SPONSORING/MONITORING AGENCY NAME(S) AND ADDRESS(ES)
Office of Naval Research
Code 1123B
Oceanic Biology/Optics/Chemistry Division
800 N. Quincy Street
Arlington, VA 22217-5000

10. SPONSORING/MONITORING AGENCY REPORT NUMBER

11. SUPPLEMENTARY NOTES
3 Manuscripts are attached
2 Manuscripts are currently in preparation and will be submitted when completed.

12a. DISTRIBUTION/AVAILABILITY STATEMENT
Unlimited

12b. DISTRIBUTION CODE

13. ABSTRACT *(Maximum 200 words)*

The objective of this project was to determine the three-dimensional distribution of phytoplankton and nutrients associated with cold filament and jet systems in the coastal transition zone. The distributions were determined with hydrographic grids, towyo mapping and nearsurface underway mapping during two cruises off northern California in July 1986 and July 1988. We have examined the relationship of nutrient and phytoplankton distributions with the physical processes of the jet/eddy system, and the role of jets and filaments in the seaward flux of nutrients and phytoplankton from the coastal region.

Results from this research indicate that seaward jets result in a significant net transport of phytoplankton offshore. Although these jets also have a large seaward transport of nutrients, the net offshore transport of nutrients may be a small proportion of the seaward transport due to associated shoreward flow. The jet/filament system also results in a net downward flux of phytoplankton as dense, coastally upwelled water is advanced seaward. Cyclonic eddies beyond the shelf break result in elevated nutrient concentrations within the euphotic zone, but not necessarily increased phytoplankton biomass. Eddies over the shelf may play role in the coupling of phytoplankton productivity with zooplankton grazing.

14. SUBJECT TERMS
Upwelling Nutrients, Chlorophyll, Phytoplankton, Light, Jets, Eddies

15. NUMBER OF PAGES

16. PRICE CODE

17. SECURITY CLASSIFICATION OF REPORT	18. SECURITY CLASSIFICATION OF THIS PAGE	19. SECURITY CLASSIFICATION OF ABSTRACT	20. LIMITATION OF ABSTRACT
Unclassified	Unclassified	Unclassified	UL

A-1

CHEMICAL AND BIOLOGICAL STRUCTURE AND TRANSPORT OF A COOL FILAMENT ASSOCIATED WITH A JET/EDDY SYSTEM OFF NORTHERN CALIFORNIA IN JULY 1986 (OPTOMA21)

Burton H. Jones[1]

Christopher N. K. Mooers[2]

Michele M. Rienecker[3]

Tim Stanton[4]

Libe Washburn[5]

[1]Department of Biological Sciences, University of Southern California, Los Angeles, 90089-0371

[2]The Institute for the Study of Earth, Oceans, and Space, University of New Hampshire
Durham, NH 03824-3525

[3]NASA Goddard Space Flight Center, Greenbelt, MD 20771

[4]Department of Oceanography, Naval Postgraduate School, Monterey, CA 93940

[5]Department of Geography, University of California, Santa Barbara, CA 93106

April 1991

Submitted to Journal of Geophysical Research

Abstract

During the OPTOMA21 cruise, from 7 to 19 July 1986, the distributions of nutrient, pigment, bio-optical and physical variables in a cool filament located between Point Reyes and Point Arena, California, were mapped to describe the three-dimensional variability of the filament and its relation to the nutrient and phytoplankton distributions offshore.

Several cool filaments were distinguishable at distances of more than 35-50 km from the coast in satellite imagery on 14 July. The juxtaposition of these features as well as the presence of an offshore anticyclone and a cyclone south of the filament (A) mapped by OPTOMA21 led to complex patterns in all of the variables, aided by the apparent alongshore variability in the source of upwelled water. Coastal upwelled water south of Point Arena was more saline (by nearly 0.4 psu) and colder (by about 0.5° C) than water north of Point Arena where subsurface chlorophyll concentrations were higher. There was, correspondingly, much higher biomass in the filament anchored north of Point Arena than in filament A. The associated offshore flowing jet entrained the coastal upwelled water, with low temperatures and high nutrient and pigment concentrations, so that the filament maintained its characteristic low temperature and high chlorophyll in the offshore zone. Filament A extended about 250 km offshore where it made a cyclonic bend and turned southeastward towards the coast. Both salinity and nutrient concentrations displayed strong gradients within the filament, their fronts not always coincident with temperature fronts; they generally increased across the filament into the cyclonic eddy almost circumscribed by the filament. Chlorophyll fluorescence maxima were clearly associated with the cool filament core, but elevated levels were also associated with the low salinity, slightly warmer water on the outer edge of the filament along its entire track. Elevated chlorophyll concentrations associated with the filament extended to a depth of about 100 m, nearly twice the estimated euphotic zone depth, probably due to subduction as the jet flowed offshore. Phytoplankton taxa within the filament were characteristic of those found within coastal upwelling regions. The cyclonic eddy contained high salinity, high nutrient yet higher temperature water at its surface, suggesting that this water may have been at the surface for several days to weeks. There was no large chlorophyll signal at the center of the eddy, in contrast to the water in the coastal upwelling region and within the filament, suggesting that there was little horizontal exchange between the cyclone and the cool filament and that the high salinity water may have originated from local (open ocean) upwelling or it may have been displaced seaward from a nearcoast origin several weeks earlier.

The high velocities associated with the filament resulted in a large transport of nutrients and phytoplankton biomass offshore, but it also flowed shoreward which reduced the net transport to the offshore region. Shoreward nitrate transport was 85 to 90 percent of seaward transport, similar in proportion to the shoreward volume transport (~90%) relative to the seaward volume transport. In contrast, shoreward chlorophyll transport was about 40 percent of seaward transport, indicating significant losses (net transport) of phytoplankton biomass to the offshore region of the filament.

1. Introduction

The presence and importance of cool filaments extending offshore 200-300 km into the California Current system have been realized only within the past decade. Initial observations of these filaments came from remote sensing (e.g., Bernstein et al., 1977) and physical programs such as CODE (Davis, 1985a,b; Kosro, 1987; Kosro and Huyer, 1986; Flament et al., 1985) and OPTOMA (Rienecker et al., 1985). Few chemical and biological observations of these features have been available until recently. (Some nearsurface observations of temperature, nutrients, and chlorophyll were made in the early 1980s of a smaller feature extending less than 100 km offshore from Pt. Sur (Traganza et al., 1980, 1981). The relationship between nearsurface temperature and nutrient concentration was generally linear in the upwelled water off Pt. Sur, allowing the inference of surface nutrient concentrations from remotely sensed sea surface temperature.) Remotely sensed ocean color measurements indicated that nearsurface high chlorophyll concentrations were correlated with the low temperature water that defined these filaments in the region off Pt. Arena and Pt. Reyes, north of San Francisco (Abbott and Zion, 1985, 1987), which substantiated and extended the results of Traganza et al. (1980,1981). Detailed physical observations of the vertical structure of these features provided significant descriptions of jets, filaments and subsidences (Flament et al., 1985; Rienecker, et al., 1985; and Rienecker and Mooers, 1989, henceforth referred to as RM), but little information on the subsurface chemical and biological structure of these features and the associated eddy field has been available until recently.

Abbott et al. (1990) used a nearsurface drifter with optical sensors and a water sampler to study the changes in nutrients, optical properties and phytoplankton abundance along a drifter path in an upwelling filament off Point Arena. They found patterns of variation along the filament which are characteristic of upwelling regions: an initial increase in chlorophyll and decrease in nutrients followed by a gradual decrease in chlorophyll and a change in the species composition as the drifter proceeded offshore. Based on observations of physical structure, chlorophyll, phytoplankton species and photosynthesis/light curves for the northern California region between 38° N (Pt. Reyes) and 41.5° N (north of Cape Mendocino), Hood (1990) found a maximum in chlorophyll concentration at the frontal boundary between the upwelled water shoreward and the more oligotrophic water seaward. Along this frontal boundary high chlorophyll concentrations were observed to a depth of 100 m. Because of the sampling scheme, it was impossible to examine details of the filament structure and its variation with distance from the coast.

Prior to the above-mentioned studies, little was known about the mesoscale three-dimensional variability of chemical and biological characteristics of the northern California upwelling region and the transition region offshore of the coastal upwelling zone. The OPTOMA21 cruise was planned to define the structure of the filament, its associated eddy field, and the variability of the structure with distance from the coast. Many of the OPTOMA21 physical hydrographic characteristics, as well as the genetic structure of the zooplankton species *Metridia pacifica*, have been described by RM and Bucklin et al. (1989). The variability of the isotopic composition of lead associated with this filament and the implications of this variability have been described by Flegal et al. (1989).

In this paper we present a summary of the nutrient and pigment distributions within the context of the physical structure observed during OPTOMA21 in July 1986. Both nearsurface and subsurface distributions of nutrients and phytoplankton obtained from CTD/rosette casts and towed bio-optical measurements are presented. Finally, estimates of the nutrient and pigment transport are used to evaluate the relative magnitudes of offshore and onshore fluxes associated with this manifestation of the filament.

2. Methods

Sampling Strategy

The OPTOMA21 cruise, from 7 to 19 July 1986, was intended to obtain detailed information about the structure of the cool filament structure and surrounding waters including onshore-offshore variability. Transects were made along the coast to examine source water variability. Offshore, cruise tracks were adaptively positioned, based on satellite AVHRR imagery, to provide an overall map of the filament (Figure 1). Three primary modes of sampling determined the variability of physical, biological, and chemical variables associated with the feature. Continuous nearsurface sampling obtained the distributions of temperature (T), salinity (S), nutrients, and chlorophyll in the upper layer throughout most of the cruise. A CTD/rosette system was used to obtain vertical profiles of physical, chemical and biological variables at hydrographic stations, interspersed with XBT casts. A towyo profiling system was used to obtain several detailed (x-z) transects (Figure 1) of T, S, micro-conductivity, beam transmission and chlorophyll fluorescence.

Nearsurface measurements of temperature, conductivity, chlorophyll fluorescence and nutrients were obtained continuously (5 second averages) from the flow from the ship's seawater intake located approximately 2 m beneath the surface. Temperature and salinity were corrected to the nearsurface measurements in accordance with the CTD and XBT profiles. Nutrient concentrations were measured

with a Technicon Autoanalyzer which continuously sampled the flow stream of nearsurface sea water (Whitledge et al., 1981). Chlorophyll fluorescence was measured continuously with a Turner Designs fluorometer and calibrated with batch samples from its outflow (Lorenzen, 1966). The calibrated and corrected data were then averaged over two minute intervals for this analysis. These two-minute averaged data have horizontal resolution of about 250 meters along the towyo transects and about 500 m along other transects.

At hydrographic stations, vertical profiles of temperature and salinity were acquired with a Neil Brown Instruments CTD with salinities post-calibrated according to the surface bottle samples. Occasionally, vertical profiles of temperature were acquired to 750 m with Sippican XBTs that were digitized with a Sippican MK 9 deck unit. Processing details are given in Wittmann et al. (1987). Along-track CTD/XBT station spacing across the filament was about 10 km. Station position fixes were obtained with LORAN C and are accurate to ~100 m.

Bottle profiles were obtained on the upcasts of CTD profiles with a General Oceanics rosette system that was tripped at approximately 20 m intervals in the upper 100 m. Nutrient concentrations were determined with a Technicon Autoanalyzer in batch mode (Whitledge et al., 1981). Chlorophyll and phaeopigment concentrations were determined from samples filtered onto Whatman GFF filters that were placed in 90% acetone and allowed to extract for 24 hours refrigerated and in the dark (Venrick and Hayward, 1984). The fluorescence of the extract was then measured before and after the addition of 5% hydrochloric acid on a Turner 111 fluorometer (Holm-Hansen et al., 1965).

A towyo instrumentation platform was winched in and out between 5 m and 120 m depth while underway at approximately 4 $m \cdot s^{-1}$, to obtain high (~800 m) spatial resolution vertical profiles of properties along the cruise track. The platform was equipped with a Neil Brown CTD sampling at 32 Hz, a Q-Instruments fluorometer, a Sea Tech 25 cm pathlength beam transmissometer (wavelength = 660 nm), a Marsh-McBirney 2-axis current meter to determine the platform velocity, and a microconductivity probe to measure thermal microstructure. By using a frequency-domain, lagged-temperature compensation, salinity was calculated from the conductivity time series and binned with 0.25 m vertical resolution. Beam transmission (%T) was transformed into the beam attenuation coefficient, c ($= \frac{1}{pathlength} \cdot \ln\left(\frac{\%T}{100}\right)$, which is generally proportional to particle concentration (e.g. Spinrad, 1986). The fluorescence voltage and beam transmission were averaged and stored with 1 m vertical resolution. The plotted data are 2-3 profile averages having a horizontal resolution of 2 to 2.5 km.

3. Description of Observed Fields

The multidisciplinary set of measurements has been used to relate the chemical (plant nutrients), biological (phytoplankton), and physical characteristics of the cool filament with its structure and to compare their distributions in the surrounding shelf and offshore waters. These relationships are presented primarily through vertical transects, both nearshore, across the coastal upwelled source regions, and offshore of the continental slope, directly across one of the several filaments in the region. First, the overall horizontal variability is summarized.

Nearsurface Patterns

The surface structure and temporal variability are clearly shown in satellite AVHRR images of SST obtained between late June and late July (see RM). For example, on 5 July a large filament (A) extended offshore south of Point Arena (Figure 2a). On 14 July three distinct filaments were evident (Figure 2b): one (B) extended seaward from north of Point Arena; the original filament (A) extended from south of Point Arena; and an additional, smaller filament (C) was evident south of Point Arena.

The surface maps of temperature, dynamic height, nitrate, and chlorophyll fluorescence from ship-based sampling (Figure 3) were similar in pattern to the SST patterns in the AVHRR imagery. As expected for coastal upwelling, nearshore temperatures were low ($<11°C$) and nutrient concentrations were relatively high ($NO_3 > 10\,\mu M$) from Point Arena southward. Nearsurface chlorophyll concentrations were high near the coast with higher concentrations near Point Reyes and immediately north of Point Arena. Near Point Arena where filament A extended seaward, chlorophyll concentrations were $\geq 5\,\mu g \cdot l^{-1}$ and nitrate concentrations $\geq 10\,\mu M$ where water temperatures were lower than $12°C$.

The region beyond about 50 km offshore can be divided into the area outside of the filament and the area including the filament. Outside of the filament, the temperatures were relatively high, generally greater than $14°C$ and the nutrient concentrations were low. Characteristic chlorophyll concentrations in this region were less than $0.2\,\mu g \cdot l^{-1}$. Nearsurface temperatures in the filament were less than $14°C$ and chlorophyll concentrations were 0.5 to 2 $\mu g \cdot l^{-1}$ at the most offshore section of the filament, about 230 km southwest of Point Arena. *In situ* observations of temperature, dynamic height, nitrate, and chlorophyll show the cyclonic bend in the filament as observed in the SST imagery. Within the area bounded by the filament, where dynamic height was <0.84 m, temperature was more than $14.5°C$ and

chlorophyll concentrations were less than 0.5 $\mu g \cdot l^{-1}$, but nitrate concentrations were high, exceeding 5 μM. The high nitrate concentration in this region seems inconsistent with general nutrient/temperature patterns observed in coastal upwelling regions.

At the surface, the coldest water in the filament was offset 5-10 km on the cyclonic side of the axis of the seaward jet that meandered through a field of anticyclones and cyclones (Figure 3). Geostrophic speeds in the seaward jet reached about 50 $cm \cdot s^{-1}$ relative to 500 db (RM), both in the seaward flow of the northern part of the filament and in the shoreward flow of the southern part of the filament. The strong shoreward flow resulted from the confluence of the seaward jet with onshore flow apparently associated with an anticyclone in the southwest of the survey region. The most intense flows (referenced to either 500 or 750 db) were vertically coherent to depths of at least 200 m, whereas the cool filament was manifest only to a depth of about 50 m.

Nearshore, Cross-Shelf Structure

Two transects are discussed to characterize the nearshore patterns. They were approximately equidistant from Point Arena; stations 27-31 (Figure 4), sampled on 8 July, were about 35 km to the south, and stations 57-61 (Figure 5), sampled on 10 July, were about 35 km to the north (Figure 1).

Coastal upwelling is indicated by cool, high salinity, nutrient-rich water near the coast and by isopleths tilted upward toward the coast (Figures 4 and 5). Salinity was about 0.2 psu lower throughout the water column and temperatures above 75 m were generally about 0.5° C higher in the northern transect compared with the southern transect. The distribution of chlorophyll in the upper 25 m was similar in both transects, with high concentrations occurring near the coast, a decrease at the middle station in the transect and higher concentrations again 45-50 km offshore. In the southern transect, the subsurface concentrations were lowest in the middle of the transect; in the northern transect, the subsurface distribution was distinct from that in the upper 25 m, with lowest concentrations near the coast and much higher concentrations than in the southern transect.

Nutrient regeneration is suggested by high ammonium concentrations in both transects. In the southern transect the ammonium concentrations were highest at the middle station in the upper 35 m and at the offshore station between 30 and 50 m, beneath the high chlorophyll of the upper 20 m. The ammonium concentrations in the northern transect were highest subsurface at 35 and 50 m at the middle station and at 50 m at the offshore station. Near the coast concentrations were relatively high in the upper 20 m of the water column. The ammonium concentrations were lowest in samples from below 50 m in

both transects suggesting that bottom regeneration and entrainment were not likely sources of ammonium in the water column, as they could be in part in other upwelling systems (e.g. Whitledge, 1980). Given the high chlorophyll concentrations in each of these transects, grazing is a likely source of the regenerated nitrogen. Although direct measurements of grazing are not available, a high ratio of phaeopigment to total pigment (chlorophyll plus phaeopigment) was expected to be indicative of recent grazing (e.g. SooHoo and Kiefer, 1982), but a low ratio would not necessarily indicate that zooplankton grazing and regeneration was low. In the southern transect the ammonium concentrations were highest at a local minimum in chlorophyll concentration where phaeopigment ratios were high (0.61 - 0.74). However, in the northern transect ammonium concentration was highest at a local maximum in chlorophyll concentration where the phaeopigment ratio was relatively low (0.19 - 0.22).

The high chlorophyll concentrations near the coast in the freshly upwelled (cool, saline) water were unexpected. Higher chlorophyll concentrations were expected offshore in a region "downstream" from where the water was upwelled. As the upwelled water is advected away from the coast and stratifies the phytoplankton are expected to adapt to the high light and nutrient conditions, increasing their growth rate and biomass away from the point of upwelling (e.g. Jones et al., 1983). In the southern transect, the nitrate/temperature plot appears to have the expected pattern of a linear increase in nitrate with decreasing temperature (Figure 6a). Temperature at the upper three sample depths of the inshore station was slightly high for the observed salinity (Figure 6b), which suggests surface warming and thus, that the water was not freshly upwelled. The nitrate concentration at the upper depths at the inshore station was low for the salinity (Figure 6c). The decrease in nitrate was sufficient to account for the high chlorophyll concentrations at this station, applying the approximate yield of 1 μg chlorophyll per 1 μM of nitrate consumed. Thus, it appears that the water had upwelled and stratified sufficiently through heating to allow significant phytoplankton growth resulting in the decreased nitrate concentrations in the nearshore region.

Offshore Patterns

The filamentary structure was distinct in transects 50 km or more offshore. The cross-filament vertical structure was sampled in two modes: 1) continuous towyo sampling, and 2) CTD/bottle transects at various locations. The towyo data provide the greatest spatial resolution and the CTD/bottle transects provide the greatest number of variables. These transects together with the underway surface mapping and satellite SST images provide insight into the three-dimensional structure of the system.

A North-South Transect 55 km West of Point Arena

To examine the cross-filament variability, a meridional transect extended from station 61 located north of Point Arena and about 45 km from the coast, to station 65, about 140 km southwest of Point Reyes (Figure 1). Underway nearsurface measurements (Figure 7), towyo mapping (Figure 8), and CTD/Rosette profiles (Figure 9) were employed along this transect on 10 and 11 July. The towyo was deployed at station 62, approximately 60 km from the northern origin of the transect. (The horizontal axes of the Figures 7 and 8 are plotted from north to south, consistent with the direction of tow. The distances along the axis are referenced to the location of towyo deployment. Therefore, distances to the north of the towyo deployment, where nearsurface measurements were obtained, appear as negative distances. All the transects that follow will use the same convention.)

Four major segments can be distinguished along this transect (Figure 7). The first segment (-60 to -30 km) at the northern end of the transect lies within filament B where the temperature was low, chlorophyll was high, and nitrate concentrations were moderate. Sharp fronts in temperature, chlorophyll fluorescence, and nitrate separated filaments B and A from the second segment (-30 to 0 km) that was warm, low in nutrients, and low in chlorophyll fluorescence. The third segment (0 to 50 km), filament A, included low temperatures, moderate chlorophyll concentrations, high beam attenuation coefficient, and high nitrate concentrations. The cool center, containing high chlorophyll and beam attenuation coefficient values was about 40 km wide. Apparently the transect ran was not perpendicular to the axis of filament A, causing the filament to appear wider than it actually was (RM). The fourth segment (50 to 160 km), south of a gradual temperature and nitrate gradient, was relatively warm, and low in nitrate and phytoplankton biomass. Each of these segments is discussed in more detail below.

The first segment of the transect was within filament B. Although the northern position of the transect appears to be at the southern edge of the filament in the 14 July AVHRR image (Figure 2b), the four-day difference between the start of the transect on 10 July and the 14 July AVHRR image is sufficient to account for the difference in location of the southern edge of the filament, which migrated about 40 km northward between 5 and 14 July (such displacements can occur rapidly, see RM). Filament B is distinguished from the other segments by its cool, saline, chlorophyll-rich upper mixed layer which was about 40 m deep. The AVHRR image and the nutrient and chlorophyll characteristics of this segment suggest that this water may have been upwelled near Cape Mendocino and was sufficiently far

downstream of the upwelling source for the phytoplankton population to have grown and consumed most of the available nitrate. The southern edge of filament B was bounded by a sharp front in temperature, nitrate and chlorophyll fluorescence.

The second segment was warm, low in nearsurface chlorophyll, and also quite low in nutrients (Figure 7). However, from the vertical profiles at station 62 (Figure 9), the surface mixed layer was a thin, low-salinity layer that overlaid a layer between 20 and 60 m containing 2-5 μM nitrate and 2-6 $\mu g \cdot l^{-1}$ chlorophyll concentrations. It appears that warm, low salinity water from offshore may have intruded nearshore between the two filaments. The low values throughout the salinity profile suggest that the source water was located offshore and was not the colder, high chlorophyll water from near the coast to the north and south. However, the chlorophyll concentrations of 5 to 6 $\mu g \cdot l^{-1}$ between 40 and 60 m seem high for water that is derived from offshore. The T, S, and chlorophyll characteristics are quite similar to those in the filament farther offshore between stations 71 and 79 (Figure 10). One possible explanation is that this water derived from the shoreward flow on the southern side of filament B and became entrained into the offshore flow of filament A. Another possible explanation is that the baroclinicity of the jet at the boundary between the warm, fresh offshore water and the cool, salty water upwelled from near the coast resulted in sufficient elevation of isopleths from the offshore region to permit phytoplankton growth. However, the available data are not sufficient to resolve this issue.

The third segment was the relatively wide segment of filament A (Figures 2 and 7). As seen in the AVHRR image on 14 July, this filament extended offshore about 90 km from Point Arena, turned southward for about 65 km and then turned toward the southwest. The meridional transect crossed the filament about 50 km west of Point Arena, probably near its southward turn. The cool anomaly was bounded on the north by a sharp temperature front that was also reflected in an increase of nitrate. The nearsurface chlorophyll fluorescence gradient was much less sharp than the temperature gradient. The core of the filament, as delineated by the lowest temperatures, was about 40 km across, but as mentioned earlier the transect was not perpendicular to the filament axis. Phytoplankton biomass was high within the filament, but was not as high as in filament B.

From the vertical structure within the filament (Figure 8), the upper 40 m layer was cool relative to the adjacent waters. Below 40 m, the isotherms underwent vertical excursions of about 40 m. This is most apparent in the deepening of the 10.5° C isotherm. The chlorophyll fluorescence isopleths deepened correspondingly. Relatively high biomass concentrations (chlorophyll fluorescence > 1; beam c >0.5

m^{-1}) extended to a depth of 100 m. This was well below the estimated euphotic zone depth of about 30 m within the high biomass region of the filament. (Deep layers of phytoplankton biomass were not seen in either of the cross-shelf transects, although the vertical extent of high biomass concentrations at station 61 (Figure 9), at the offshore end of the northern transect and within filament B, may not have been fully resolved since there was no bottle tripped at 80 m.) The bottom boundary of the biomass maximum tended to follow the 10° C isotherm between 20 and 50 km. At 50 km, there was a very sharp biomass front extending from the surface to 50 m, which corresponded with the location of a weak surface temperature front. Nearsurface nitrate decreased at about 60 km and remained measurable at the surface for an additional 40 km.

At station 63, immediately south of the phytoplankton front, chlorophyll concentrations were less than $0.5 \mu g \cdot l^{-1}$ throughout the water column (Figure 9). However, the water at this station was relatively saline and had higher nitrate concentrations than at station 61 in filament B. The low chlorophyll biomass within this segment is not consistent with water derived from the coastal region (Figure 3, 4, and 5). The saline, high nitrate, low chlorophyll water is similar to the high nitrate water farther offshore within the cyclonic region circumscribed by the filament, described later.

Temperature remained high and phytoplankton biomass relatively low in the fourth segment. At 100 km, nitrate concentrations had become barely detectable.

A Downstream Cross-Filament Transect

Immediately following the transect described in the previous section a second cross-filament transect was sampled between 11 and 13 July, from station 65 in the southeast to station 84 in the northwest (Figure 1). The transect crossed the filament nearly perpendicular to its axis at a location approximately 100 km downstream from the previous crossing of filament A. Niskin bottle profiles were obtained at 9 km intervals along a 46 km segment of the transect crossing the filament (Figure 11).

The filament was narrower (15-20 km) at this location than in the previous crossing (Figures 2b and 11). The width of the offshore jet within which the filament was embedded was about 50 km (RM). The temperature at the center of the filament was $<11.5°C$, comparable to temperatures in the filament nearer the coast. Temperatures on either side of the filament were $>14°C$. Nearsurface salinity was relatively fresh (<32.7 psu) north of filament and increased to >33.1 psu south of the cool filament.

Nitrate isopleths tended to follow salinity isopleths resulting in relatively high nitrate concentrations in the upper layer, 14° C water south of the filament. Ammonium concentrations were high within the filament, particularly below 30 m, and at 35 to 50 m depth in the south.

North of the filament the chlorophyll concentration was highest in a subsurface layer that included the samples taken from 35 and 50 m (Figure 11). The concentrations were highest in the relatively fresh northern boundary of the filament at 26 km and within the cool core of the filament at 34 km. At the cool core station, elevated concentrations extended at least to a depth of 100 m, similar to the vertical distribution in the section across the filament from Tow 1. South of the filament the chlorophyll concentrations were less than $0.5\,\mu g \cdot l^{-1}$.

The high chlorophyll concentrations immediately north of the filament core and within the filament core may have resulted from at least two processes. The upward tilting of isopycnals at the outer edge of the filament that is characteristic of the seaward jet would support the upwelling of deeper, nutrient-containing water into the euphotic zone enabling net primary production to occur. This would explain the high biomass at station 62 in the previous section and at the 26 and 34 km stations of this transect. However, the biomass in this offshore section may have been entrained into the filament near the coast and advected seaward with minimal cross-filament mixing. This would explain the similarity in the T/S characteristics (Figure 10) between station 62 and this section. Decreases in nutrient concentration and biomass between the two sections could be attributed to either physical losses such as sinking and/or mixing, or to biological losses such as grazing. It is likely that both advection and upwelling contribute to the phytoplankton biomass observed on this transect.

A Continuous, Nearsurface Cross-Filament Transect

A more complete set of nearsurface measurements was obtained on the next transect to the west, which was a meridional towyo transect (Tow 2 in Figure 1). This transect crossed the filament on 14 July, approximately 45 km southwest of the previous crossing, and it crossed the shoreward flow farther to the south (Figure 2). Bio-optical measurements were not obtained; the hydrographic structure has been discussed by RM.

The two segments of the filament were clearly evident in the temperature and fluorescence structure (Figure 12). The seaward-flowing portion of the filament was centered at 45 km and the shoreward-flowing portion was centered at 95 km. Salinity increased from north to south across the seaward-flowing portion of the filament and remained high until the track entered the shoreward-flowing

segment of the filament. The nitrate pattern was similar to salinity, increasing across the filament in the northern segment and decreasing across the southern segment of the filament. Chlorophyll fluorescence maxima were associated with the cool core of the filament, even within the low salinity segment between 30 and 40 km. Within the high salinity segment bounded by the filament, chlorophyll fluorescence remained higher than in the low salinity regions outside of the filament and the associated cyclonic feature. Fluorescence increased again in the southern segment of the filament, then decreased gradually in the low salinity segment south of the filament, reaching minimum levels at 110 km and beyond. It is therefore evident that elevated chlorophyll concentrations in relatively low salinity were associated with the filament along its entire track. It is also clear that high nitrate concentrations were associated not only with the cool filament but also spanned the high salinity segment between the two arms of the filament as might be expected with a cyclonic upwelling feature. However, this high nitrate region within the cyclonic feature did not have the high phytoplankton biomass found in the core of the filament.

A North-South Transect of the Filament 145 km Southwest of Pt. Arena

A third meridional hydrographic transect through the filament was made on 18 July. This transect included stations 167-176 which crossed the filament about 15 km southwest of where stations 71-79 crossed the filament on 13 July and was about 30 km east of Tow 2 (Figure 1). It originated north of the seaward-flowing portion of the filament, continued through the cyclonic region between the two arms of the filament, and extended south into the shoreward-flowing arm of the filament. (Phytoplankton taxonomic information is also available for this transect.)

The cool core of the northern, seaward-flowing portion of the filament, located about 25 km from the northern end of the transect (Figure 13), was narrow and the minimum temperature was less than 12° C. The 12° C isotherms extended from the surface to a depth in excess of 60 m. The general pattern of the isotherms was similar to the patterns in Tow 1 and in stations 70-79: isotherms shoaled in the upper 50-60 m of the filament and deepened below 60 m depth. There was a steep horizontal salinity gradient across the filament from low salinity water north of the filament to high salinity to the south, in the cyclonic feature. The horizontal salinity gradient contributed to the rise in isopycnals associated with the geostrophic component of the offshore jet. In the center of the cyclonic feature the surface salinity was more than 33.3 psu. This isohaline rose to the surface from a depth of nearly 100 m at the north end of the transect and deepened to nearly 100 m as the transect crossed into the shoreward flow of the filament at the southern end. The nitrate distribution across this segment was similar to the

temperature distribution in the northern part of the transect and to the salinity distribution in the southern part. For example, the highest surface nitrate concentrations (>4 μM) coincided with the high salinity core of the cyclonic feature. In the vicinity of the filament, surface concentrations were more than 2 μM.

Regenerated forms of nitrogen, nitrite and ammonium were also high in the vicinity of the filament. Ammonium concentrations were high beneath the filament in the depth range of 40 to 100 m. High concentrations extended laterally somewhat, especially to the south, but the concentrations were lower than those within the filament and were similar to the concentrations in the nearshore transects. Nitrite also showed a deep maximum in this segment. However, nitrite concentrations were highest south in the center of the cyclonic eddy feature at a depth of 60 m coincident with the local subsurface chlorophyll maximum.

As in the previous snapshots of the filament, the nearsurface chlorophyll concentrations were highest within the filament. The horizontal chlorophyll gradient was relatively steep on the southern boundary of the northern arm of the filament and was less steep across the northern boundary, consistent with the structure in Tow 1, Tow 2 and stations 70-79. High biomass concentrations extended vertically to a depth of at least 100 m in the filament, similar to Tow 1. The concentrations in the southern arm of the filament near 110 km increased at the surface, but did not exceed 1 $\mu g \cdot l^{-1}$. The biomass maximum did not extend as deeply in the southern, shoreward flowing section of the filament as it did in the northern section.

Direct phytoplankton counts were obtained for the water samples from this transect. These counts provide an additional indication of the biomass and the phytoplankton taxonomic composition. The cell abundance distribution generally followed the chlorophyll distribution with the highest abundance for most groups of phytoplankton occurring in the northern arm of the filament, between 6 and 30 km, and secondarily in the southern arm of the filament. Diatoms had the greatest spatial variability with horizontal abundance maxima in the seaward flow and the shoreward flow of the filament (Figure 14). Diatom abundances were low in the center of the cyclonic feature. The *Chaetoceros* species had the greatest range of abundance. Their abundance was low within the cyclonic feature, especially below 40 m depth. The *Chaetoceros* accounted for more than 90 percent of the diatom abundance in some samples from the filament (cf. Hood, 1990). The high abundance of diatoms, particularly *Chaetoceros*, within the

filament is consistent with a significant proportion of filament water deriving from coastal upwelled water. The deep chlorophyll distribution in the filament is consistent with the uniformly high numbers of diatoms occurring between the surface and 100 m in the filament.

Dinoflagellates had less spatial variability than the diatoms. However, large dinoflagellates were more abundant within the filament. (Dinoflagellates have routinely been a major component of the phytoplankton in other upwelling regimes (e.g., Estrada and Blasco, 1979).) Both large and small dinoflagellates varied more vertically than horizontally. There was a much less abundance variation in the smaller phytoplankton, which included flagellates, monads, and coccolithophorids ("other taxa" in Figure 14), than in either diatoms or dinoflagellates.

The doming of isopleths of T, S, and nitrate between the two arms of the filament reflects the cyclonic nature of the feature around which the filament flows. High salinity and nitrate concentrations (Figure 13) extended to the surface in the center of the feature. However, temperatures were higher in the upper 50 m of this feature suggesting that this water may have been at the surface for several days or weeks. (This high-salinity, high-nutrient feature was also apparent in Tows 1 and 2.) The phytoplankton biomass in this region was less than one would expect given the elevated nutrient concentrations available within the surface layer. The low phytoplankton biomass and the taxonomic composition suggest that there had been relatively little horizontal exchange between the center of the cyclonic feature and the cool filament surrounding it. The source for the high salinity water may have been local (open ocean) upwelling, or that the cyclonic feature had been formed much earlier as part of the coastal upwelling process and propagated offshore.

Within the cool filament (stations 171-174) there was substantial T/S variability (Figure 15). For example, at station 172 the nearsurface water is relatively warm and fresh. At 20 and 40 m, the temperature decreased slightly, but the salinity increased markedly. At 60 and 80 m, the salinity decreased, returning to the T/S characteristics defined by the low salinity California Current water. This variability was also apparent in the segment (stations 170 to 176) between the filament and the low salinity water to the north. At the southern end (station 167) of the transect, where the jet flowed shoreward, T/S characteristics were similar. Using the high resolution towyo transects RM described this water mass variability as indicative of intrusive features. By the time of the transect of stations 167 to 176, RM noted increased "diffusion" of the filament as manifest in the AVHRR imagery, which may have contributed to the complexity of structure observed here.

4. Transport of Inorganic Nitrogen and Biomass

A major question regarding the role of the meandering jets and their associated cool filaments is whether or not they result in a net seaward transport of nutrients, planktonic biomass and other dissolved and suspended material into the offshore region of the California Current System (Mooers and Robinson, 1984). Previous work resulting from the California Cooperative Fisheries Investigations (CalCOFI) program has demonstrated that large scale zooplankton variability in the California Current can be correlated with large scale equatorward volume transport variability (Chelton et al., 1982). However, a broad region of cool, upwelled water exists near the coast and could provide an alternative source of nutrient and phytoplankton variability for offshore waters. The horizontal continuity of isotherms and isopleths of pigment color obtained with the coastal zone color scanner (CZCS) (Abbott and Zion, 1985; Traganza et al., 1981), and previous physical observations of meandering jets and eddies in the region (Mooers and Robinson, 1984), suggest that seaward transport could contribute to the enrichment of the offshore region with nutrients and phytoplankton.

An estimate of the nitrogen and chlorophyll transport for the upper 100 m of the water column is presented below. The estimate is based on the snapshot of the filament from the hydrographic transects (stations 167 - 176) obtained on 17-18 July, a period of reduced wind stress (RM).

Horizontal Transport

The horizontal advective fluxes of the filament are estimated using geostrophic velocities (RM) and the nutrient and biomass distributions presented above. To calculate the fluxes, the velocity field and the transported variable (nutrients or chlorophyll) were interpolated onto a uniform grid overlaying the sample domain. The flux was calculated at each grid point as the product of the variable concentration and the velocity estimate. The transport, J, was estimated by integrating the flux over the area of the rectangle centered on the grid point, i.e.

$$J = \sum_{i,j} J_{i,j}$$

where

$J_{i,j} = \vec{v}_{i,j} \cdot C_{i,j} \cdot L_x \cdot L_z$

$\vec{v}_{i,j}$ = velocity perpendicular to section plane at the grid point

$C_{i,j}$ = concentration of variable at the grid point i,j

and L_x, L_z = length of the box around the grid point i,j in the horizontal and vertical directions,

respectively.

The transect of stations 167 to 176 was chosen for this estimate because it had the best horizontal coverage of nutrients and pigments with casts every 20 km (more frequent across the filament), of any transect crossing the filament. The calculated geostrophic velocities (relative to 500 db) for this transect ranged from about 30 $cm \cdot s^{-1}$ seaward at the northern end to about 40 $cm \cdot s^{-1}$ shoreward at the southern end (Figure 16). These velocities are not as high as have been observed on other surveys in the region (e.g. Kosro and Huyer, 1986), nor were they the highest velocities observed during OPTOMA21 (see RM for other transects).

The transport has been partitioned into two depth ranges, 0-50 m and 0-100 m. It is expected that the nitrogen transport must lie within the euphotic zone if it is to have a substantial influence on the offshore productivity. The offshore euphotic zone depth within the filament was conservatively chosen as 50 m (cf. Washburn et al., 1991). The seaward transport in the upper 50 m of the northern subsection (65 km horizontally x 50 m vertically) was approximately 1170 M $NO_3 \cdot s^{-1}$. The shoreward transport in the upper 50 m of the southern subsection (45 km horizontally x 50 m vertically) was 1000 M $NO_3 \cdot s^{-1}$ (Table 1A). Hence, the net seaward transport was 170 M $NO_3 \cdot s^{-1}$ (15 percent of the seaward transport) in the upper 50 m and 590 M $NO_3 \cdot s^{-1}$ (about 11 percent of the seaward transport) between the surface and 100 m depth.

The net transport of chlorophyll gave a somewhat different picture. The seaward transport for the upper 50 m was 300 g chlorophyll$\cdot s^{-1}$ (Table 1B), and the shoreward transport was 130 g chlorophyll$\cdot s^{-1}$, 44 percent of the seaward transport. In contrast to nitrate, integrating the chlorophyll transport over the upper 100m resulted in a smaller percentage increase in overall transport. The seaward transport was 460 g chlorophyll$\cdot s^{-1}$ and the shoreward transport was 180 g chlorophyll$\cdot s^{-1}$. The shoreward transport was 39 percent of the seaward transport , a slightly smaller percentage than for the upper 50 m. The difference (280 g chlorophyll$\cdot s^{-1}$) between the seaward and shoreward transports of chlorophyll may be overestimated. It is not clear in examining the transects in Figure 13 that the transect crossed the entire temperature minimum, chlorophyll maximum region of the southern arm of the filament. Of course, errors could be introduced by the assumed reference surface for the geostrophic flow.

The estimates of volume transport for this transect provide a reference for the estimates of nitrate and chlorophyll mass transport. In the upper 50 m the seaward transport was 0.45 Sv and the shoreward transport was 0.40 Sv, ~89 percent of the seaward transport (Table 1C). The transport for the upper 100

m was 0.80 Sv seaward and 0.72 Sv shoreward (90% of seaward transport). Thus the fractional differences between seaward and shoreward volume transport are about the same as the fractional differences between seaward and shoreward nitrate transport. In contrast, the fractional differences for chlorophyll transport are much greater than for either nitrate or volume transport. Therefore, it appears that there is a significant loss of phytoplankton biomass between the seaward and shoreward portions of the filament. The result is a net loss of 50-60% of the seaward transport of phytoplankton biomass into the region seaward of this transect.

The transect may have covered an adequate distance to compare the nitrate transports in the upper 50 m since nitrate concentrations fell to below 1 μM at either end. Even with relatively high velocities the low concentrations would result in only small increases in transport for the upper 50 m. The net loss of nitrate in the region offshore of the transect is a modest (11 to 15%) fraction of the seaward transport of nitrate in the filament . Because chlorophyll values appear to remain above 0.5 $\mu g \cdot l^{-1}$ at some depths at either end of the transect, the estimated net loss of 50 to 60% of the chlorophyll in the offshore region may be biased by incomplete sampling of both the seaward and shoreward flows.

Vertical Transport

A vertical flux of phytoplankton pigments is suggested by the distributions of chlorophyll, phytoplankton abundance, and particle abundance (proportional to beam attenuation coefficient) in the four cross-filament transects.

The first transect that suggests a significant downward transport of phytoplankton is Tow 1 on 10-11 July, 1986 (Figures 8). Elevated levels of phytoplankton biomass, indicated by beam c and chlorophyll fluorescence, extended to depths as great as 100 m in the first 60 km of the transect, well below the estimated euphotic zone depth of 30 m in the region of high biomass. Whether the deep phytoplankton abundance resulted from physical transport (mixing, downward advection) or was biologically mediated (vertical migration, physiologically induced sinking, etc.) may be suggested by the other data. The depth of the 10° C isotherm corresponded closely with the 1 $\mu g \cdot l^{-1}$ isopleth of chlorophyll fluorescence between 0 and 60 km along this transect (Figure 8). This correspondence between isotherms and chlorophyll fluorescence isopleths is also apparent for the 9 to 11° C band.

The distribution of chlorophyll and beam c had a similar pattern on the other cross-filament transects farther offshore. For example, in the north-south transect (stations 167-176), about 150 km offshore, high values of chlorophyll concentration and phytoplankton abundance extended to at least 100 m at some

stations (Figure 13). As in Tow 1, the 9 to 11° C band deepened below 50-60 m, similar to the pattern of the chlorophyll isopleths at the base of this deep feature. In another towyo transect west of stations 167-176, the beam c distribution associated with the northern transect of the filament extended to about 80 m depth (not shown). As with the other transects there was a deepening of the 9 to 11° C band in this region. The deepening of these isotherms was associated with the presence of almost isothermal layers in the vertical profiles and were usually associated with smaller vertical scale saline intrusions (see RM). The correspondence between isotherms and biomass isopleths suggest that the elevated biomass levels to depths of 100 m were the result of physical processes such as subduction. This conclusion is consistent with the conclusions of Kadko, et al. (1991) and Washburn, et al. (1991).

In addition to the deep biomass feature in the offshore region of seaward flow, there was also a deep chlorophyll feature in the shoreward flow of the southern arm. This particular feature extended to about 60 m depth, and did not appear to have the same variation of isotherm depth as in the northern segment of the filament. In addition, the water was fresher (by up to 0.3 psu) between 60 and 80 m compared with the northern anomaly. The shallowing of the high biomass feature from at least 100 m in the northern segment to about 60 m in the south suggests that the large difference between seaward and shoreward chlorophyll transport may be partially due to the physical loss of some of the higher salinity water found in the seaward flow. Perhaps this occurred when the filament made its cyclonic turn shoreward.

5. Discussion and Summary

The observations from OPTOMA21 provided one of the first overviews of the physical, chemical, and biological distributions of a coastal upwelling/cool filament/meandering jet system manifest in the California Current System and many other eastern boundary currents. It is clear from the satellite imagery of sea surface temperature and ocean color (Abbott and Zion, 1985) that the system is complex and highly variable. Several distinct regions and their associated processes appear to contribute to the structure and dynamics of this coastal transition zone: the coastal upwelling region near the coast, the offshore cool filaments and their associated jets, the cyclonic upwelling feature, and the offshore, lower salinity region beyond the filament and cyclonic feature.

The nearshore region can generally be characterized as a coastal upwelling region. Both satellite imagery and *in situ* observations show manifestations of the coastal upwelling. The coastal stations were characterized by low temperatures (<11° C), high salinity, and high nutrient concentrations. Chlorophyll concentrations were also high in the coldest, surface coastal water. Higher biomass concentrations are

generally expected "downstream" from where the water is upwelled. As the upwelled water is advected away from the coast and stratifies, the phytoplankton are expected to adapt to the high light and nutrient conditions, increasing their growth rate and biomass away from the point of upwelling (Jones et al., 1983; MacIsaac et al., 1985; Dugdale and Wilkerson, 1989). Localized warming and reduced nutrient concentrations in the high biomass, high salinity, upper layer water near the coast suggest that the phytoplankton were growing rapidly in the upwelled water. Based on the high salinity of this water, it is unlikely that the high seed population resulted from lateral mixing with the surrounding lower salinity surface water. Resuspension of cells from the bottom into the upwelled water is a possible source of the seed population. Another possible source is the sinking of cells from the surface layer into the water as it is being advected toward the coast. This is not a new idea, but this process is difficult to verify.

There was alongshore variability in the source of the upwelled water. Water upwelled from south of Point Arena had salinities in excess of 33.9 psu, while water from north of Point Arena had salinities of about 33.5 psu. The higher temperatures and lower salinities of the water from north of Point Arena suggest that either the source water for upwelling was different from that south of Point Arena or that it may have undergone more mixing with lower salinity water present over the shelf break and slope. Given the location of the transect where the lower salinity water was observed, both explanations are possible.

During OPTOMA21, several cool filaments were distinguishable at distances of more than 35-50 km from the coast and were embedded in a large-scale cool anomaly which included a cyclone south of filament A. Satellite imagery suggests that the filaments incorporated some of the cool, chlorophyll-rich coastal water entrained by the associated jet. Filament A extended about 250 km offshore where it turned southeastward, following the perimeter of a cyclonic eddy feature located offshore from Point Reyes. The filament maintained its characteristics of low temperatures and high chlorophyll in the offshore zone. Both salinity and nutrient concentrations displayed strong gradients within the filament, their fronts not always coincident with temperature fronts. Salinity and nutrient concentrations generally increased across the filament and into the cyclonic eddy feature (e.g. Figures 10, 12 and 13). Their values remained high within the cyclonic feature consistent with the uplifting of isopleths that one would expect with a cyclonic upwelling feature. The water in the filament warmed as it moved offshore and turned southeastward; where surface transects crossed both arms of the filament, temperature was usually lower in the northern, seaward-flowing segment. Chlorophyll concentration also decreased along the filament from near the shelf break progressing seaward. However, the chlorophyll concentration was highly variable.

The cool filaments had a complex subsurface structure. It was shown by RM that the upper 30-40 m of the filament contained cool, low salinity water and that beneath the upper 50 m the water may be warm and relatively salty compared to the adjacent water. Another significant characteristic of the filaments was the deep penetration of relatively high concentrations of phytoplankton biomass. Concentrations of phytoplankton biomass were high between 80 and 100 m depth, nearly twice the estimated euphotic zone depth, in each of the transects across the offshore flow of the northern segment of the filament. Estimates of phytoplankton sinking rates in upwelling regions are generally less than 2 m per day (e.g. Bienfang, 1985). Assuming a euphotic zone depth of about 30 m in the coastal region, approximately 35 days would be required for phytoplankton sinking at 2 m per day from the lower part of the euphotic zone to reach 100 m depth. This is too long a period for sinking to be significant given the characteristic advection rates of the jet. The consistency of the relationship between the chlorophyll concentrations and the isotherms at various distances and times along the filament combined with what is known about phytoplankton sinking rates suggest that the deep chlorophyll resulted from physical processes such as sinking (subduction) of the denser, coastally upwelled water as it advects seaward. Similar conclusions have been reached for this region from radon measurements (Kadko, et al, 1991) and from more extensive bio-optical measurements (Washburn et al., 1991).

From 50 to 250 km offshore the highest regenerated nutrient concentrations, especially ammonium, were associated with the filament. The highest ammonium concentrations tended to occur in the depth range of 40-100 m, the deeper depth range of the high chlorophyll concentrations. These concentrations were of the same order of magnitude ($\sim 0.5\ \mu M$) as those in the cross-shelf transects and in the stations along Tow 1. The ammonium may have resulted from zooplankton grazing. Observations of zooplankton biomass and reproduction indicated higher levels within the filament (R. Bohrer, personal communication). (Also, Abbott et al. (1990) presented indirect evidence of higher zooplankton concentrations within a cool filament during night-time along the path of a drifter that was deployed in the Point Arena region in June 1987.) The low levels of ammonium in the upper 40 m probably resulted from uptake by phytoplankton within the euphotic zone (estimated to have been 40-50 m deep in the offshore portion of the filament). Another possible source of the ammonium is advection from the coastal region. The ammonium concentrations were $0.5\ \mu M$ or more at the four stations along Tow 1, which varied in distance offshore from 50 to 100 km. The zone below 50 m is also the depth range where RM observed warm, saline intrusions beneath the filament consistent with a nearshore source for this water. However, it is likely that this water

was nearer the surface in the coastal region and that phytoplankton uptake of ammonium would have been significant. It is therefore likely that a significant proportion of the high ammonium concentrations associated with the filament came from *in situ* regeneration within the offshore flow, but that a portion of the ammonium may have been advected from the shelf and slope region.

The cyclonic upwelling feature between the filament and the coastal region was observed in several of the transects. There was some evidence for this feature in Tow 1, but it was especially apparent in the nearsurface values of Tow 2 and in stations 167-176. Isotherms, isohalines, and nutrient isopleths dome in this region consistent with a cyclonic feature. However, the upper 50 m of this feature was relatively warm, in contrast to most of the high-salinity, high-nutrient water that extended to the surface in this region. This suggest that the saline, nutrient-rich water may have been at the surface for a sufficient period for significant heating to occur.

It is surprising that the cyclonic eddy feature did not develop higher chlorophyll concentrations in the presence of the higher nutrient concentrations in the surface layer. There are several possible explanations for this. First, the biomass was low suggesting that the seed population in the upwelled water was not large to begin with. Second, the phytoplankton populations were not able to increase their physiological capability sufficiently to take advantage of the upwelled nutrients. Dugdale and Wilkerson (1990) have suggested, that unless nitrate concentrations exceed 5-6 μM, the range of nitrate concentrations within the upper layer of the cyclonic upwelling feature, the phytoplankton cannot physiologically "shift-up" to take advantage of the available light and nutrients. Another possibility is that the phytoplankton contained within the water upwelled offshore lacked the high growth rate potential often characteristic of diatoms in coastal water. Diatoms, which are generally considered to be fast-growing and most able to exploit the nutrient and light regime characteristic of upwelling regions (e.g. Margalef, 1978), had particularly low abundance in the cyclonic feature. The physical and biological development of these cyclonic features and their importance to the physical and biological dynamics of the coastal transition zone remain as important topics for understanding eastern boundary current regions.

North of the filament and cyclonic eddy feature the temperature was higher and the salinity was lower consistent with California Current water. Chlorophyll biomass was low in this region, although not as low as in an open ocean oligotrophic region.

The filament/jet-associated offshore advection and cyclonic-eddy upwelling provide two mechanisms for the introduction of nutrients into the euphotic zone in the region offshore from the coastal upwelling zone off northern California. Although the rate of vertical transport into the surface layer by the cyclonic eddy system is not known, the area covered by the cyclonic feature indicates that it could provide a major portion of the nutrients within the region bounded by filament A. The net advective transport of nutrients into the offshore region was less than 15 percent of the transport of the seaward-flowing jet in the upper 50 m, comparable to the difference in volume transport between the seaward and shoreward flows in our estimate. In contrast, The net phytoplankton transport into the offshore region was more than 50 percent of the offshore transport, much greater than either the volume or nitrate differences. However, the southern segment of the filament and hence the shoreward transport of phytoplankton may not have been completely covered. The long term effect of these two mechanisms on offshore productivity is unknown. It may be that there are events which enhance the horizontal exchange between the chlorophyll-rich filament water and chlorophyll-poor, nutrient-sufficient core of the cyclonic feature. If so then the nutrient flux from the eddy could provide a significant contribution to the offshore productivity.

Acknowledgements: We are grateful to the captain and crew of the R/V *Point Sur* for their cooperation in the OPTOMA21 field survey. The acquisition of this data set was enhanced by the technical assistance of Eric Olson, Dennis O'Neill, and Terry Garrett of USC. Dolors Blasco provided the phytoplankton taxonomy. This research is a contribution to the OPTOMA Program and to the CTZ Program, both of which were sponsored by the Office of Naval Research, Oceanic Biology and Physical Oceanography Programs.

6. References

Abbott, M.R., and P.M. Zion (1985) Satellite observations of phytoplankton variability during an upwelling event. *Continental Shelf Research* 4: 661-680.

Abbott, M.R., and P.M. Zion (1987) Spatial and temporal variability of phytoplankton pigment off northern California during Coastal Ocean Dynamics Experiment 1. *Journal of Geophysical Research* 92:1745-1755.

Abbott, M.R., K.H. Brink, C.R. Booth, D. Blasco, L.A. Codispoti, P.P. Niiler, and S.R. Ramp. 1990. Observations of phytoplankton and nutrients from a Lagrangian drifter off northern California. *Journal of Geophysical Research 95*:9393-9409.

Bernstein, R.L., L. C. Breaker, and R. Whritner. (1977) California Current eddy formation: ship, air and satellite results. *Science 195*:353-359.

Bienfang, P. (1985) *Sedimentation of Suspended Microparticulate Material in the Point Conception Upwelling Ecosystem, a Technical Report of Research Performed During the 1983 OPUS II Fieldwork*. Waimanalo, Hawaii: The Oceanic Institute, pp. 1-24.

Bucklin, A., M.M. Rienecker, and C.N.K. Mooers (1989) Genetic tracers of zooplankton transport in coastal filaments off northern California. *Journal of Geophysical Research 94*:8277-8288.

Chelton, D.B., P.A. Bernal, and J.A. McGowan (1982) Large-scale interannual physical and biological interaction in the California Current. *Journal of Marine Research 40*:1095-1125.

Davis, R.E. (1985a) Drifter observations of coastal surface currents during CODE: The method and descriptive view. *Journal of Geophysical Research* 90:4741-4755.

Davis, R.E. (1985b) Drifter observations of coastal surface currents during CODE: The statistical and dynamical views. *Journal of Geophysical Research* 90:4756-4772.

Dugdale, R.C. and F.P. Wilkerson (1989) New production in the upwelling center at Point Conception, California: temporal and spatial patterns. *Deep-Sea Research 36*:985-1007.

Dugdale, R.C. and F.P. Wilkerson (1990) Evidence for a critical nitrate concentration in upwelling systems: implications for operation of the biological pump in the CO_2 cycle. *EOS 71*:111

Estrada, M. and D. Blasco (1979) Two phases of the phytoplankton community in the Baja California upwelling. *Limnology and Oceanography 24*:1065-1080.

Flament, P., L. Armi, and L. Washburn (1985) The evolving structure of an upwelling filament. *Journal of Geophysical Research 90*:11765-11778.

Flegal, A.R., T.F. Duda and S. Niemeyer. (1989) High gradients of lead isotopic composition in north-east Pacific upwelling filaments. *Nature* 339:458-460.

Holm-Hansen, O., C.J. Lorenzen, R.W. Holmes, and J.D.H. Strickland (1965) Fluorometric determination of chlorophyll. *Journal Du Conseil* 30:3-15.

Hood, R.R. 1990. *Phytoplankton Biomass, Photosynthetic Light Response, and Physical Structure in a Northern California Upwelling System.* Ph.D. Dissertation, University of California, San Diego, 141 p.

Jones, B.H., K.H. Brink, R.C. Dugdale, D.W. Stuart, J.C. VanLeer, D. Blasco, and J.C. Kelley. 1983. Observations of a persistent upwelling center off Point Conception California. In: E. Suess and J. Thiede (eds.), *Coastal Upwelling, Its Sediment Record, Part A: Responses of the Sedimentary Regime to Present Coastal Upwelling,* Plenum Press, pp. 37-60.

Kadko, D. C., L. Washburn, and B. H. Jones. 1991. Evidence of subduction within cold filaments of the N. California Coastal Transition Zone. *Journal of Geophysical Research*, submitted.

Kosro, P.M. (1987) Structure of the Coastal Current Field off Northern California During the Coastal Ocean Dynamics Experiment. *Journal of Geophysical Research 92*:1637-1654.

Kosro, P.M. and A. Huyer. (1986) CTD and velocity surveys of seaward jets off northern California, July 1981 and 1982. *Journal of Geophysical Research 91:*7680-7690.

Lorenzen, C.J. 1966. A method for continuous measurement of *in vivo* chlorophyll concentration. *Deep-Sea Research 13:*223-227.

MacIsaac, J.J., R.C. Dugdale, R.T. Barber, D. Blasco, and T.T. Packard (1985) Primary production cycle in an upwelling center. *Deep-Sea Research 32*:503-529.

Margalef, R. 1978. Life forms of phytoplankton as survival alternatives in an unstable environment. *Oceanologica Acta 1:*493-509.

Mooers, C.N.K. and A.R. Robinson. 1984. Turbulent jets and eddies in the California Current and inferred cross-shore transports. *Science 223:*51-53.

Rienecker, M. M., C. N. K. Mooers, D. E. Hagan, and A. R. Robinson. (1985) A cool anomaly off northern California: an investigation using IR imager and in situ data. *Journal of Geophysical Research 90:*4807-4818.

Rienecker M.M. and C.N.K. Mooers (1989) Mesoscale eddies, jets and fronts off Pt. Arena, July 1986. *Journal of Geophysical Research 94:*12555-12570.

SooHoo, J.B. and D.A. Kiefer (1982) Vertical distribution of phaeopigments - I. A simple grazing and photooxidative scheme for small particles. *Deep-Sea Research 29*:1539-1551.

Spinrad, R. W. 1986. A calibration diagram of specific beam attenuation. *Journal of Geophysical Research 91:*7761-7764

Traganza, E. D., J. C. Conrad, and L. C. Breaker (1981) Satellite observations of a cyclonic upwelling system and giant plume in the California Current. In: F. A. Richards (ed.), *Coastal Upwelling,* American Geophysical Union, Washington, D.C., pp. 228-241.

Traganza, E.D., D.A. Nestor, and A.K. McDonald (1980) Satellite observations of a nutrient upwelling off the coast of California. *Journal of Geophysical Research* 85:4101-4106.

Venrick, E.L. and T.L. Hayward (1984) Determining chlorophyll on the 1984 CalCOFI surveys. *CalCOFI Reports* 25:74-79.

Washburn L., D.C. Kadko, B.H. Jones, T.J. Cowles, and T.L. Hayward. (1991) Water mass subduction in a coastal upwelling system. *Journal of Geophysical Research*, submitted.

Whitledge, T.E. (1980) Nitrogen recycling and biological populations in upwelling systems. In: F. A. Richards (ed.), *Coastal Upwelling,* American Geophysical Union, Washington, D.C., pp. 257-273.

Whitledge, T.E., S.C. Malloy, C.J. Patton, and C.D. Wirick. (1981) *Automated nutrient analysis in seawater, BNL 51398, Brookhaven National Laboratory*, New York, 216 pp.

Wittmann P.A., M.L. Ciandro, A.A. Bird and C.N.K. Mooers (1987) *Hydrographic data from the OPTOMA Program. OPTOMA21, 7-20 July 1986.* Naval Postgraduate School Technical Report NPS-68-87-001, Monterey, CA, 58 pp.

7. Transport Tables:

Table 1. Nitrate, Chlorophyll, and Volume Nitrogen Transport

Stations 167-176, 18 July 86

(110 km x 100 m grid)

A. Nitrate Transport

Depth Range	Seaward (65 km)	Shoreward (45 km)	Difference
0-50 m	1170 Moles/s	1000 Moles/s	170 Moles/s
0-100 m	5200 Moles/s	4610 Moles/s	590 Moles/s

B. Chlorophyll Transport

Depth Range	Seaward (65 km)	Shoreward (45 km)	Difference
0-50 m	300 g/s	130 g/s	170 g/s
0-100 m	460 g/s	180 g/s	280 g/s

C. Volume Transport

Depth Range	Seaward (65 km)	Shoreward (45 km)	Difference
0-50 m	0.45 Sv	0.40 Sv	0.05 Sv
0-100 m	0.80 Sv	0.72 Sv	0.08 Sv

8. Figure Legends

Figure 1. Station locations for the OPTOMA21 cruise for the period of July 7 - July 19, 1986. The cruise track is indicated with the dotted line. Diamonds indicate the station locations and numbers indicate the station numbers at the end points of hydrographic transects. The three towyo transects are indicated with solid lines.

Figure 2. Sea surface temperature images from NOAA-9 AVHRR satellite for a) July 5 and b) July 14, 1986, showing coastal upwelling and several filaments extending seaward from the coast. The cruise track is overlaid on the July 14 image.

Figure 3. Near-surface map constructed from the observations along the ship track shown in Figure 2. The contour plots include measurements from the ship's nearsurface sea water intake and from hydrographic casts. The plotted variables include a) temperature ($^{\circ}C$); b) dynamic height (decimeters); c) nitrate plus nitrite (μM); and d) chlorophyll a fluorescence ($\mu g \cdot l^{-1}$).

Figure 4. Hydrographic transect from near the coast about 35 km south of Point Arena and north of Point Reyes (Stations 27-31) on July 8, 1986.

Figure 5. Hydrographic transect from near the coast about 35 km north of Point Arena (Stations 57-61) on July 10, 1986.

Figure 6. a) Nitrate/temperature; b) temperature/salinity; and c) nitrate/salinity from stations 27-31, cross-shelf transect south of Point Arena. The data point labels indicate the station/depth for nearshore, upper layer observations.

Figure 7. Nearsurface values for the north-south transect from station 61 to 65 (Tow 1) for T (from ship intake and towyo), NO_3, chlorophyll fluorescence (from ship intake and towyo) and beam c from the towyo. Vertical dashed lines are used to indicate the approximate boundaries of the segments of the transect discussed in the text. Numbers between the dashed lines in the towyo temperature plot indicate the segment number. Distances along the track are referenced to the towyo deployment point; positive distances are distances southward from the deployment point and negative distances extend northward from the point of deployment to station 61.

Figure 8. Transects of temperature (°C), beam attenuation coefficient (m^{-1}), and chlorophyll fluorescence (volts; note 1 volt≈1 $\mu g \cdot l^{-1}$) from Tow 1. There are no chlorophyll fluorescence contour lines greater than 4.5 because the fluorometer saturated at 5 volts. Distances are referenced to the position of the towyo deployment at station 62, as in Figure 7.

Figure 9. Hydrographic profiles of T, S, sigma t, NO_3, ammonium, and chlorophyll for stations 61-64 (Figure 1) along line A-B on July 10-11, 1986. Locations of profiles are also indicated on the nearsurface space series in Figure 7.

Figure 10. Temperature/salinity plot for stations 70-79 and for station 62 from the Tow 1 transect.

Figure 11. Hydrographic bottle transects for stations 70-79: a) temperature (°C); b) salinity (psu); c) sigma t; c) nitrate (μM); e) ammonium (μM); and f) chlorophyll *a* ($\mu g \cdot l^{-1}$).

Figure 12. Nearsurface temperature, salinity, nitrate, and chlorophyll fluorescence for Tow 2 on July 13-14, 1986. The transect distances are referenced to the towyo deployment point as in Tow 1 (Figure 7).

Figure 13. Hydrographic bottle transects for stations 167-176: a) temperature (°C); b) salinity (psu); c) nitrate (μM); d) ammonium (μM); e) nitrite (μM); and f) chlorophyll *a* (μM).

Figure 14. Abundance of major phytoplankton taxa for station 167-176. The abundance is presented as the Log_{10} of the counts for the 50 ml settled volume of the sample.

Figure 15. The T/S plot for stations 167-176, July 17-18, 1986.

Figure 16. The geostrophic velocity relative to 500 db for the transect between stations 167 and 176 (see Figure 1 for station locations).

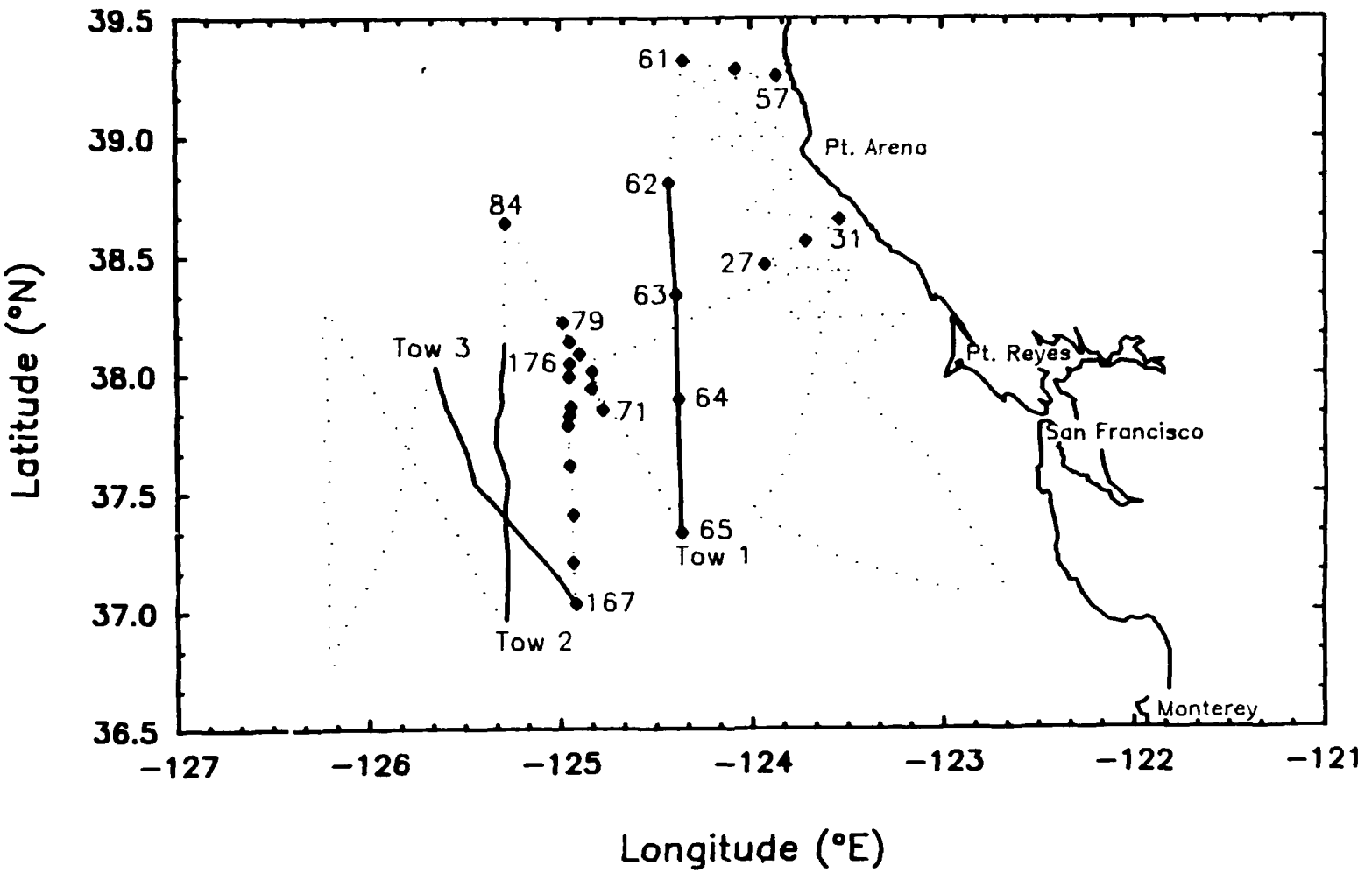
39.5
39.0
38.5
38.0
37.5
37.0
36.5
Latitude (°N)
−127
−126
−125
−124
−123
−122
−121
Longitude (°E)
61
57
Pt. Arena
62
84
31
27
63
79
Tow 3
176
Pt. Reyes
71
64
San Francisco
65
Tow 1
167
Tow 2
Monterey

Figure 1

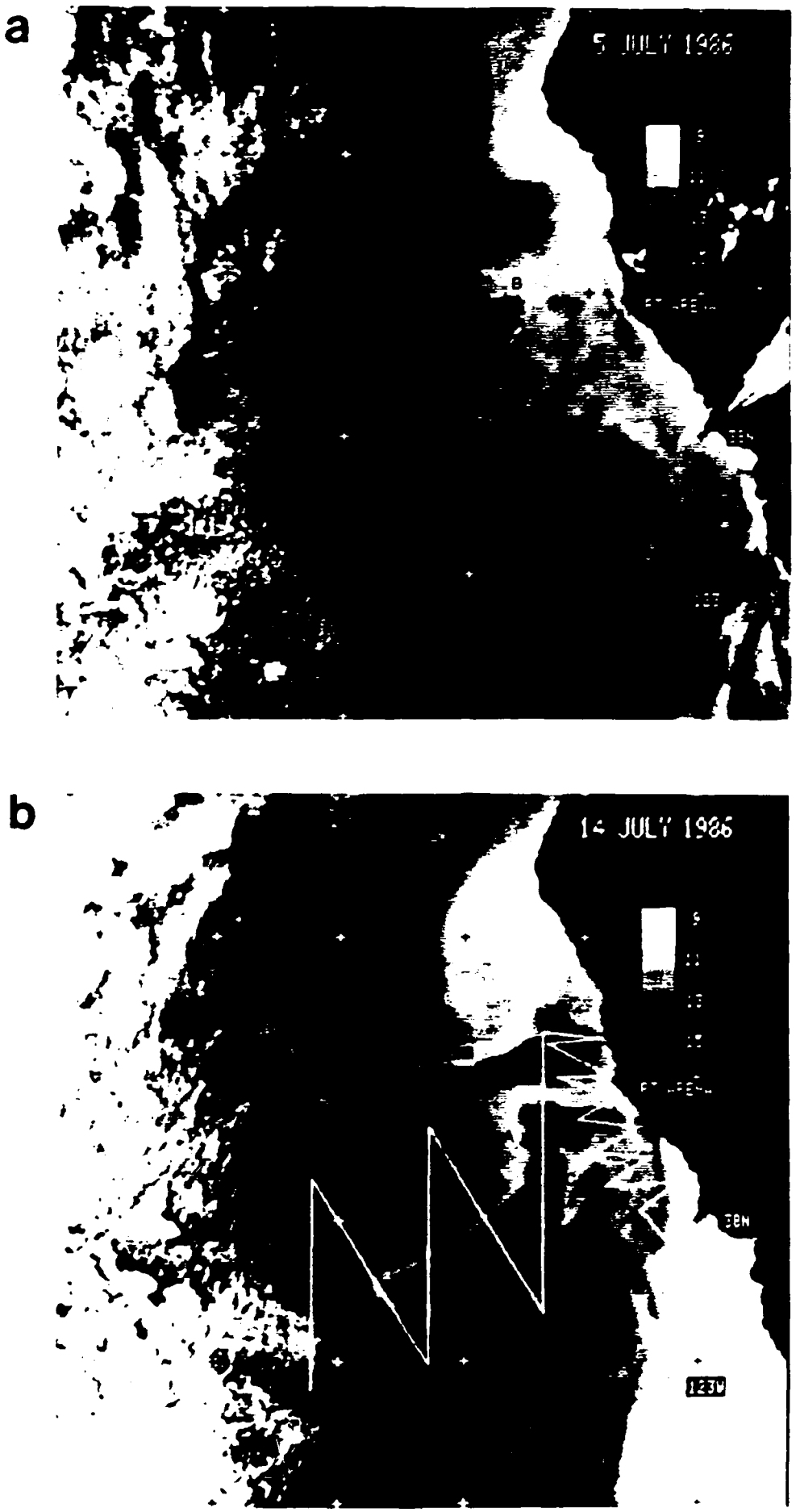

Figure 2

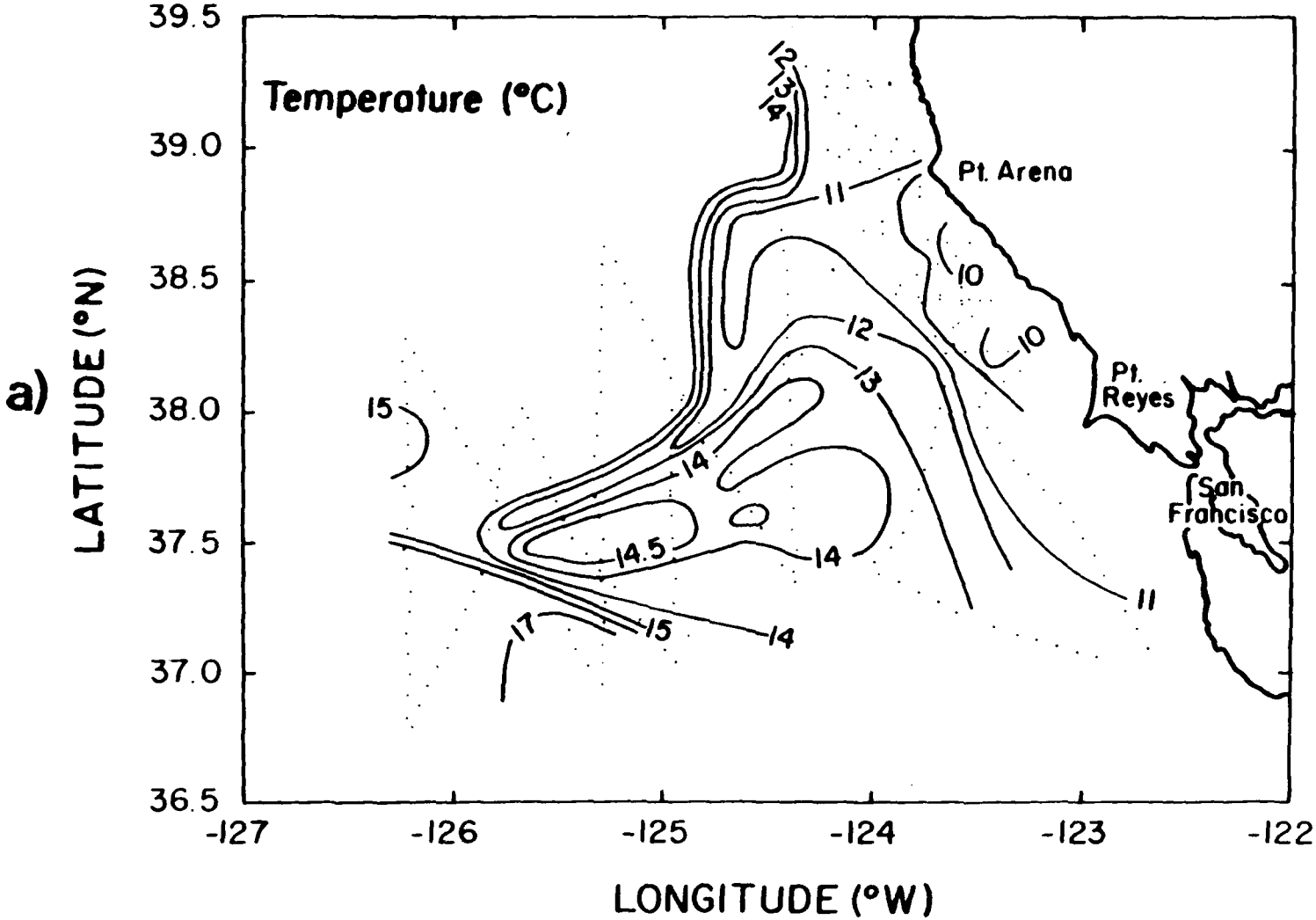
a)
Temperature (°C)
LATITUDE (°N)
LONGITUDE (°W)
39.5
39.0
38.5
38.0
37.5
37.0
36.5
-127
-126
-125
-124
-123
-122
Pt. Arena
Pt. Reyes
San Francisco
12
13
14
11
10
10
12
13
15
14
14.5
14
17
15
14
11

Figure 3

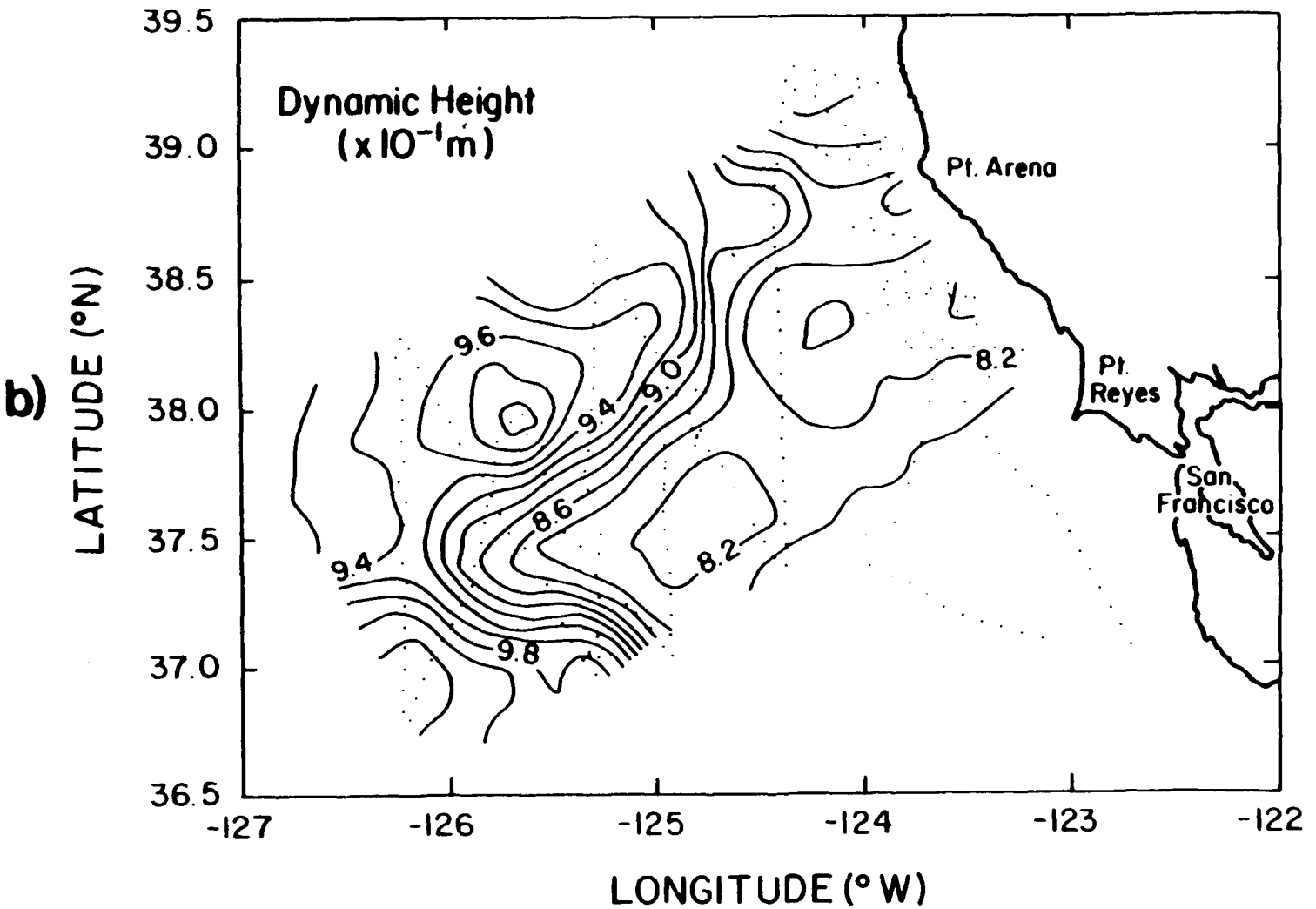
b)
Dynamic Height
(x 10⁻¹m)
39.5
39.0
38.5
38.0
37.5
37.0
36.5
LATITUDE (°N)
-127
-126
-125
-124
-123
-122
LONGITUDE (° W)
Pt. Arena
Pt. Reyes
San Francisco
9.6
9.4
9.0
8.6
8.2
9.4
8.2
9.8

Figure 3

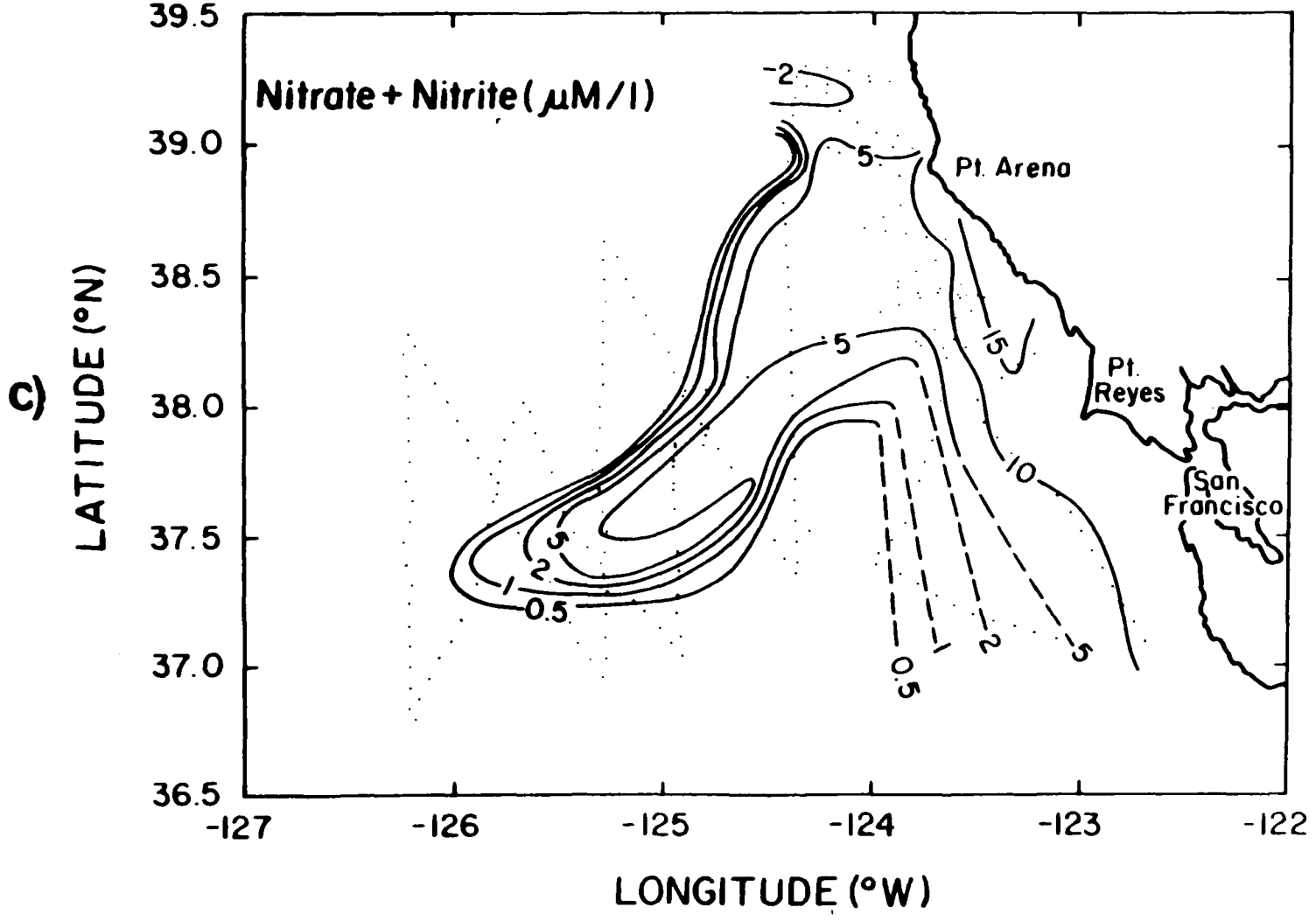
c)
Nitrate + Nitrite (μM/l)
LATITUDE (°N)
LONGITUDE (°W)
39.5
39.0
38.5
38.0
37.5
37.0
36.5
-127
-126
-125
-124
-123
-122
Pt. Arena
Pt. Reyes
San Francisco
2
5
5
15
10
5
2
1
0.5
0.5
1
2
5

Figure 3

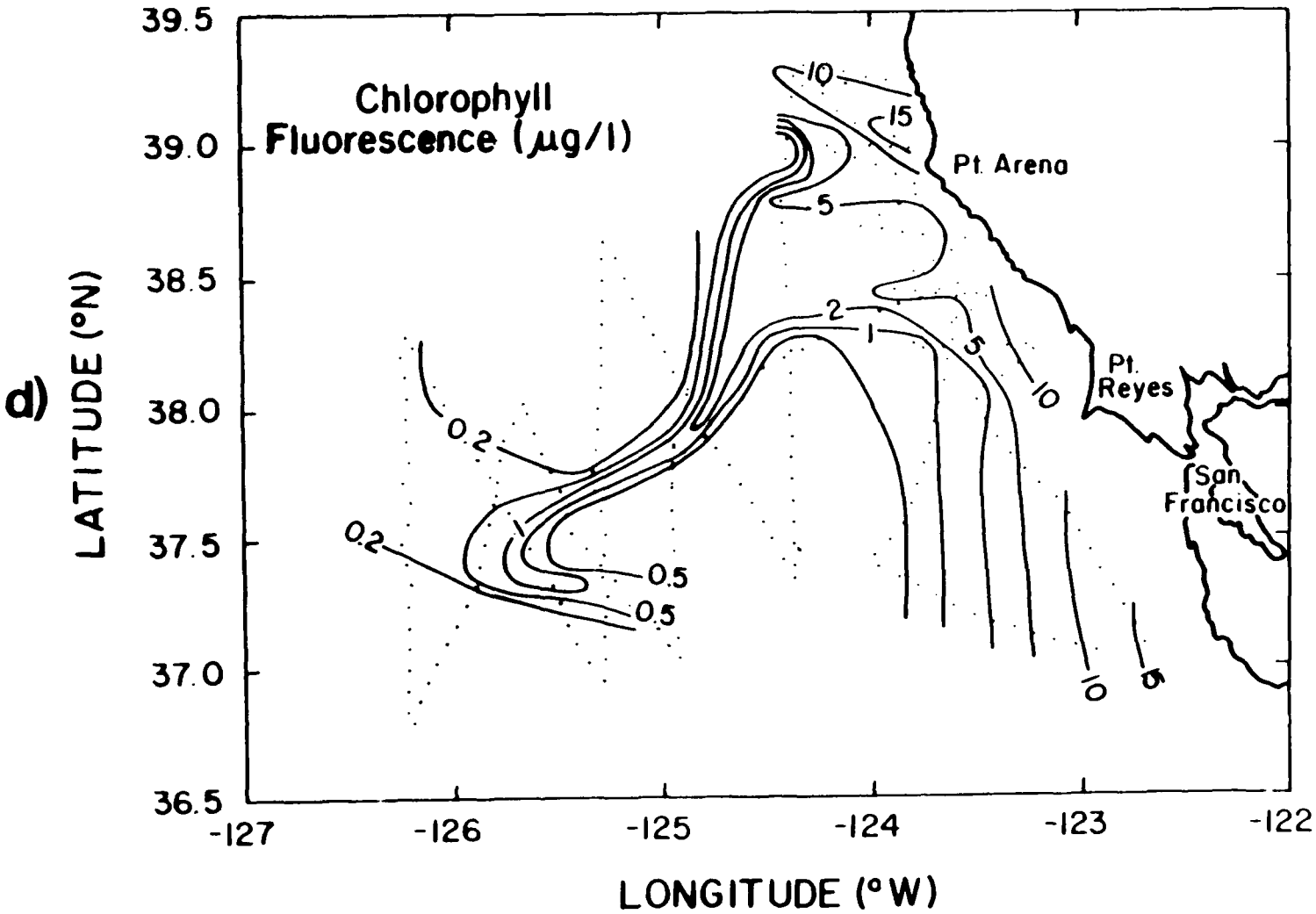
d)
Chlorophyll
Fluorescence (µg/l)
39.5
39.0
38.5
38.0
37.5
37.0
36.5
LATITUDE (°N)
-127
-126
-125
-124
-123
-122
LONGITUDE (°W)
Pt. Arena
Pt. Reyes
San Francisco
10
15
5
2
1
0.2
0.2
1
0.5
0.5
5
10
10
5

Figure 3

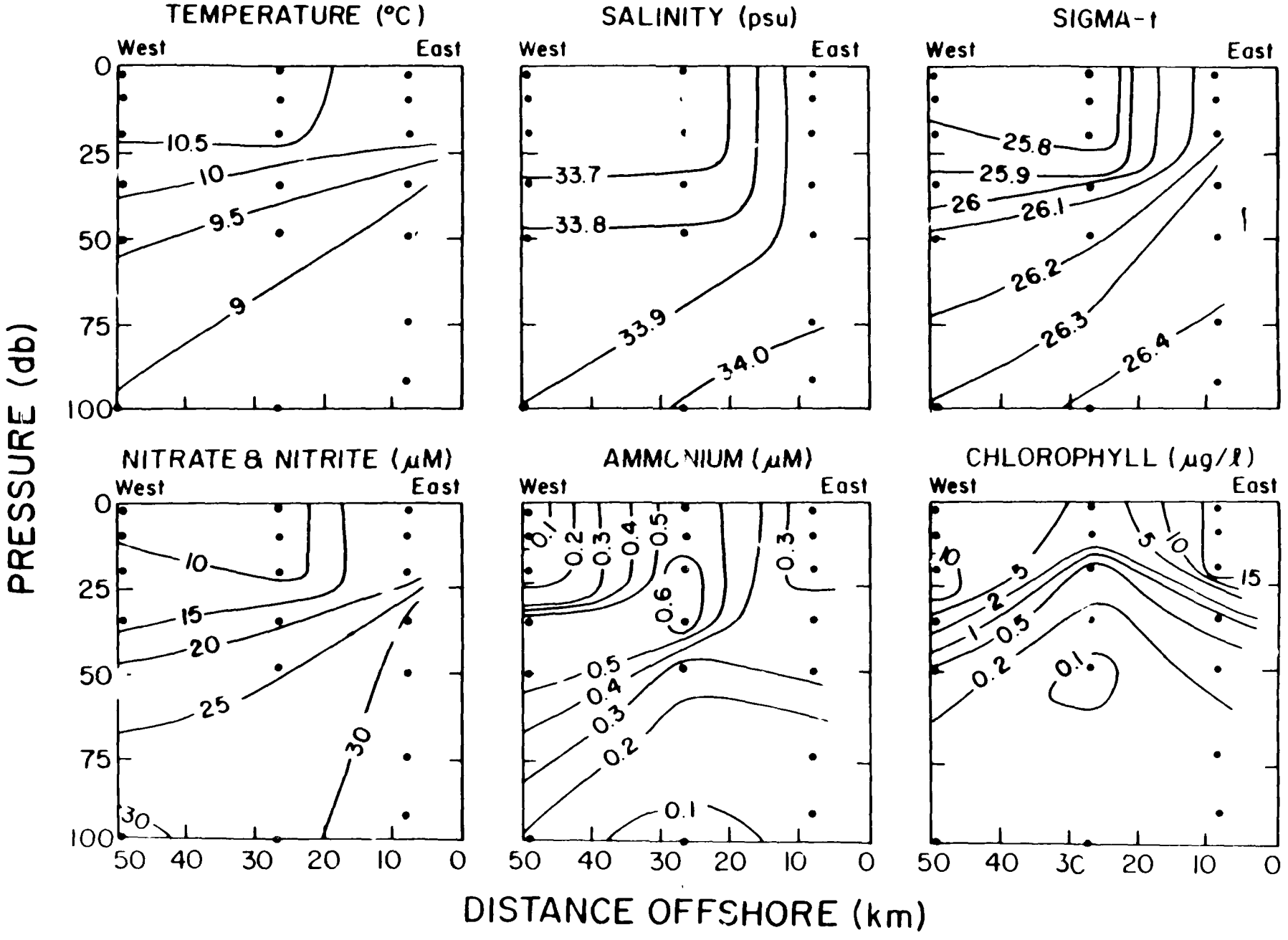
TEMPERATURE (°C)
SALINITY (psu)
SIGMA-t
NITRATE & NITRITE (μM)
AMMONIUM (μM)
CHLOROPHYLL (μg/ℓ)
West
East
PRESSURE (db)
DISTANCE OFFSHORE (km)
0
25
50
75
100
50 40 30 20 10 0
10.5
10
9.5
9
33.7
33.8
33.9
34.0
25.8
25.9
26
26.1
26.2
26.3
26.4
15
20
25
30
0.1
0.2
0.3
0.4
0.5
0.6
1
2
3
5
10

Figure 4

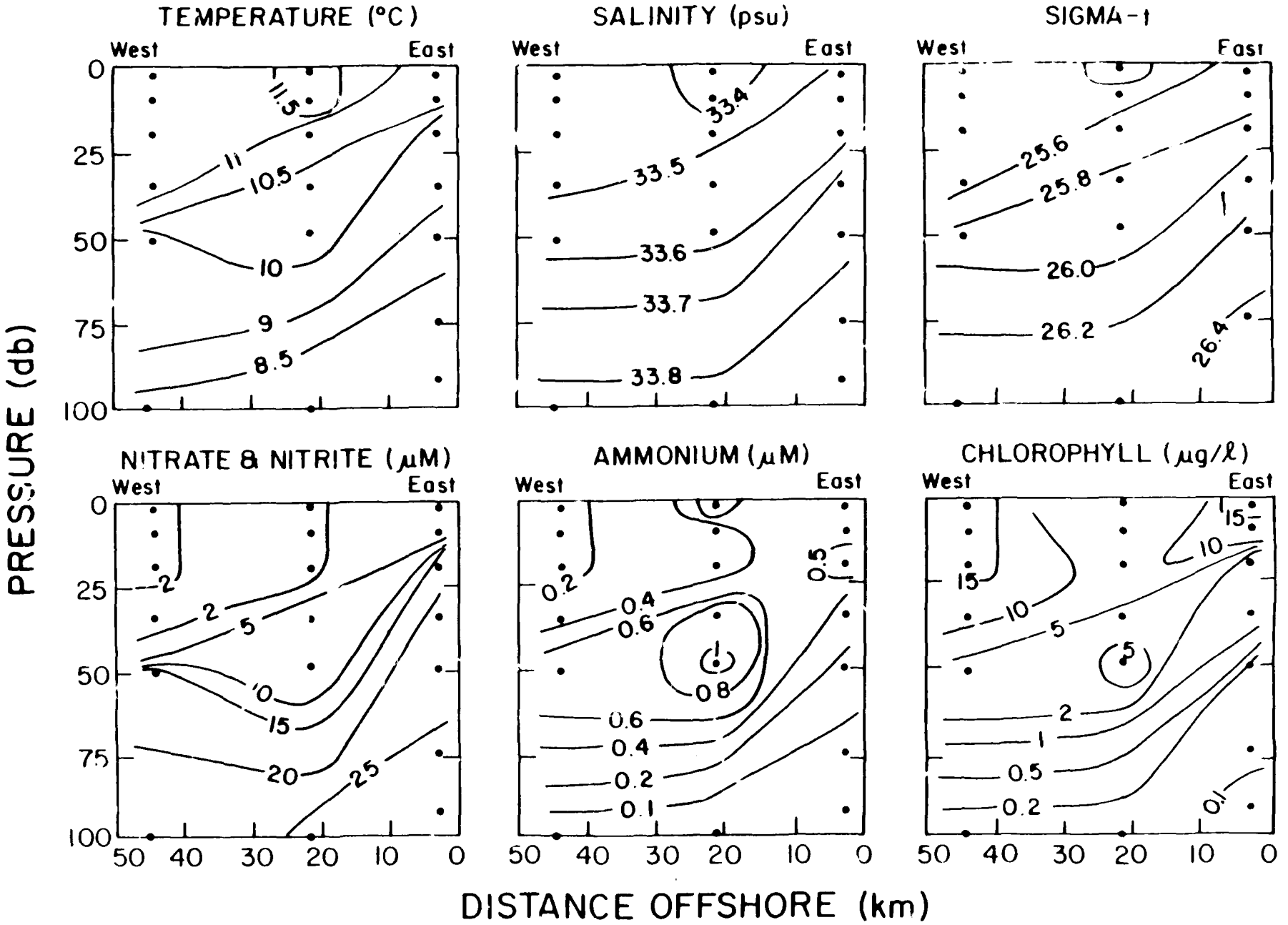
TEMPERATURE (°C)
SALINITY (psu)
SIGMA-t
NITRATE & NITRITE (μM)
AMMONIUM (μM)
CHLOROPHYLL (μg/ℓ)
West
East
PRESSURE (db)
DISTANCE OFFSHORE (km)
0
25
50
75
100
50 40 30 20 10 0
11.5
11
10.5
10
9
8.5
33.4
33.5
33.6
33.7
33.8
25.6
25.8
26.0
26.2
26.4
2
5
10
15
20
25
0.2
0.4
0.6
0.8
0.5
1
15
10
5
2
1
0.5
0.2
0.1

Figure 5

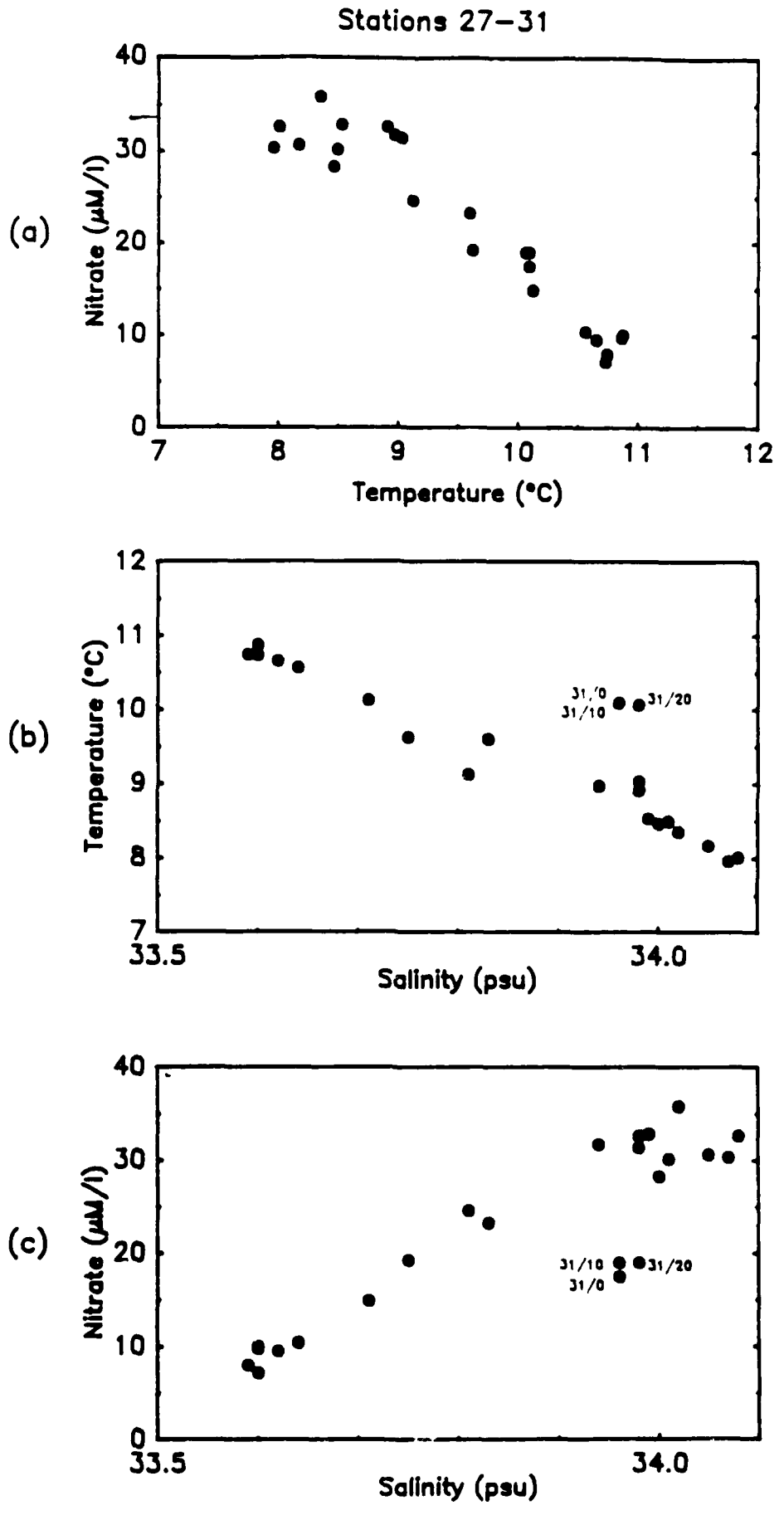
Stations 27–31
(a)
Nitrate (μM/l)
Temperature (°C)
(b)
Temperature (°C)
Salinity (psu)
31/0
31/10
31/20
(c)
Nitrate (μM/l)
Salinity (psu)
31/10
31/0
31/20

Figure 4

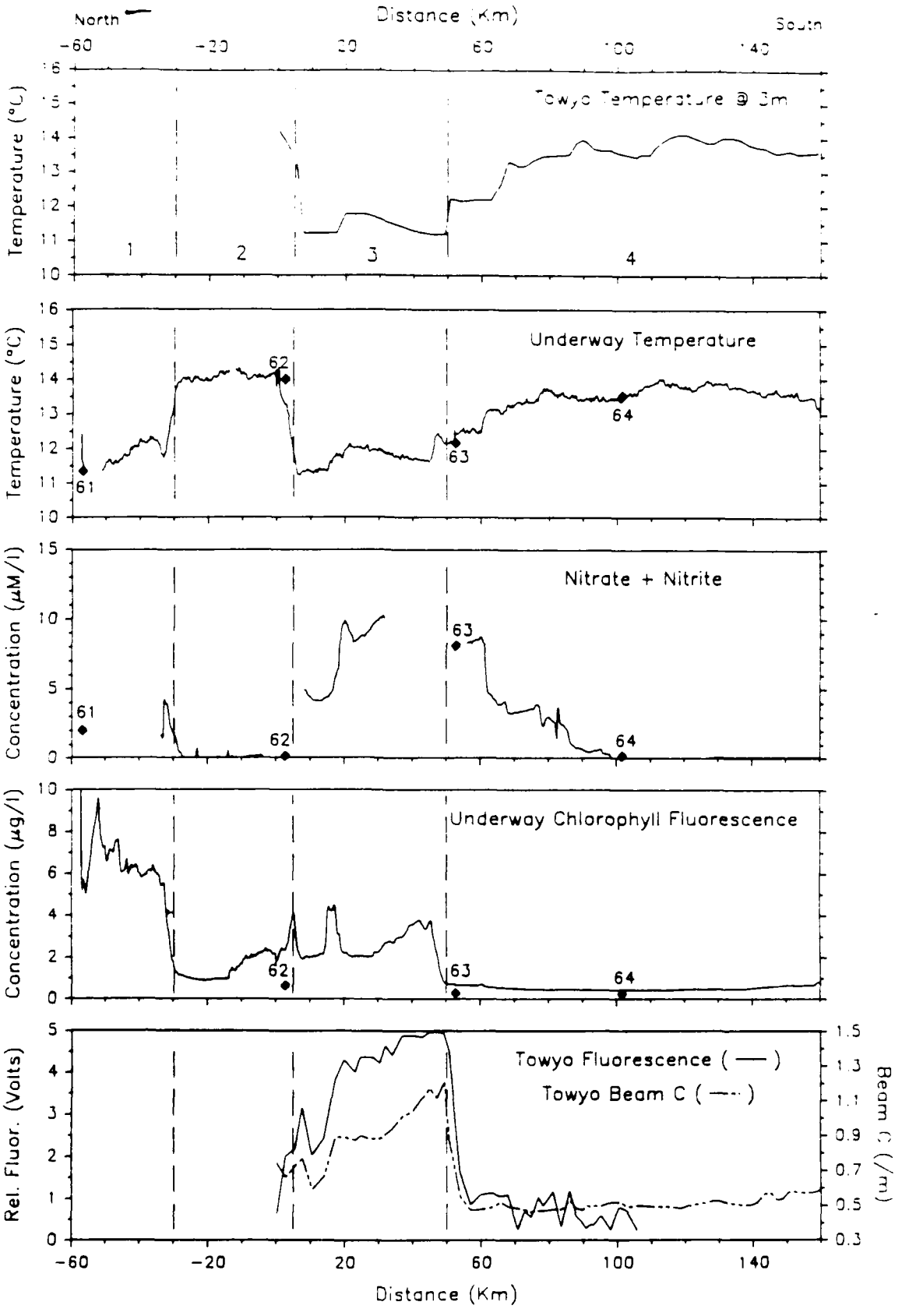
North
Distance (Km)
South
-60
-20
20
60
100
140
Towyo Temperature @ 3m
Temperature (°C)
1
2
3
4
Underway Temperature
61
62
63
64
Nitrate + Nitrite
Concentration (µM/l)
Underway Chlorophyll Fluorescence
Concentration (µg/l)
Towyo Fluorescence (——)
Towyo Beam C (—·—)
Rel. Fluor. (Volts)
Beam C (/m)
Distance (Km)

Figure

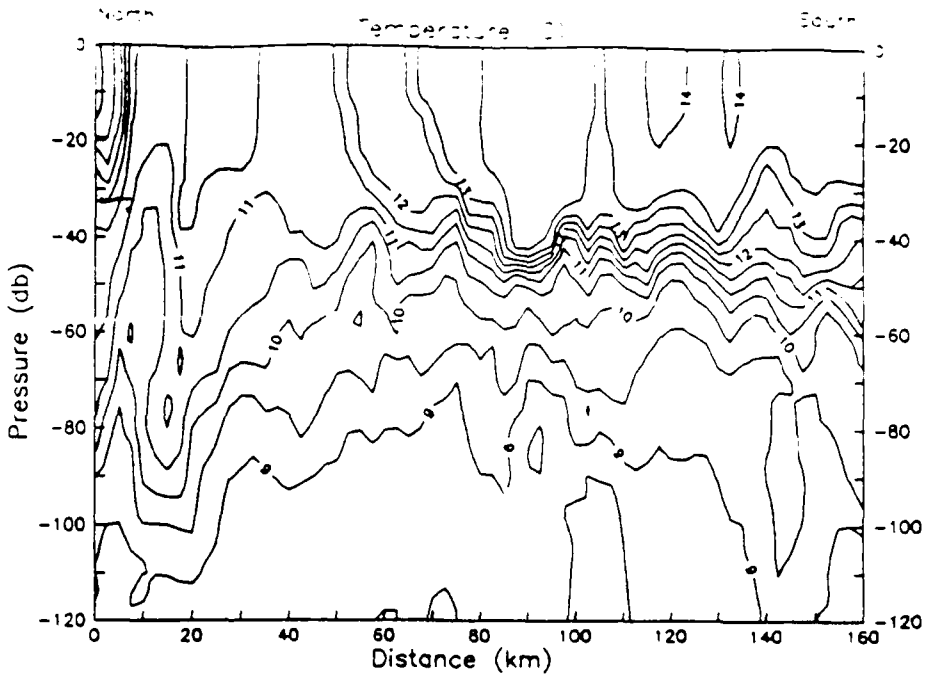
Pressure (db)
Distance (km)

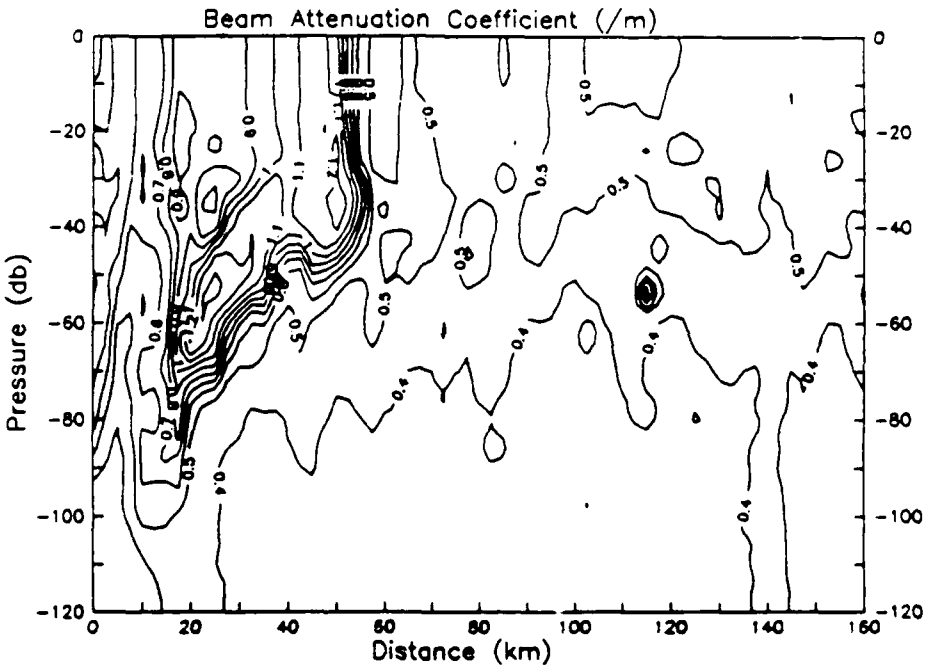
Beam Attenuation Coefficient (/m)
Pressure (db)
Distance (km)

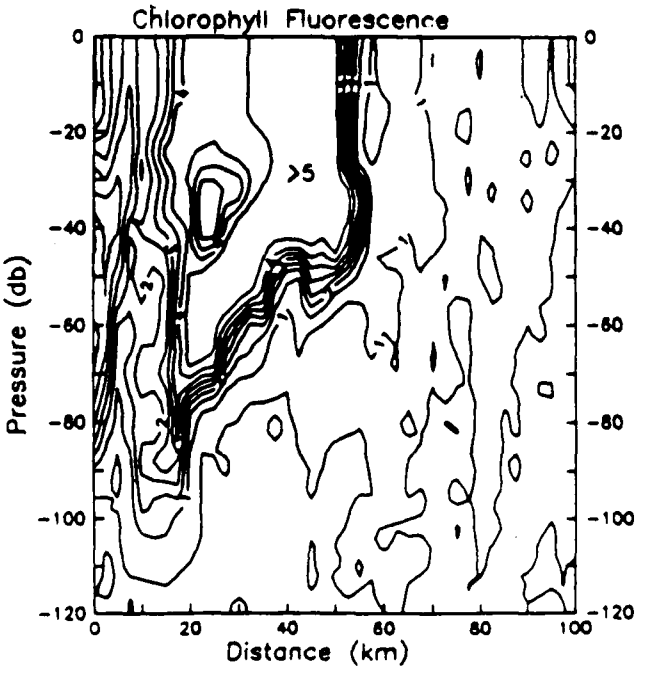
Chlorophyll Fluorescence
>5
Pressure (db)
Distance (km)

Figure 5

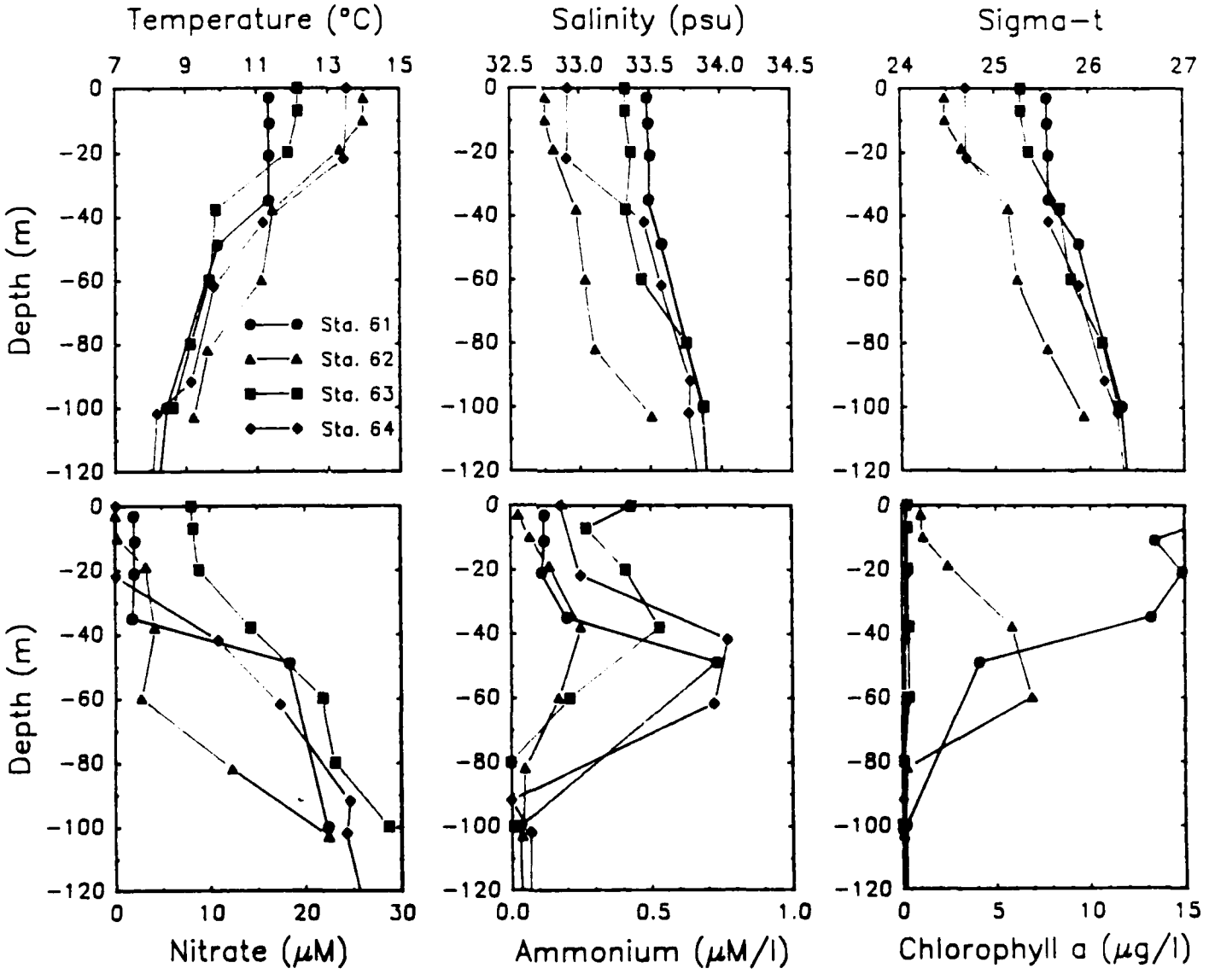
Temperature (°C)
Salinity (psu)
Sigma–t
Depth (m)
Sta. 61
Sta. 62
Sta. 63
Sta. 64
Nitrate (μM)
Ammonium (μM/l)
Chlorophyll a (μg/l)

Figure

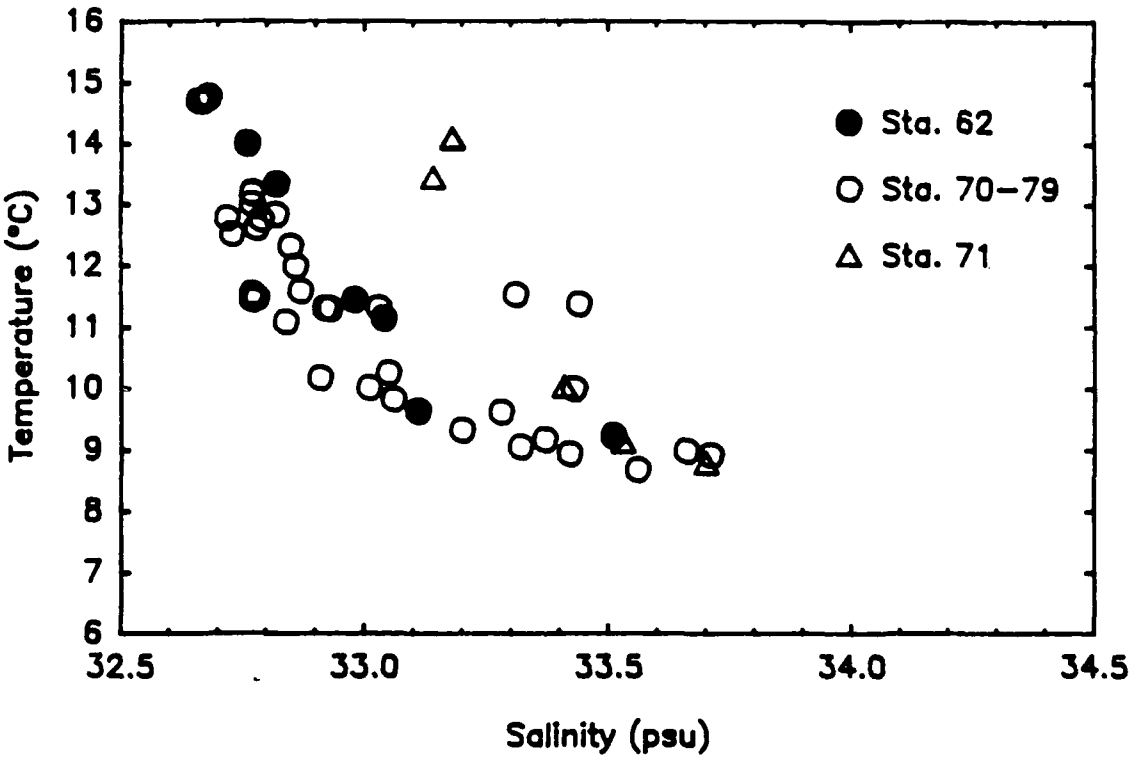
16
15
14
13
12
11
10
9
8
7
6
Temperature (°C)
32.5
33.0
33.5
34.0
34.5
Salinity (psu)
Sta. 62
Sta. 70–79
Sta. 71

Figure 10

Figure 11

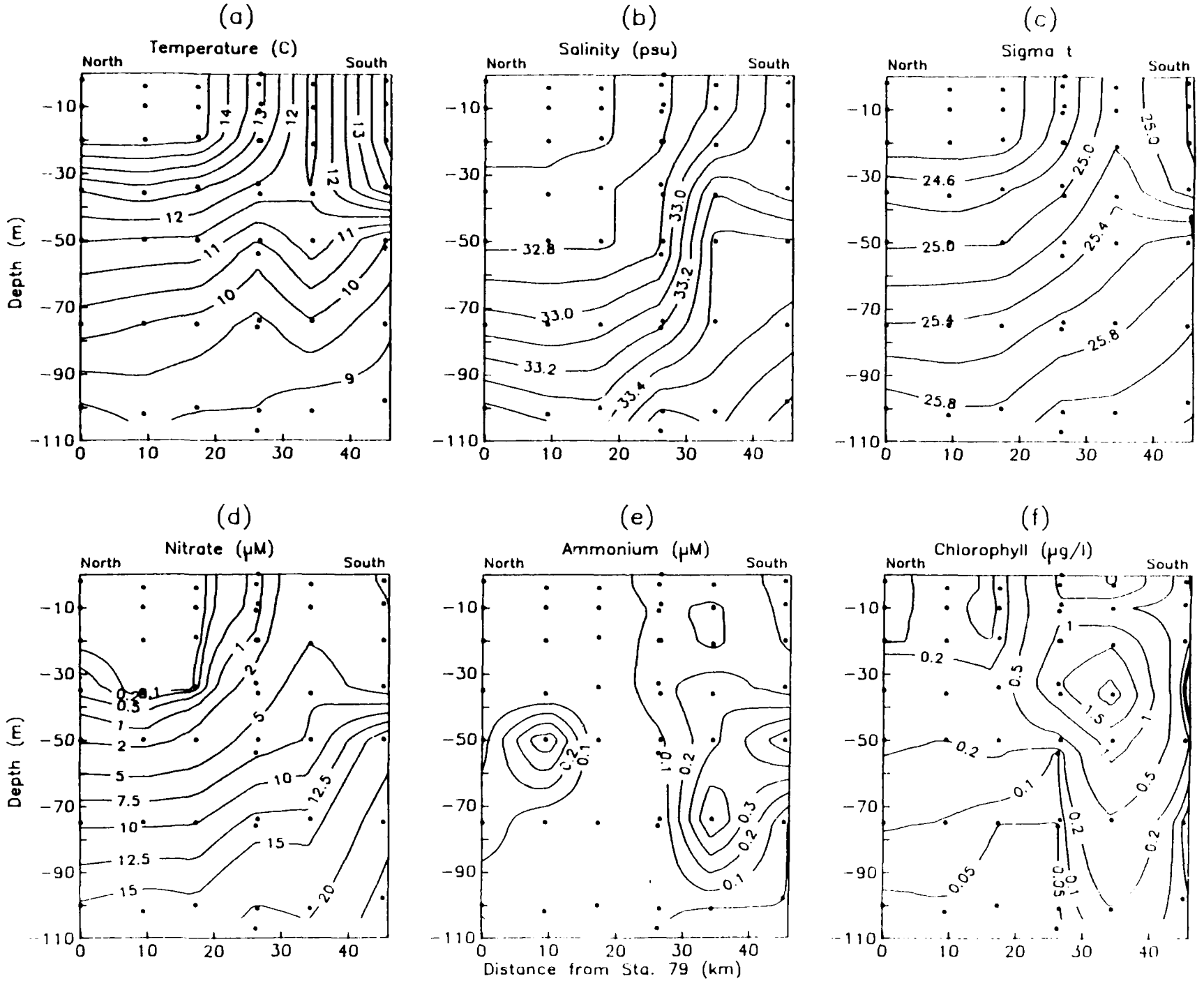
(a)
Temperature (C)
North
South
Depth (m)
(b)
Salinity (psu)
North
South
(c)
Sigma t
North
South
(d)
Nitrate (μM)
North
South
Depth (m)
(e)
Ammonium (μM)
North
South
Distance from Sta. 79 (km)
(f)
Chlorophyll (μg/l)
North
South

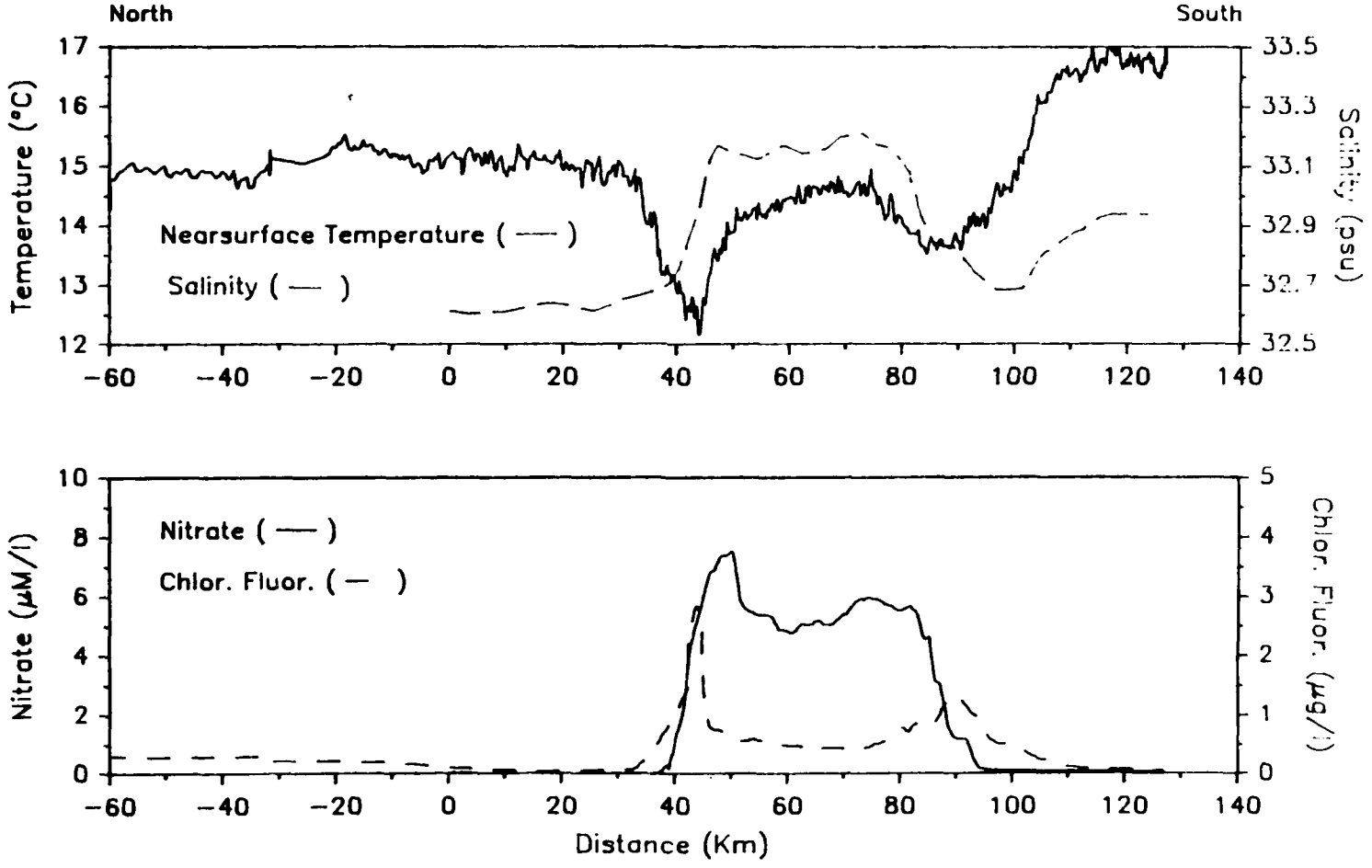
North
South
Temperature (°C)
Salinity (psu)
Nearsurface Temperature (—)
Salinity (—)
Nitrate (μM/l)
Chlor. Fluor. (μg/l)
Nitrate (—)
Chlor. Fluor. (—)
Distance (Km)

Figure 12

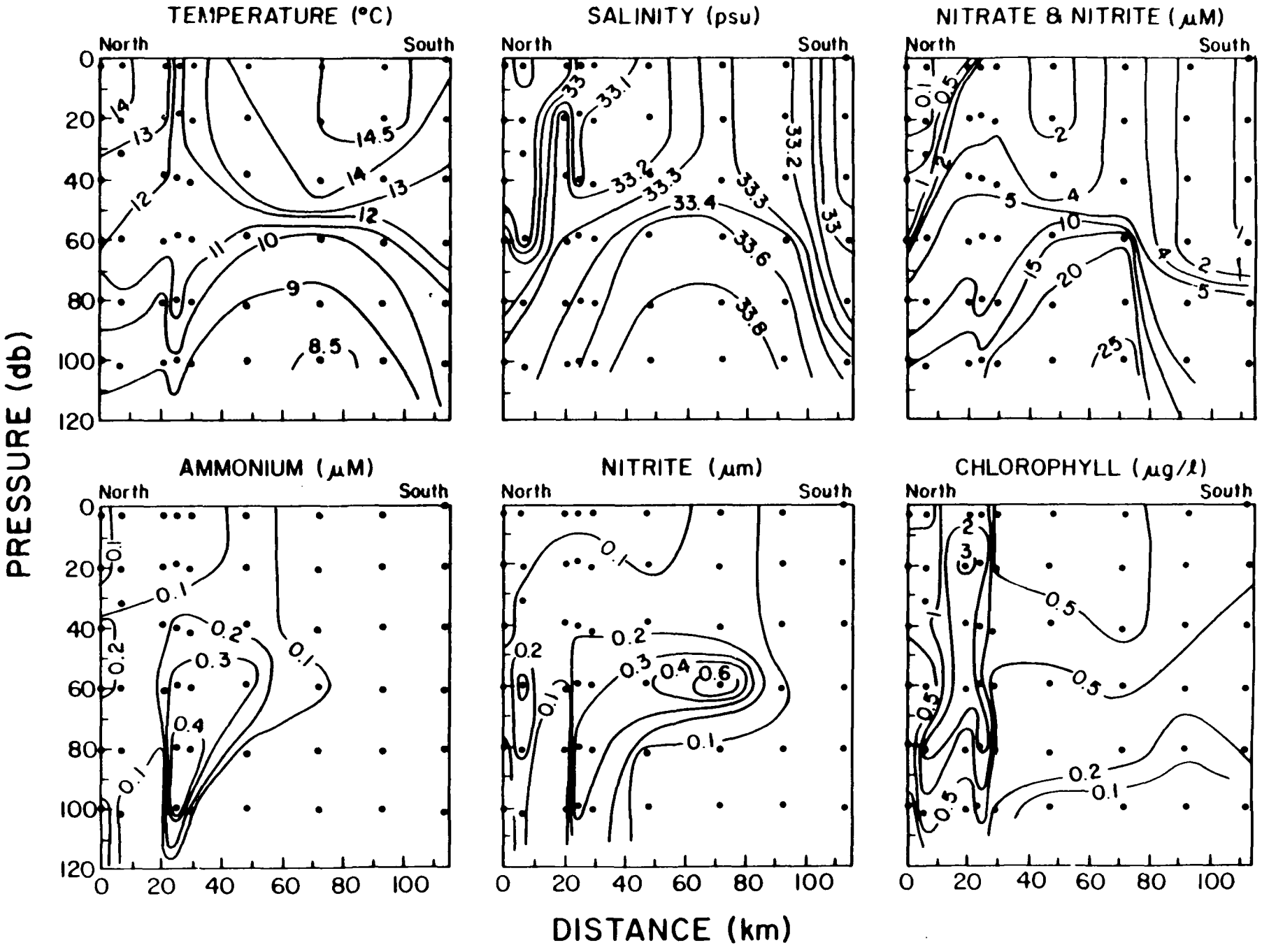
TEMPERATURE (°C)
SALINITY (psu)
NITRATE & NITRITE (μM)
AMMONIUM (μM)
NITRITE (μm)
CHLOROPHYLL (μg/ℓ)
North
South
PRESSURE (db)
DISTANCE (km)
0
20
40
60
80
100
120

Figure 13

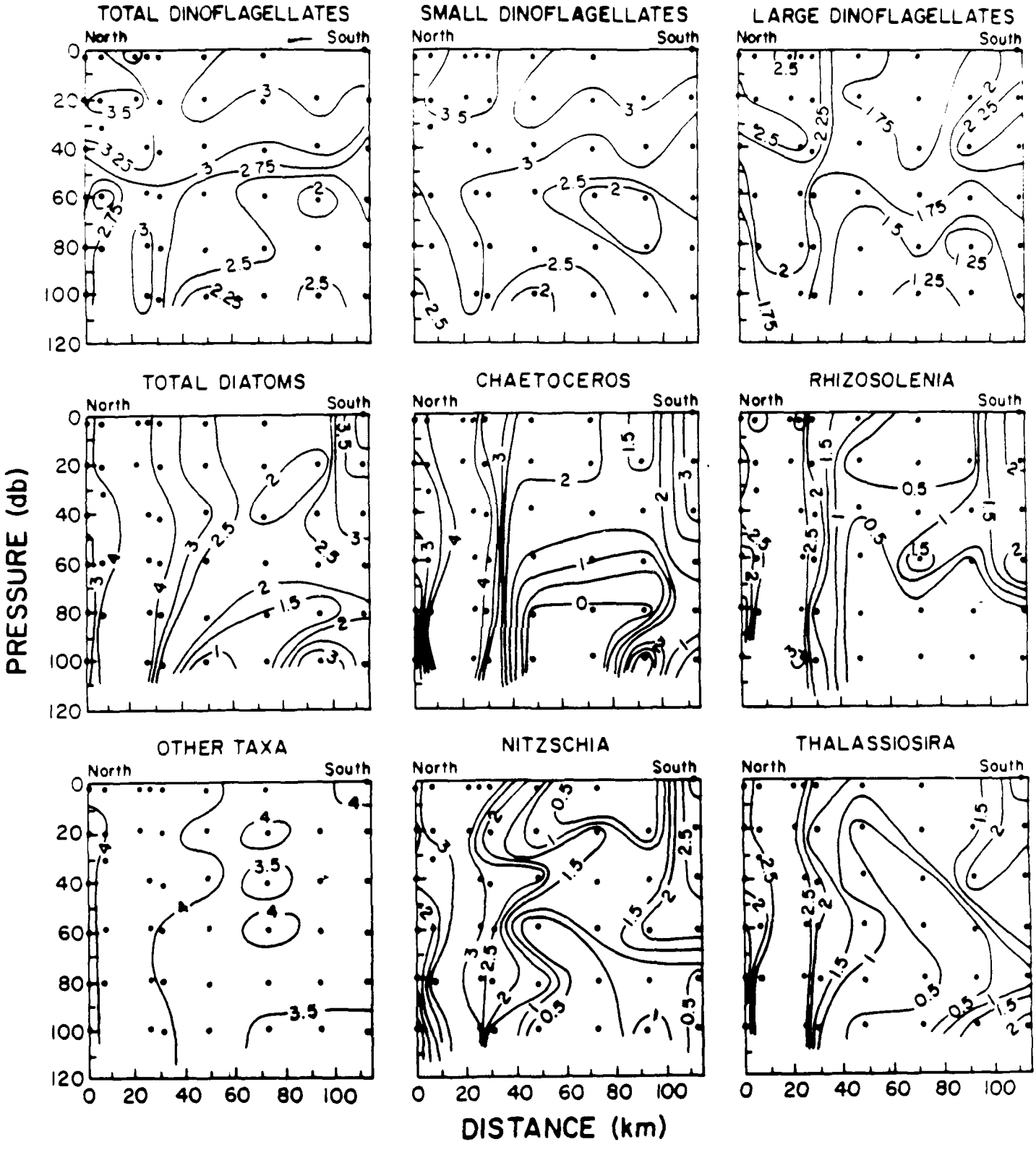
TOTAL DINOFLAGELLATES
SMALL DINOFLAGELLATES
LARGE DINOFLAGELLATES
TOTAL DIATOMS
CHAETOCEROS
RHIZOSOLENIA
OTHER TAXA
NITZSCHIA
THALASSIOSIRA
North
South
PRESSURE (db)
DISTANCE (km)
0
20
40
60
80
100
120

Figure 14

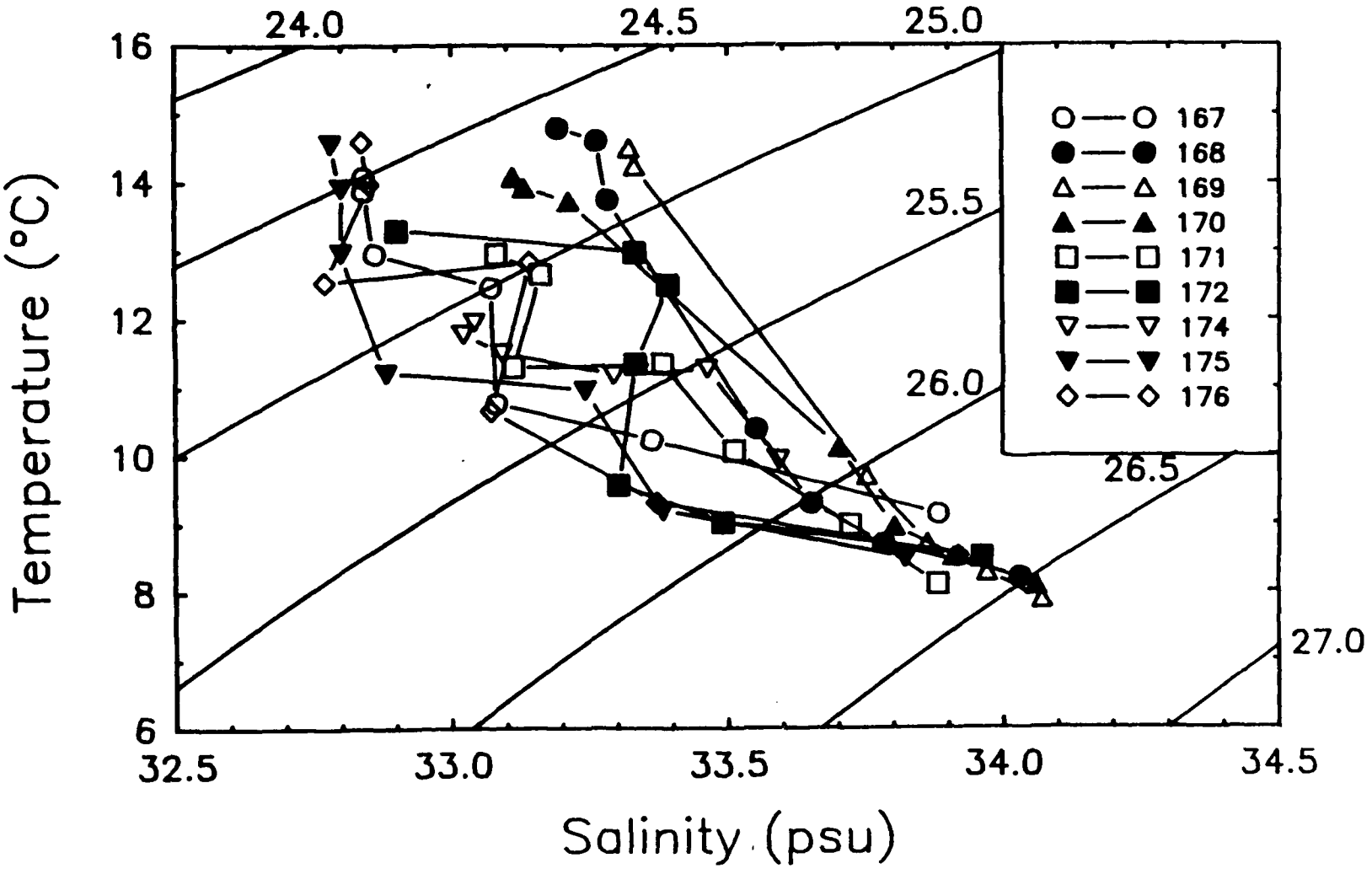
24.0
24.5
25.0
25.5
26.0
26.5
27.0
16
14
12
10
8
6
Temperature (°C)
32.5
33.0
33.5
34.0
34.5
Salinity (psu)
167
168
169
170
171
172
174
175
176

Figure 15

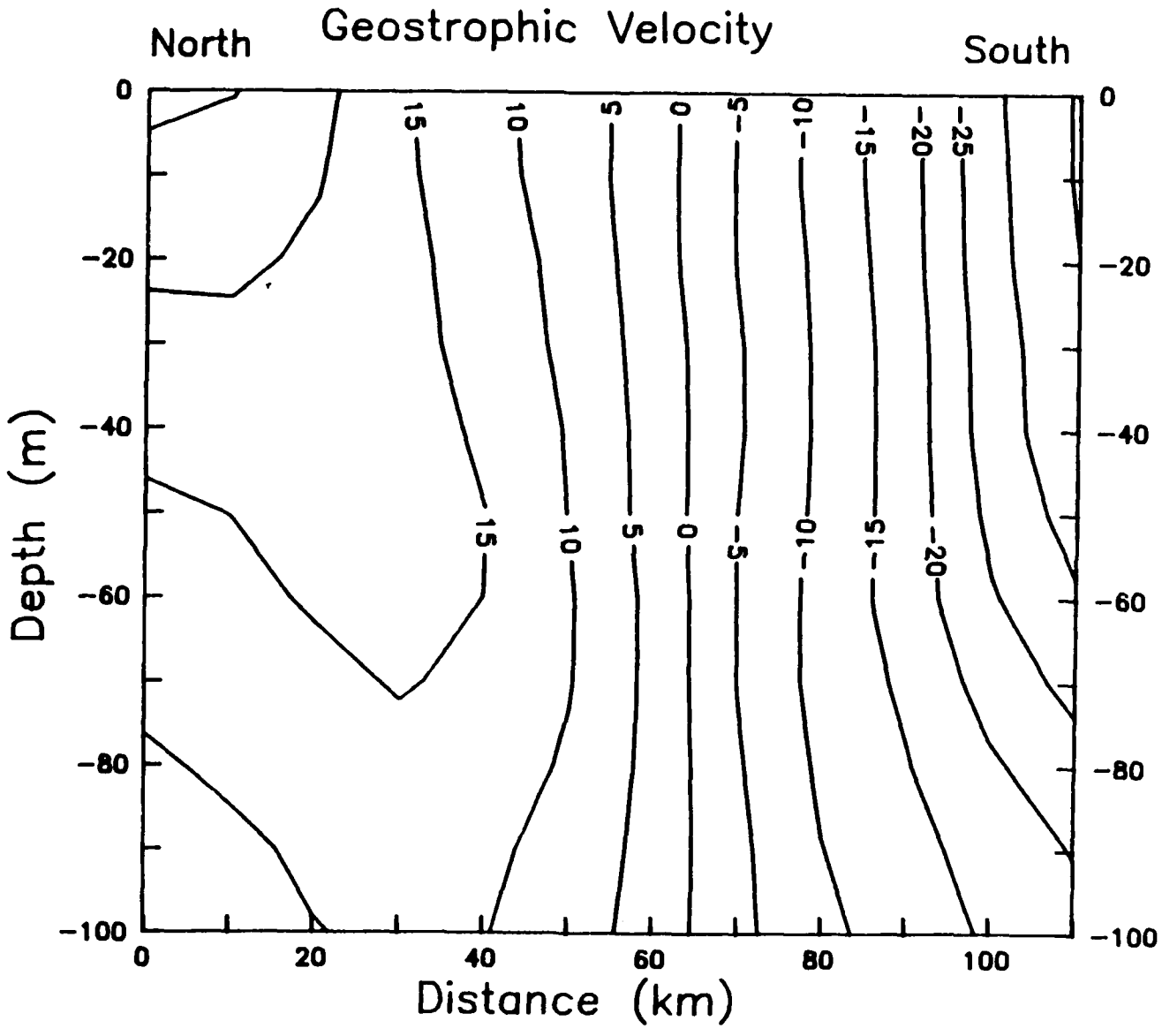
Geostrophic Velocity
North
South
Depth (m)
Distance (km)
0
-20
-40
-60
-80
-100
0
20
40
60
80
100
15
10
5
0
-5
-10
-15
-20
-25

Figure 16

"Water mass subduction and the transport of phytoplankton in a coastal upwelling system"

Libe Washburn[1,5], David C. Kadko[2,6], Burton H. Jones[1], Thomas Hayward[3], P. Michael Kosro[2], Timothy P. Stanton[4], Steve Ramp[4], and Timothy Cowles[2]

[1]University of Southern California, Los Angeles, CA
[2]College of Oceanography, Oregon State University, Corvallis, OR
[3]Scripps Institution of Oceanography, La Jolla, CA
[4]Naval Postgraduate School, Monterey, CA
[5]now at: Dept. of Geography, University of California, Santa Barbara, CA
[6]now at: Rosentiel School for Marine and Atmospheric Science University of Miami, Miami, FL

Submitted to Journal of Geophysical Research

ABSTRACT

Observations during the Coastal Transition Zone (CTZ) experiment in summer, 1988 reveal the presence of deep phytoplankton layers in a coastal upwelling system. The layers occur throughout the CTZ study area, including a strong baroclinic jet which was present over the period of the experiment. Based on a variety of bio-optical, hydrographic, and geochemical indicators, it is concluded that the water masses associated with the layers result from subduction processes. Criteria are developed to identify subducted water masses based on the beam attenuation coefficient, chlorophyll fluorescence, and distribution of light in the water column. Temperature-salinity characteristics are consistent with two source regions for the subducted layers, one near shore and a second farther offshore. Most of the layers correspond to the inshore source which is apparently distributed alongshore. Subducted water masses are found in all 6 grid surveys of the CTZ experiment and probably result from a variety of physical processes. One of these is flow along sloping isopycnal surfaces due to advection and mixing processes. Advection timescales for flow out the axis of the jet range from a few days to a few weeks, depending on the depth of a particular surface, and the bio-optical indicators for subduction processes persist over these time scales.

1. INTRODUCTION

An unanticipated observation during the Coastal Transition Zone (CTZ) experiment is the occurrence of layers of high concentrations of phytoplankton at depths often greatly exceeding the euphotic zone. These layers are found both near shore and offshore within a productive coastal upwelling system off northern California and are often observed in a strong offshore jet that was present in the CTZ study area in 1988. We explore the hypothesis that the water masses associated with these layers originate near the surface in the euphotic zone and are subsequently transported downward by vertical circulation processes or subduction (other terms such as subsidence or downwelling are equally descriptive). The subduction hypothesis is supported by a variety of physical, biological, and geochemical indicators including ^{222}Rn, dissolved O_2, and chlorophyll (Kadko et al. 1990).

This movement of large volumes of water out of the surface layer (euphotic zone) is potentially important to the vertical transport of heat, mass, salt, and other scalars. Furthermore, geochemical data indicate that this transport can be rapid with vertical velocities of order 20 - 30 m/day (Kadko et al. 1990). It also may result in a high vertical flux of organic carbon and represents a mechanism which could quickly remove large concentrations of phytoplankton from the euphotic zone in a productive coastal environment.

At this point, the characteristics of subducted water masses and the mechanisms leading to their subduction in a coastal region are not well understood. Some basic questions include. What are the thicknesses, horizontal extents, and volumes of subducted water masses? Are subducted water masses only associated with offshore jets or are they more widely distributed in the CTZ? Where are the source regions for the subducted water masses? Are the source regions local in the sense that subduction results from vertical sinking with little horizontal advection? Or, is horizontal advection strong enough to move subducted water masses away from the region where sinking occurs? Are subducted waters transported offshore and, if so, at what rates? What physical processes lead to subduction?

Experimentally, it is necessary to determine quantities and criteria that can be used to establish that an observed water mass has been subducted. It is also important to determine the effective decay times for various subduction indicators.

2. EXPERIMENTAL PROCEDURE

A more complete description of the shipboard observations from the CTZ experiment during the summer, 1988 is presented by

Huyer et al. (1991). Basically, the overall strategy was to sample a region of the CTZ between Pt. Reyes and Pt. Arena, California over a period of several weeks in order to observe the evolution of strong coastal jets which have been observed previously in the area (cf. Flament et al., 1985 and Davis, 1985). To do this, six hydrographic grid surveys of more or less uniform spatial coverage were made sequentially from three ships: R/V's Wecoma, Pt. Sur, and Thomas Washington (leg 1). (The sampling grids for 5 of these surveys are indicated in Fig. 4.) Due to adverse weather conditions, the entire leg 1 grid survey from the Thomas Washington could not be completed (This incomplete grid is shown in Fig 12). However, the inshore part was completed and is used here to examine near shore water properties. In addition, during leg 2 of the Thomas Washington survey, sampling was specifically directed at observing physical, biological and chemical distributions in the offshore jet with some limited sampling outside the jet (station locations are indicated by triangles in Fig. 5). The period of this "process sampling" was 18 days (4 July to 21 July) and coincided with the first two hydrographic grid surveys of the Pt. Sur which were conducted from 6 to 18 July.

Measured variables from all vessels include conductivity, temperature, depth (CTD), chlorophyll fluorescence, beam transmission and meteorological observations. Fluorometers and transmissometers were manufactured by Sea-tech, Inc. of Corvallis, Oregon and each transmissometer has a 0.25 m path length with a 660 nm wavelength light source. Rosettes with Niskin bottles were used in conjunction with the CTD instrumentation to provide bottle sampling for salinity calibration, dissolved O_2, nutrients, chlorophyll, and pigments. Continuous profiles of photosynthetically available radiation (PAR) were made from the Thomas Washington using a sensor manufactured by Bio-spherical Instruments, Inc. of San Diego, California.

3. EVIDENCE FOR SUBDUCTION

The primary evidence for subduction processes discussed here is layers of phytoplankton which are observed at depths below the euphotic zone. Because phytoplankton are green plants, they require light for photosynthesis and grow in the illuminated layers of the upper ocean. The presence of phytoplankton in the water column is detected by a combination of chlorophyll fluorescence and beam attenuation coefficient (beam c) profiles. Beam c is a quantitative measure of water column turbidity which depends upon various aspects of the particle field such as particle concentrations, size distribution, and index of refraction (cf. Jerlov, 1976; Baker and Lavelle, 1984). Vertical profiles of beam c and chlorophyll fluorescence at stations containing phytoplankton layers are highly correlated and the presence of phytoplankton in these layers is verified by bottle

samples. Such a station located 50 km west of Pt. Arena and in a region of strong southward flow is shown in Fig. 1.

Beam c values exceed 0.4 m^{-1} and the chlorophyll fluorescence signal is above the noise level almost everywhere above 190 db (Fig. 1B). The measured 1% light level here is 31 db and three distinct layers are found: 1) a near surface layer above the 1% light level where chlorophyll concentrations are as high as 8.6 μg/l, 2) a deeper layer which extends from the 1% light level to about 110 db, and 3) a very deep layer with low beam c and and fluorescence levels which extends from 125 to 190 db. No surface mixed layer is observed and gradients in all measured quantities extend to the surface. A weak temperature inversion is present on the upper boundary of layer 2 (Fig. 1C) and suggests that this layer is intrusive, a conclusion also supported by the T-S diagram for this station. Examples of several T-S diagrams showing an association between deep fluorescence layers and relatively warm, salty anomalies are given by Kadko et al.(1991).

A very different type of profile is typically found in offshore waters away from the jet, such as at station E-4 (Fig. 1A). A deep fluorescence layer is centered at about 93 db, well below the 60 db deep surface mixed layer, and lies just below the 1% light level at 85 db (Fig. 2A and 2B). Chlorophyll concentrations from bottle samples are about 0.5 μg/l just above and below the fluorescence peak; apparently the peak itself was missed in sampling. However, chlorophyll and fluorescence are highly correlated and nearby stations show peak concentrations of about 1 μg/l. Chlorophyll layers of this type, which occur in association with the base of the euphotic zone, are common features of the California Current system (cf. Anderson, 1969 and Cullen, 1982). They may result from a number of processes such as an increase in phytoplankton biomass due to growth at the intersection of the euphotic zone and nutricline (Herbland and Voituriez, 1979). Two other possibilities are photoadaptation, where the chlorophyll per cell increases in response to low light conditions (Prezelin, 1981 and Beers et al. 1975), or variability in fluorescence yield of the phytoplankton (Kiefer, 1982). At station E-4 and nearby stations the increase in beam c indicates increased biomass while the fluorescence per unit chlorophyll, or fluorescence yield, is relatively constant throughout the water column. However, the chlorophyll per unit beam c increases with depth at E-4 and suggests that the chlorophyll content per cell or per unit biomass also increases with depth.

To objectively examine CTZ data sets for the occurrence of phytoplankton layers which may have been moved out of the euphotic zone by subduction processes, it is necessary to differentiate the deep layers like those of Fig. 1 from those which probably result from in situ photosynthesis as in Fig. 2. Furthermore, it is necessary to rule out other processes which might also result in the presence of layers of fluorescent

particles below the euphotic zone. A step in this process is to establish the relationship between the light field in the water column throughout the region and the vertical positions of layers of phytoplankton.

The penetration of light into the water column is examined by comparing vertical profiles of PAR throughout the CTZ. A total of 17 stations from legs 1 and 2 of the Thomas Washington survey, all recorded within one hour of local noon, is used to examine the variability of the light field (Fig. 3A). Stations close to local noon were chosen in order to observe the maximum penetration of light into the water column. Following Huyer et al. (1991), three regions are identified based on dynamic height (5/500 db): the jet corresponds to the range 0.82 to 0.96 m, inshore and southern waters below 0.82 m, and offshore and northern waters greater than 0.96 m. These ranges are somewhat different from those used by Huyer et al. (1991), but are more appropriate to the Thomas Washington data. Considerable variation in the depth of light penetration is found within the jet waters: typical values of the 1% light level in the most turbid waters are in the range of 20 to 30 db and are almost 80 db in the more clear waters (Fig. 3B). This depth range also spans that observed for the inshore and southern waters. Offshore waters are generally more clear with a typical 1% light level of about 85 db; much of the phytoplankton in the water column lies below this level.

Observations obtained during leg 2 of the Thomas Washington survey show that almost one fourth of the water column with high chlorophyll fluorescence levels (>1.0 volts) is found at depths below the 1% light level of the clearest offshore waters (Fig. 3C). About 6.4% occur below the 0.1% light level which ranges from about 115 to 125 db based on the three offshore profiles of Fig. 3B. The threshold fluorescence value of 1.0 v is chosen because it represents a high signal level; the noise level of the fluorometer and CTD acquisition system used on the Thomas Washington is about a factor of 4 smaller. The tail of the distribution of Fig. 3C extends down to 200 db, although layers exhibiting high fluorescence are found at depths exceeding 200 db in some of the other surveys. For stations within the jet, the fluorescence threshold used in producing the histogram of Fig. 3C corresponds to a chlorophyll concentration of about 1 μg/l and in the offshore waters to a level of about 0.3 μg/l. The points sorted into the histogram also have beam c values exceeding 0.4 m^{-1}. Thus much of the phytoplankton lies below the euphotic zone.

4. SUBDUCTION CRITERIA

Because phytoplankton require light for growth and reproduction, it is unlikely that local production of particles by photosynthesis can account for particle layers below the euphotic zone. These correspond to the hatched regions of Fig.

3B, particularly those below the 0.1% light level. This suggests that other processes are responsible for these deep layers such as vertical circulation out of the euphotic zone, particle sinking, resuspension of bottom sediments containing chlorophyll, or diapycnal mixing. We have no microstructure measurements to assess diapycnal mixing rates and assume that this is not an important mechanism for vertical particle transport here.

The hypothesis that vertical circulation, or subduction, accounts for these layers has been investigated by Kadko et al. (1991) and is supported by a variety of indicators. In addition to high levels of chlorophyll, these layers often contain deficiencies of ^{222}Rn ($\lambda_{1/2}$ = 3.85 days) with respect to ^{226}Ra activity, which indicates recent gas exchange with the atmosphere. The radon observations are perhaps the most unambiguous of all subduction indicators, since no other process can produce the deficiencies. The layers are often associated with local maxima in dissolved oxygen and often appear in water masses which are warmer and saltier than waters above and below in θ-S diagrams. All of these observations are consistent with vertical movement of water masses away from the surface. However, a limitation of these indicators is that they are based on bottle sampling and therefore have very limited vertical resolution. Furthermore, the indicator ^{222}Rn is available for a relatively small number of stations and only as part of the Thomas Washington survey. In this analysis, we focus on the distributions of chlorophyll fluorescence and beam c as subduction indicators because they can be measured to about the same vertical resolution as CTD variables and because they are available from all surveys.

The possible role of particle sinking in forming the deep fluorescent layers is difficult to assess, although a number of factors suggest that it is not the dominant process. First, oceanic phytoplankton generally tend to sink slowly at vertical velocities of less than 1 m/day (Bienfang, 1981; Bienfang and Szyper, 1982; Bienfang et al. 1982; Smayda, 1970). Observations from the Pt. Conception area of California indicate that phytoplankton sinking rates within 50 km of the upwelling center are less than 2 m/day (Bienfang, 1984). These estimates are much smaller than a vertical subduction velocity of 27 m/day obtained by Kadko et al. (1991) based on Rn^{222} samples.

Second, θ-S relationships observed in these deep layers found in offshore regions of the jet appear related to those found near shore in the euphotic zone, as is shown later. If particle sinking were dominant, then the θ-S relationship of a layer would have no correspondence to properties in the euphotic zone from which the particles were derived. The θ-S of the layer would simply be the local relationship at the time and depth at which the particle layer is observed as it sinks downward. As an additional check on the possible role of particle sinking in

forming the deep layers, the densities corresponding to layers near shore in the jet were compared with those found offshore. No consistent increase in density is observed offshore as might be expected as a result of particle sinking over the time required to advect out the jet (a few days to a few weeks, depending on the position of a layer in the water column).

Third, many of the deep regions of phytoplankton are in thin, well defined layers which are more or less Gaussian in shape (eg. Fig. 6F). A distribution of descending particles all falling at different rates (but strongly weighted toward large numbers of small particles; cf. Spinrad, 1986), for many days would tend to be spread vertically throughout the water column and would not concentrate in layers. Finally, in cross axis sections of the jet, where the station spacing is about 10 km, distributions of fluorescence and beam c approximately parallel σ_θ surfaces. This would not be expected if particle sinking across density surfaces were dominant.

It is possible that particle sinking may work in combination with subduction processes in layer formation. In near shore areas where chlorophyll concentrations are large, particle coagulation effects may be important (Jackson, 1991) and could result in much higher sinking rates, greater than 100 m/day (Smetacek, 1985). However, the coagulated particles would have to have combined effective densities equal to the seawater density at some point in the water column to remain suspended. Otherwise they would sink to the bottom.

Another possible mechanism which might result in fluorescent particles appearing below the euphotic zone is resuspension of bottom sediments containing phytoplankton. Deep nepheloid layers due to resuspension processes have been observed over the continental shelf off Oregon by Pak and Zaneveld (1977). Turbidity layers with high values of beam c are commonly observed below 100 m in all of the CTZ hydrographic data sets, particularly near shore. Typically these layers occur near the sea floor and exhibit no measurable fluorescence. However, deep turbidity layers from a few profiles exhibit very low, but measurable fluorescence signals. Comparison of signal levels indicates that the ratio of fluorescence to beam c is much lower in these bottom resuspended layers than in the phytoplankton layers higher in the water column. These layers are easily differentiated because their θ-S relationships are very different from those found anywhere in the euphotic zone and the corresponding seawater densities are much greater. Another difference between the subducted layers and these deep turbidity layers is the ratio of phaeopigment to total pigment present. In the deep turbidity layers the ratio is often larger than 0.8 while in the subducted layers it is typically less than 0.4 (separate analysis by one of the authors, BHJ)

Based on the preceding analysis, we conclude that the

phytoplankton layers observed well below the euphotic zone, which exhibit high values and correlated distributions of fluorescence and beam c, result primarily from subduction processes. However, some clarification about "well below the euphotic zone" is required. The presence of phytoplankton below the 1% light level at a specific station does not necessarily mean that the phytoplankton were not produced in situ, because the depth of light penetration can change. For example, a layer of phytoplankton might initially grow near the deepest observed 1% light level of 80 to 90 db in clear water. After this growth, energetic near-surface advection could transport a second, more shallow layer of particles, over the deeper layer and produce a much shallower 1% light level. The result would be a deep layer of phytoplankton produced in situ which is observed below the euphotic zone. Other scenarios might also produce a similar situation. For this reason we generally limit our analysis to those layers found below the deepest 0.1% light levels which are found in clear, offshore waters. We have used a pressure of 120 db, about the midpoint of the range in 0.1% light levels in offshore waters (Fig. 3C), to represent this point in the water column. While this is a very restrictive criteria it does reduce the possibility that the observed particles result from in situ photosynthesis.

To objectively search each of the CTZ data sets for subducted water masses we applied three criteria based on the preceding analysis. If all three of the following criteria are satisfied, we consider the water mass to have been subducted. The criteria are: 1) pressure > 120 db, 2) beam c > 0.4 m^{-1}, and 3) fluorescence signal exceeds the instrumental noise level. For these data, a beam c threshold of 0.4 m^{-1} or larger is found to differentiate turbid layers from more clear ambient waters. Minimum observed levels of beam c in individual profiles from all of the data sets fall in the range 0.35 - 0.40 m^{-1} and are taken to be representative of the effective clear water values of beam c (c_w). This range of c_w falls within that given by Lavelle and Baker (1987) of 0.31 - 0.42 m^{-1}. The range is also comparable to two experimental results for c_w presented by Jerlov (1976, Table XIII): 0.319 m^{-1} and 0.385 m^{-1} (interpolated to 660nm).

The threshold fluorescence signal level had to be determined individually for each of the surveys because the effective noise level for each fluorometer and CTD data acquisition system was different. The procedure for determining this threshold is basically subjective and is based on comparing signal levels in fluorescent layers with minimum observed levels which are taken to be the instrumental noise level. Minimum signal thresholds are derived from all of the survey data and are used in identifying subducted water masses. It proved impractical to use a uniform chlorophyll or total pigment concentration as a criteria for these data because of high scatter in the observed relationship between fluorescence voltage and pigment

concentrations derived from bottle samples. Much of this scatter is apparently due to regional differences in the regression coefficients and may result from differences in phytoplankton species composition (Hood, 1990).

To search for subducted water masses, all of the CTZ data sets were sorted based on the criteria developed above. Profiles from all surveys identified as containing subducted layers were individually examined to verify that noise spikes or other data problems were not present. This sorting procedure also identified a few layers near the sea floor with relatively high beam c, but very weak fluorescence levels that barely exceeded the threshold. Water properties of these points are typical of the ambient deep water and they are usually found at depths exceeding 300 m. These points were excluded from the analysis.

5. DISTRIBUTION OF SUBDUCTED WATER MASSES

Subducted water masses occur frequently in the CTZ based on the numbers of profiles from each grid survey which contain them (Fig. 4). They are found both in the seaward flowing jet and near shore, and a few are found in offshore waters south of the jet. Beam c and fluorescence anomalies in the layers from these latter profiles were very weak as were all of the layers in the first survey. In the first three surveys from 20 June - 18 July, no layers are found in offshore waters to the north and east of the jet and those farthest offshore during this time are in the jet itself. A different situation is observed during the fourth survey from 21-27 July when subducted layers are found near the offshore boundary of the grid. They are also seaward of the strongest flow in the jet. Over the time period from the third to fourth grid surveys, the orientation of the jet rotated abruptly from offshore flow to along shore flow where it remained constant at least through the end of the fifth survey. The change in orientation coincided with a general relaxation in the wind field at this time (Stanton et al., 1991), a pattern which has been observed previously in the same area (Strub et al., 1991).

Leg 2 of the Thomas Washington survey was designed to sample selectively the seaward flowing jet and is therefore useful for examining the distribution of subducted water masses here. In addition, this survey included some stations outside of the jet for comparison. Application of the criteria developed in Section 4 shows that subducted water masses are found frequently out along the jet axis with the most seaward of these stations lying almost 300 km from Pt. Arena (Fig. 5). A few stations south of Pt. Arena and inshore of the jet are located in an anti-cyclonic eddy (Swenson and Niller, 1991) and also contain subducted water masses.

Profiles from a group of five stations from those identified in Fig. 5 suggest a gradual sinking of phytoplankton layers along

isopycnal surfaces out the jet axis (Fig. 6A). These stations were not occupied sequentially and do not follow any particular water parcel in a Lagrangian sense. Rather, they illustrate where particle layers can be found in different regions of the jet. At the near shore station 46, high levels of fluorescence and beam c are observed above 80 db. Radon deficiencies at this station indicate recent gas exchange throughout this depth range (Kadko et al., 1991) even though no surface mixed layer is present. Surface mixed layers in density are apparent only at offshore stations 67 and 33 in the upper 20 db. Out the axis of the jet, beam c, fluorescence, and chlorophyll levels are frequently high on and above the 25.8 isopycnal, which deepens from about 23 db at station 46 to 150 db at station 33. Discrete layers around this level are evident (Figures 6C, 6E, and 6F), but are not continuous in profiles from nearby stations. Measurable beam c and fluorescence levels are not limited to the depth of the 25.8 isopycnal and above, but exceed 200 dbar in some stations such as 17A (Fig. 6D) and in stations from the five grid surveys of Fig. 4 as well.

Figure 6 suggests that the vertical distribution of phytoplankton layers may be related to the position of isopycnal surfaces. Because of this we use an isopycnal coordinate system in much of the following analysis. In particular, the distributions of properties on two isopycnal surfaces are examined in some detail: (1) the 25.8, which frequently lies within the euphotic zone; and (2) the 26.2, which is generally below the euphotic zone.

Comparison of the distributions of beam c and pressure on isopycnal surfaces indicates that the lateral extent of subducted layers may be large. Offshore, where the 25.8 surface is below 120 db, beam c > 0.4 m^{-1} at stations 33, 34, 72, and 75 (Figures 7A and 7B); the along axis separation of the 33-34 pair and the 72-75 pair is about 50 km while the cross axis dimension of this layer of particles is at least 28 km. The pattern of isopycnal contours of fluorescence (not shown) is very similar to that for beam c in Fig. 7A. The highest levels of beam c (c > 0.7 m^{-1}) on the 25.8 isopycnal occur inshore where this surface lies within the euphotic zone (above 50 db based on Fig. 3B) and is consistent with in situ production of phytoplankton. One of these areas where the 25.8 isopycnal is warped upwards is centered on 124.25 W, 38.75 N and results from the combination of the southward jet flow and the strong northward flow due to an anticyclonic eddy (Fig. 11).

On the deeper 26.2 isopycnal the highest levels of beam c (c > 0.5 m^{-1}) are found near shore at depths below 120 db (Figures 8A and 8B), except for the area immediately south of Pt. Arena which is very shallow and reaches above 50 db. Farther offshore and west of 125.5 W, all points having c > 0.4 m^{-1} lie below 120 db. Again the pattern of fluorescence on this surface (not

shown) is very similar. We conclude from this that most of the phytoplankton found on the 26.2 isopycnal in the area covered by the survey were not produced in situ where observed, but instead, have been moved vertically and horizontally by subduction and advection processes out of the euphotic zone in their source regions. This suggests that subduction processes play an important role in governing water mass properties on this isopycnal surface. In contrast, in situ production within the survey area may account for much of the phytoplankton on the 25.8 surface near shore with subduction processes being more important offshore.

6. SOURCES OF SUBDUCTED WATER MASSES

The distribution of beam c and fluorescence on isopycnals like the 26.2 indicate that many of the deep phytoplankton layers probably originate in the euphotic zone away from where they are observed. Because isopycnals slope steeply upward toward the coast in the CTZ area, some lie within the euphotic zone near shore, but at much greater depths farther offshore (Figures 7B and 8B). We hypothesize that these inshore areas where the isopycnals rise into the euphotic zone are the major source regions for the phytoplankton and subducted water masses, although some sources probably lie to the north of the area covered by the surveys. Use of the term "source region" for subducted water masses simply means that they were near the surface there.

If the deep phytoplankton layers originate near shore, then the θ-S relationships in the layers found offshore should be similar to those near shore in the euphotic zone if isopycnal and diapycnal mixing rates are not too large and if particle sinking is not important. For purposes of tracing vertical water mass movement, the phytoplankton act as a dye which identifies water masses which have previously been in the euphotic zone. The θ-S characteristics are potentially useful for tracing horizontal movement of these water masses if remote source regions can be unambiguously identified in θ and S. In contrast to θ and S which are conservative away from the mixed layer, beam c and fluorescence levels are likely to change substantially since phytoplankton concentrations are non-conservative over time scales of a few days and levels change due to a variety of processes such as photosynthesis and grazing by zooplankton. Therefore, the usefulness of fluorescence and beam c as vertical water mass tracers will be limited by their effective loss rates.

In the remainder of this section, the θ-S characteristics of subducted water masses are compared with those of potential source regions for two (overlapping) time periods: first, over the entire experimental period including the time when the jet orientation changed rapidly (late July to early August); and second, during the time when the jet orientation was fairly

stable (late June to mid-July). Higher resolution sampling from the Thomas Washington during this latter period allows more detailed inferences to be drawn regarding near shore source regions.

The locus of all θ-S points from the five grid surveys of Fig. 4 which satisfy the subduction criteria of Section 4 cluster into two areas of distinct characteristics (Fig. 9A). Most of the points fall within a σ_θ range 25.9 - 26.6 (Group A) while a second group is clustered between 25.1 - 25.5 (Group B). Most of the points in the second group are found at the offshore stations in Fig. 4D when the jet orientation changed abruptly. The one exception is offshore station 163 (Fig. 4B) from the first Pt. Sur survey which also falls in Group B. The differences in θ-S characteristics of Group B suggest that the subducted layers found offshore, particularly after the jet reorientation, are not derived from the same sources as those found elsewhere.

Subducted water masses corresponding to the main group of points (Group A) in Fig. 9A are probably derived from near shore sources based on comparisons with upper ocean θ-S characteristics in the CTZ area. All θ-S points in the upper 50 db of the water column from each inshore line of the grid surveys are plotted in Fig. 9B along with the envelope of points from the subducted layers shown in Fig. 9A (Group A). The extensive overlap of the Group A θ-S points with points from the inshore lines is consistent with near shore source regions for the subducted water masses. In contrast, very little overlap is found between the Group A subducted layer θ-S points and those from all of the other (offshore) lines from the grid surveys (Fig. 9C). The upper 50 db of the water column is chosen because this range falls within the euphotic zone throughout most of the survey area (Fig. 3). However, this may underestimate the depth range of the euphotic zone in near shore areas since some of the θ-S points in the subducted layers correspond to higher densities than found near shore above 50 db.

It is also likely the majority of the subducted water masses observed within the jet during the process sampling from the Thomas Washington (Fig. 5) result from near shore sources. During this sampling, the position and water mass composition of the jet were fairly constant for about a month covering the period 20 June to 18 July (Huyer et al., 1991). The consistent orientation of the jet may be seen in the first three geopotential anomaly fields of Fig. 4. Most of the θ-S points within the subducted layers of the jet, identified in Fig. 5, fall within the Group A envelope of θ-S points in Fig. 9A. However, a few such as those from Station 35 which is located far offshore, fall within the Group B envelope and may indicate another source farther offshore (Figures 10A and 10B).

The θ-S points for the subducted water masses within the jet are consistent with formation by isopycnal mixing of waters from different near shore source regions. Based on θ-S distributions in the upper 50 db of the water column, two potential source regions are identified: (1) the waters offshore and north of Pt. Arena (and possibly north of the study area), represented by station A3, and (2) waters immediately north of Pt. Reyes, represented by station A13 (Fig. 10B). Points lying between the A3 and A13 curves could be formed by advection and isopycnal mixing of waters from these two source regions. However, source water contributions from the area around Pt. Reyes require a northward coastal flow inshore of the jet. The θ-S curves of Fig. 10B (solid lines) are obtained from leg 1 data of the Thomas Washington survey (25 June - 2 July) and show that waters on the southern end of the inshore line are generally saltier on a given isopycnal than those to the north. This situation persisted during all of the grid surveys based on isopycnal plots of "spiciness" presented by Huyer et al. (1991).

On some isopycnals near shore, a correspondence is observed between flow direction and θ-S properties which is consistent with the hypothesis that the subducted layers originate from at least two inshore source regions. A detailed θ-S diagram containing only points in subducted water masses below 120 db which lie on σ_θ = 26.2 (Fig. 10C) shows that θ-S points at stations 9A and 47, in the southward flow of the jet (Fig. 10A), are very similar to those at Station A3 located north of Pt. Arena. The southward flow of the jet at station 47 penetrates to about 300 db and the maximum near surface geostrophic velocity is 0.7 m/s (Fig. 11). Contours of geostrophic velocity (reference level of 500 db) of Fig. 11 are based on a line of stations extending offshore from just south of Pt. Arena (stations 47 - 53 in Fig. 14A). In contrast, at stations 51 and 52, which are in northward flow (Fig. 11), θ-S points are nearly identical to those at Station A13 located just off Pt. Reyes. The remaining points lie between these end members. The combination of northward flow in the center of the line of stations 47 - 53 with southward flow on the east end of the line (Fig. 11) is due the presence of the anticyclonic eddy just inshore of the jet mentioned previously. This eddy is evident in drifter tracks reported by Swenson et al. (1991). A similar pattern of geostrophic velocity is also observed 20 km to the south on the line of stations 57 - 65 (station locations shown in Fig. 14A.

Further evidence that Pt. Reyes may be a source region for some of the subducted layers is the distribution of S on σ_θ = 26.2 from legs 1 and 2 of the Thomas Washington survey. Salinities exceeding 33.82 are found on the two lines of stations from leg 2 that extend offshore from just south of Pt. Arena (Fig. 12); these points generally are found below 90 db (Fig. 8B) and have high levels of beam c (Fig. 8A) and fluorescence. Two

of these stations, 51 and 52, satisfy the subduction criteria of Section 4. The high salinity of these waters (S > 33.82) is consistent with northward (and downward) advection from the Pt. Reyes area along the 26.2 isopycnal. The more comprehensive inshore survey (leg 1) obtained about 18 days earlier shows that S > 33.82 on σ_θ = 26.2 at three stations (A11, A12, and A13) near Pt. Reyes, but nowhere to the north (Fig. 13A). Clearly, considerable evolution of the near shore salinity field occurred over this time period. Northwestward advection of high salinity water along σ_θ = 26.2 from the vicinity of Pt. Reyes would require an average speed of about 0.07 m/s to account for the changes in S near Pt. Arena. This estimate falls well within the range of northward geostrophic velocities on the 26.2 isopycnal along the line of stations 47 - 53 (Fig. 11).

Not only is the salinity distribution consistent with the idea that Pt Reyes is a subduction source region, but so are the distributions of beam c, fluorescence, and pressure on σ_θ = 26.2. In the waters off Pt. Reyes, the 26.2 isopycnal reaches vertically to within about 40 db of the surface (ie. within the euphotic zone) at station A13 (Fig. 13B) and has c > 0.8 m^{-1} (Fig. 13C). High levels of beam c at pressures of about 90 db and less are evident at stations A11, A12, and 13. The fluorescence contours (not shown) are very similar to the beam c contours here. Thus, waters found near Pt. Arena below 120 db, such as stations 51 and 52, may originate in the near the surface waters off Pt. Reyes where similar S, beam c, and fluorescence characteristics are found.

7. VERTICAL TRANSPORT BY ISOPYCNAL SINKING

One mechanism that could result in vertical movement of water masses out of the euphotic zone and subsequent transport offshore to depths exceeding 120 db is simply flow along sloping isopycnal surfaces out the axis of the jet. Evidence for water mass sinking in the jet comes from a sequence of CTD stations made daily alongside a surface drifter (path shown with solid line in Fig. 14A). Averages of densities in the upper 10 m of the water column progressively decrease and the total change from the beginning to the end of the track is about 0.7 kg/m^3. Fluid particles traveling on the 25.8 or 26.2 isopycnal surfaces could experience depth changes of well over 100 m based on the distributions of pressure of these surfaces (Figures 7B and 8B). A particle moving on a density surface would probably not change depth monotonically because local depth variations result from processes like mesoscale eddy activity.

The time required for a water particle to move out the jet axis on a particular isopycnal varies greatly because of strong vertical shear in the jet. Depending upon the mean advective speed and the depth of a particular isopycnal, the time scale for this process to occur ranges from a few days to a few weeks.

This advective time scale is of interest because it puts a lower bound on the persistence time for the subduction indicators used in this analysis (beam c and fluorescence) and it gives an estimate of the order of magnitude of typical vertical velocities. To illustrate how this isopycnal sinking out of the euphotic zone might proceed, the advection times and vertical and horizontal velocities are computed along hypothetical drifter tracks located on the 25.8 and 26.2 isopycnal surfaces.

Advective time scales for flow along these isopycnals are estimated from 8 sections of geostrophic velocity which cross the jet at approximately right angles to the flow (Fig. 14A). The sections were obtained over a two week period (7 - 21 July) during the time when the position of the jet was relatively constant (Huyer et al. 1991). Geostrophic velocity profiles are computed from adjacent pairs of stations on these transects and use a reference level of 500 db. Some sections show sloping density surfaces down to 500 db so actual velocities may be larger. Geostrophic velocities are then interpolated onto the isopycnals based on the average pressure of the given isopycnal for each pair of stations; examples of isopycnal velocity profiles on σ_θ = 26.2 are shown in Figures 14B to 14E. Negative velocities indicate generally southward or offshore flow and the shapes of the profiles are approximated by polynomial fits to data points from station pairs.

On the two inshore lines 47 - 53 and 65 - 57, a region of strong cyclonic vorticity separates the southward flowing jet from the northward flow of the anti-cyclonic eddy (Fig. 14B and 14C). The region of southward flow in the eddy is barely resolved on the east end of each line. Farther out the jet along the line of stations 17A - 21, the flow field exhibits lower vorticity and is offshore everywhere in the profile (Fig. 14D). The mean velocity from this profile is -0.14 m/s. The offshore flow of the jet is still detectable at the most offshore line 73 - 76, 360 km from shore, and shows lower vorticity with a mean velocity of -0.11 m/s.

Advective time and velocity scales along the hypothetical drifter tracks at three levels in the jet are summarized in Table 1. Mean velocity and time scales are based on averages of only the portions of each profile which are in the jet (southward or offshore flow); eddy or recirculating portions of isopycnal velocity profiles are not included in the means. The minimum time scales and maximum velocity scales are based on the maximum jet velocity in each section. We take minimum transit times and maximum velocities to be more representative of the jet axis while the maximum times and minimum velocities are representative of off axis conditions. The end points for the hypothetical drifter tracks are stations 48 and 75 and the track length is 321 km (dotted line, Fig. 14A). The hypothetical drifter on the 25.8 isopycnal begins at about 20 db at station 48, well within the euphotic zone, and requires from 12 to 21 days to reach station

75 where it would be at about 140 db. The corresponding times on the 26.2 surface are about double these times while those at 5 db are about half. For comparison, the track of an actual surface drifter is also shown in Figure 14A (solid line). This drifter took 5.1 days to travel from station 6 to station 32 which compares favorably with minimum and mean times (between stations 48 and 32A) of 4.5 - 9.8 days using the geostrophic velocities at 5 db/500 db in the cross-jet sections of Fig. 14A.

8. DISCUSSION AND CONCLUSIONS

Shipboard CTD and bio-optical observations made during the summer upwelling season in 1988 reveal the presence of deep phytoplankton layers below the euphotic zone in many areas of the coastal transition zone (CTZ), including a strong baroclinic jet which was present throughout the observational period. A principal conclusion of this study is that the water masses associated with the phytoplankton have been moved downward by subduction processes. This finding is supported by the distributions of several hydrographic and geochemical tracers, including ^{222}Rn, chlorophyll, and dissolved oxygen (Kadko, et al. 1991). Criteria to objectively identify subducted water masses have been developed and are based on the light field in the water column and levels of chlorophyll fluorescence and the beam attenuation coefficient (beam c). Subducted water masses are observed in all six hydrographic grid surveys of the CTZ experiment which covered the period 20 June - 4 August, 1988.

The θ-S relationships corresponding to the subducted water masses fall into two distinct groups and are consistent with two near surface subduction regions, one near shore and a second much farther offshore. The scatter in θ-S points suggests that the near shore source is distributed along shore and has contributions from the area in the vicinity of Pt. Reyes and from an area north of Pt. Arena, or possibly north of the study area. Subducted water masses from the near shore source region were present throughout the experimental period, while those from the offshore source were most frequently observed just after the strong baroclinic jet changed orientation from offshore to alongshore flow.

The positions of layers of phytoplankton in the water column indicate that some water masses sink over 100 m as they are advected out along the jet axis. Similar, but much larger, vertical displacements resulting from isopycnal advection in a strong, meandering baroclinic jet (the Gulf Stream) have been observed in RAFOS float trajectories by Bower and Rossby (1989). Vertical displacements could also result from mixing processes acting along sloping isopycnals, both along and across the jet xis. Vertical advection rates based on geostrophic flow on sloping density surfaces are 6-10 m/day for the 25.8 surface and

2-4 m/day for the deeper 26.2 surface. These estimates are averages based on advection over 320 km of the jet axis and probably underestimate maximum vertical velocities. This is because isopycnals rise up into higher velocity flow near shore where isopycnal slopes are generally the largest. Kadko et al. (1991) estimate vertical velocities as high as 27 m/day based on ^{222}R deficiencies. Advective time timescales out the jet are about 2 - 3 weeks along the 25.8 isopycnal and about double this along the 26.2 isopycnal. This indicates that detectable levels of beam c and fluorescence from subducted phytoplankton can persist for several weeks.

A variety of other physical processes may lead to water mass subduction and not all of them are associated with the jet since subducted layers are found at several stations outside of the jet (Figures 5 and 6). Drifter observations of Brink et al. (1991) show that convergence zones exist offshore in the jet with associated downwelling velocities of order 10 m/day. Vertical velocities of order 20 m/day and larger which result from changes in relative vorticity are reported by Swenson et al. (1991) from clusters of drifters deployed in the jet. Persistent vertical velocities of this same magnitude are found in the vorticity and vertical velocity analysis of Dewey et al (1991). Another mechanism that could lead to water mass subduction is the interaction of the jet with a large scale deformation field. The resulting ageostrophic, cross jet transport leads to downwelling on the cyclonic side of flank of the jet (Onken et al, 1990). Numerical modeling experiments for the CTZ area also result in downward vertical velocities consistent with our observations (Hoffman, et al., 1991)

Two important issues concerning the impact of subduction processes on the circulation in this coastal transition zone are the total volume of subducted water and the vertical volume flux. A lower bound on the subducted volume in the jet may be estimated by assuming that the fraction of all profiles in the jet satisfying the subduction criteria developed in Section 4 is representative of the jet volume as a whole. During Leg 2 of the Washington cruise, a total of 50 profiles were obtained in the jet (ie. 5/500 db dynamic height in the range 0.82 to 0.96 m) and just over 1% of all the water column from these profiles satisfy the criteria. The total volume of the jet above 500 m in the survey area is about 9000 km^3 so the subducted volume is of order 100 km^3. Assuming that the total subducted volume is transported out the jet axis in 12 to 21 days (the transit times on the 25.8 isopycnal from Table 1) and that a steady state volume of subducted water is maintained in the jet, the required vertical volume flux is of order 5 to 8 km^3/day. An estimate of the vertical mass flux of chlorophyll may be made using the average fluorescence level in the subducted layers and a chlorophyll calibration derived for the depth range from the 1% light level to 150 m (separate analysis by one of the authors, CHJ). The

mean chlorophyll concentration is about 1 μg/l and the resulting vertical mass flux of chlorophyll is of order of $(5 - 9)x10^3$ kg/day.

The subducted volume estimate of 100 km^3 is likely an underestimate for the study area as a whole, possibly by as much as an order of magnitude, for two reasons. First, the depth criteria of 120 m is very conservative since it is based on the deepest 0.1% light level in the clearest offshore waters. If this criteria is relaxed to say the average 0.1% light level found in the jet, about 83 m, then the fraction of the water column satisfying the subduction criteria would be 4 times larger based on Fig. 3C. (This average 0.1% light level is based on analysis, not presented here, by one of the authors, BHJ.) Second, only about one third of the stations from all of the grid surveys showing evidence of subduction is found in the jet (Fig. 5). Combining these factors, the total subducted volume in the entire study area may be as large as 1000 km^3 and, if the vertical processes leading to subduction have similar rates inside and outside the jet, the vertical volume flux might be as much as 80 km^3/day. The corresponding vertical mass flux of chlorophyll in this case would be of order $9x10^4$ kg/day. For illustration, the areas of a 50 m deep euphotic zone which would be subducted by vertical volume fluxes of 5 and 80 km^3/day are indicated by squares in Fig. 5. The larger square is 40 km on a side. Clearly, more observations are required to constrain the subducted volumes and rates and to determine the impacts of subduction processes on coastal circulation and ecology.

ACKNOWLEDGEMENTS

Ken Brink and Dave Mackas provided helpful comments on an early draft of the manuscript. This work was supported by the Office of Naval Research, Coastal Sciences Program.

REFERENCES

Anderson, G.G., 1969, Subsurface chlorophyll maximum in the Northeast Pacific Ocean, Limnol. Oceanogr., 14, 386-391.

Baker, E.T., and J.W. Lavelle, 1984, The effect of particle size on the light attenuation coefficient of natural suspension, J. Geophys. Res., 89, C5, 8197-8203.

Beers, J.R., F.M.H. Reid, and G.L. Stewart, 1975, Microplankton of the NORTH Pacific central gyre. Population structure and abundance, June 1973, Int. Rev. Gesamten Hyrobiol., 60, 607-638.

Bienfang, P., J. Szyper, and E. Laws, 1982, Sinking rate and pigment responses to light-limitation of a marine diatom: implications to dynamics of chlorophyll maximum layers, Oceanol. Acta, 6, 1, 55-62.

Bienfang, P., and J. Szyper, 1982, Effects of temperature and salinity on sinking rates of the centric diatom Ditylum Brightwelli, Bio. Oceangr., 1, 3, 211-223.

Bienfang, P.K., 1981, Sinking rate dynamics of Cricosphaera Carterae Braarud. 1. Effects of growth rate, limiting substrate, and diurnal variations in steady-state populations, J. Exp. Mar. Ecol., 49, 217-233.

Bishop, J.K.B., 1986, The correction and suspended particulate matter calibration of Sea Tech transmissometer data, Deep-Sea Res., 33, 1, 121-134.

Bower, A.S., and T. Rossby, 1989, Evidence of cross-frontal exchange processes in the Gulf Stream based on isopycnal RAFOS float data, J. Phys. Oceanogr., 19, 9, 1177-1190.

Brink, K.H., R.C. Beardsley, P.P. Niiler, M. Abbott, A. Huyer, S. Ramp, T. Stanton, and D. Stuart, 1991, Statistical properties of near surface flow in the California coastal transition zone, J. Geophys. Res., (submitted).

Cullen, J.J., 1982, The deep chlorophyll maximum: comparing vertical profiles of chlorophyll a, Canadian J. of Fisheries and Aquatic Sci., 39, 791-803.

Davis, R.E., 1985. Drifter observations of coastal surface currents during CODE: the statistical and dynamical views, J. Geophys. Res., 90, 4756-4772.

Dewey, R.K., J.N. Moum, C.A. Paulson, D.R. Caldwell, and S.D. Pierce, 1991, Structure and dynamics of a coastal filament, J. Geophys. Res., (submitted).

Flament, P.J., A. Armi, and L. Washburn, 1985, The evolving structure of an upwelling filament, J. Geophys. Res., 90, 11,765-11,778.

Hoffman et al., 1991.

Hood, R., 1990, Phytoplankton biomass, photosynthetic light response, and physical structure in a Northern California upwelling system, Ph.D. dissertation, Scripps Institution of Oceanography.

Huyer, A., F. Chavez, T. Cowles, J. Fleischbein, P.M. Kosro, S. Ramp, L. Small, T. Stanton, and L. Washburn, 1991, Evolution of the Coastal Transition Zone off Northern California, June to August 1988, submitted to J. Geophys. Res.

Jackson, G., 1991, A model of formation of marine algol flocs by physical coagulation processes, in press, Deep-Sea Res.

Jerlov, H.G., 1976, Marine Optics, Elsevier, New York, 231 pp.

Kadko, D.C., L. Washburn, and B.H. Jones, 1991, Evidence of subduction within cold filaments of the N. California coastal transition zone, submitted, J. Geophys. Res.

Kiefer, D.A., 1973, Fluorescence properties of natural phytoplankton populations, Mar. Bio., 22, 263-269.

Onken, R., J. Fischer, and J.D. Woods, Thermohaline finestructure and its relation to frontogenesis dynamics, J. Phys. Oceanogr., 20, 9, 1379-1394.

Pak, H., J.R.V. Zaneveld, 1977, Bottom nepheloid layers and bottom mixed layers observed on the continental shelf off Oregon during the upwelling season, J. Geophys. Res., 82, 3921-3931.

Prezelin, B.B., 1981, Light reactions in photosynthesis, Physiological bases of phytoplankton ecology, Canadian Bulletin of Fisheries and Aquatic Sci. (T. Platt, Ed.), 210, 1-43.

Smayda, T.J., 1970, The suspension and sinking of phytoplankton in the sea, Oceanogr. Mar. Biol. Ann. Rev., 8, 353-414.

Smetacek, V.S., 1985, Role of sinking in diatom life-history cycles: ecological, evolutionary, and geological significance, Mar. Bio., 84, 239-251.

Spinrad, R.W., 1986, A calibration diagram of specific beam attenuation, J. Geophys. Res., 91, C6, 7761-7764.

Stanton, T.P., J. Stockel, M.L. Batteen and S. Ramp, 1991, Upper ocean response to a wind relaxation event in the coastal transition zone, submitted to J. Geophys. Res.

Strub, P.T. and the CTZ Group, 1991, The nature of the cold filaments in the California Current System, submitted to J. Geophys. Res.

Swenson, M., P.P. Niiler and K. Brink, 1991, The dynamical and thermodynamical structure of the flow associated with a cold filament off Pt. Arena, California in July 1988, submitted to J. Geophys. Res.

Table 1. Advection times and velocities along jet*

Level	Time (days) Min. - Mean	Horizontal Velocity (m/s) Max. - Mean	Vertical Velocity (m/s) Max. - Mean
5 db	5 - 11	0.70 - 0.33	
σ_θ = 25.8	12 - 21	0.30 - 0.17	10 - 6
σ_θ = 26.2	20 - 42	0.18 - 0.09	4 - 2

*Stations: 48-62-88-19-26-39-32A-75
Total distance = 321 km

FIGURE CAPTIONS

Fig. 1A. Locations of stations E4 and 6. Contours of geopotential anomaly (0/500 db) are from first Pt. Sur survey, 6 - 12 July 1988.

Fig. 1B. Profiles of photosynthetically available radiation (PAR), beam c, and fluorescence at station 6 along with chlorophyll concentrations at discrete depths from bottle samples.

Fig. 1C. Profiles of potential temperature, potential density, and salinity at station 6.

Fig. 2A. As in 1B, but for station E4.

Fig. 2B. As in 1C, but for station E4.

Fig. 3A. Location of PAR profiles obtained within one hour of local noon (triangles). Contours of geopotential anomaly (0/500 db) are from first Pt. Sur survey, 6 - 12 July 1988. Offshore extension of geopotential anomaly contours from leg2 of Thomas Washington survey.

Fig. 3B. PAR profiles obtained within one hour of local noon in: the offshore jet (solid lines), southern and inshore waters (dotted lines), and offshore waters (dashed lines). Vertical bar shows range in 1% light level in jet. Arrows indicate depths of 1% and 0.1% light levels in clear offshore waters.

Fig. 3C. Histogram showing distribution of fluorescence in water column from all CTD profiles obtained during leg 2 of Thomas Washington survey.

Fig. 4. Locations of stations containing subducted water masses shown with filled triangles. Dots show other station locations. (A) first Wecoma survey, 20-27 July; (B) first Pt. Sur survey, 6-12 July; (C) second Pt. Sur survey, 12-18 July; (D) third Pt. Sur survey, 21-27 July; (E) and second Wecoma survey, 29 July - 4 August. Contours of geopotential anomaly (0/500 db).

Fig. 5. Locations of all stations during leg 2 of Thomas Washington survey (triangles). Filled triangles indicate stations with subducted water masses. Contours of geopotential anomaly (0/500 db) are from first Pt. Sur survey, 6 - 12 July 1988. Offshore extension of geopotential anomaly contours from Thomas Washington survey.

Fig. 6A. Locations of profiles in jet shown in Figures 6B to 6F.

Fig. 6B. - 6F. Profiles of potential density, beam c, and fluorescence at five stations along jet axis. Diamonds indicate chlorophyll concentrations from bottle samples.

Fig. 7A. Contour section of beam c on σ_θ = 25.8. The x's show station locations.

Fig. 7B. Contour section of pressure on σ_θ = 25.8. The x's show station locations.

Fig. 8A. Contour section of beam c on σ_θ = 26.2. The x's show station locations.

Fig. 8B. Contour section of pressure on σ_θ = 26.2. The x's show station locations.

Fig. 9A. θ-S points corresponding to subducted water masses from the five grid surveys of Fig. 4. Water masses of points in Group A are from near shore sources and Group B from offshore sources.

Fig. 9B. θ-S points in upper 50 db of water column for the most inshore line of the five grid surveys of Fig. 4. Envelope of θ-S points of subducted water masses in Group A (Fig. 9A) shown by dashed lines.

Fig. 9C. θ-S points in upper 50 db of water column for the offshore lines of the five grid surveys. Envelope of θ-S points of subducted water masses (Fig. 9A) shown by dashed lines.

Fig. 10A. Locations of various stations whose θ-S relationships are shown in Figures 10B and 10C.

Fig. 10B. θ-S profiles shown with solid lines are for the stations on line A from leg 1 of the Thomas Washington survey. θ-S points shown with open circles are for subducted water masses observed below 120 db from leg 2 of the Thomas Washington survey. Station locations shown in Fig. 10A.

Fig. 10C. θ-S points of subducted water masses on σ_θ = 26.2 and θ-S profiles for the upper 50 db of the water column at stations A3 and A13 (solid lines). Station locations shown in Fig. 10A.

Fig. 11. Vertical section of geostrophic velocity (5/500 db) computed from stations 47 - 53. Station locations shown in Fig. 14A. Stippled areas indicate flow to the south.

Fig. 12. Horizontal contour section of salinity on σ_θ = 26.2 from leg 2 of Thomas Washington survey. Station locations indicated with x's.

Fig. 13. Horizontal contour sections on $\sigma\theta$ = 26.2 from leg 1 of Thomas Washington survey of: A. salinity, B. pressure, C. beam c. Station locations indicated with x's.

Fig. 14 A. Cross-jet transects used for computing sections of geostrophic velocity. Track of surface drifter indicated with solid line and hypothetical drifter track with dotted line.

Fig. 14B. - 14E Isopycnal profiles of geostrophic velocity on $\sigma\theta$ = 26.2 for: (B) stations 47 - 53, (C) stations 65 - 57, (D) stations 17A - 21, and (E) stations 76 - 73.

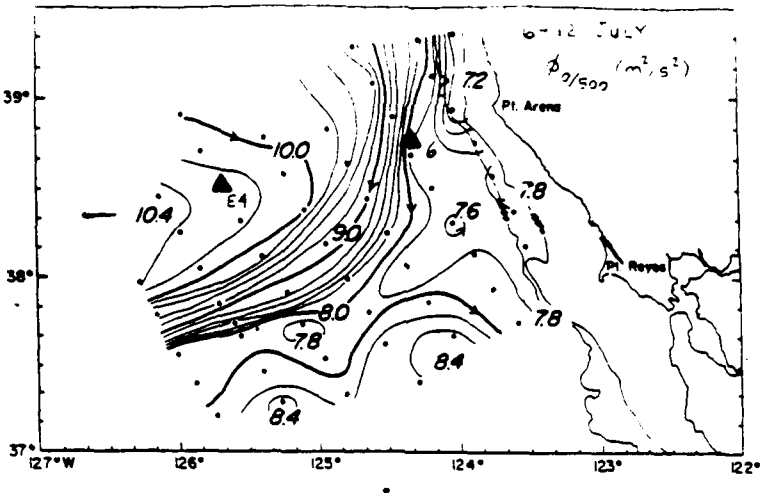
6-12 JULY
$\phi_{0/500}$ (m^2, s^2)
Pt. Arena
Pt. Reyes
E4
10.4
10.0
9.0
8.0
7.8
7.6
7.2
8.4
39°
38°
37°
127°W
126°
125°
124°
123°
122°

A.

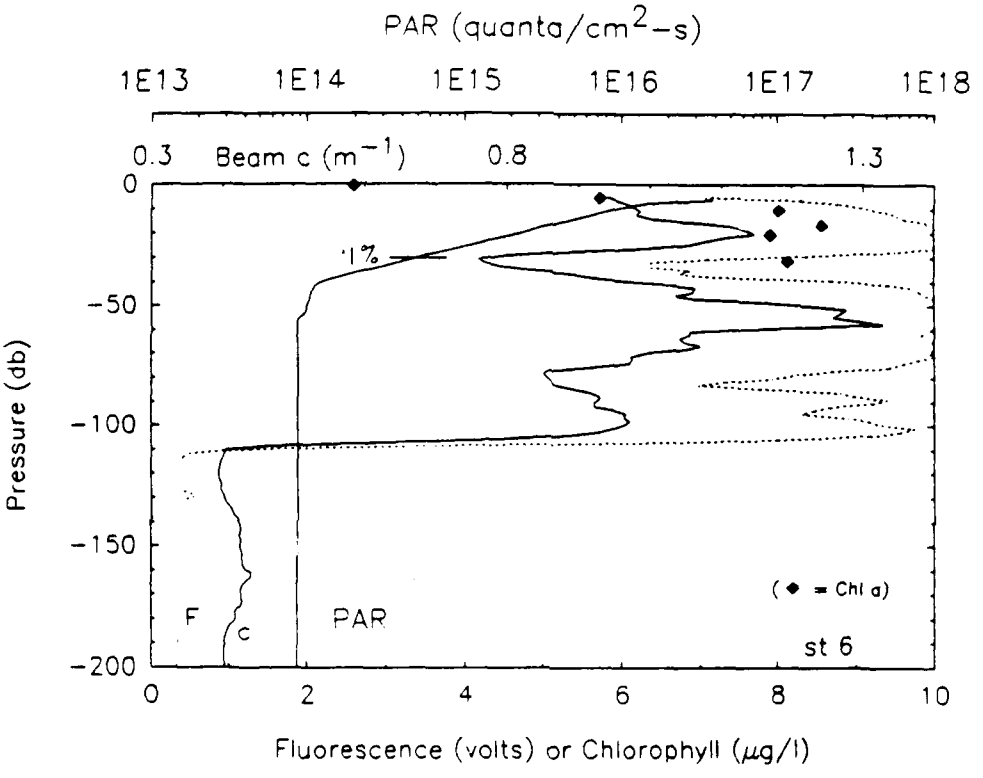
PAR (quanta/cm^2-s)
1E13
1E14
1E15
1E16
1E17
1E18
0.3
Beam c (m^{-1})
0.8
1.3
0
-50
-100
-150
-200
Pressure (db)
1%
F
c
PAR
(◆ = Chl a)
st 6
0
2
4
6
8
10
Fluorescence (volts) or Chlorophyll (μg/l)

B.

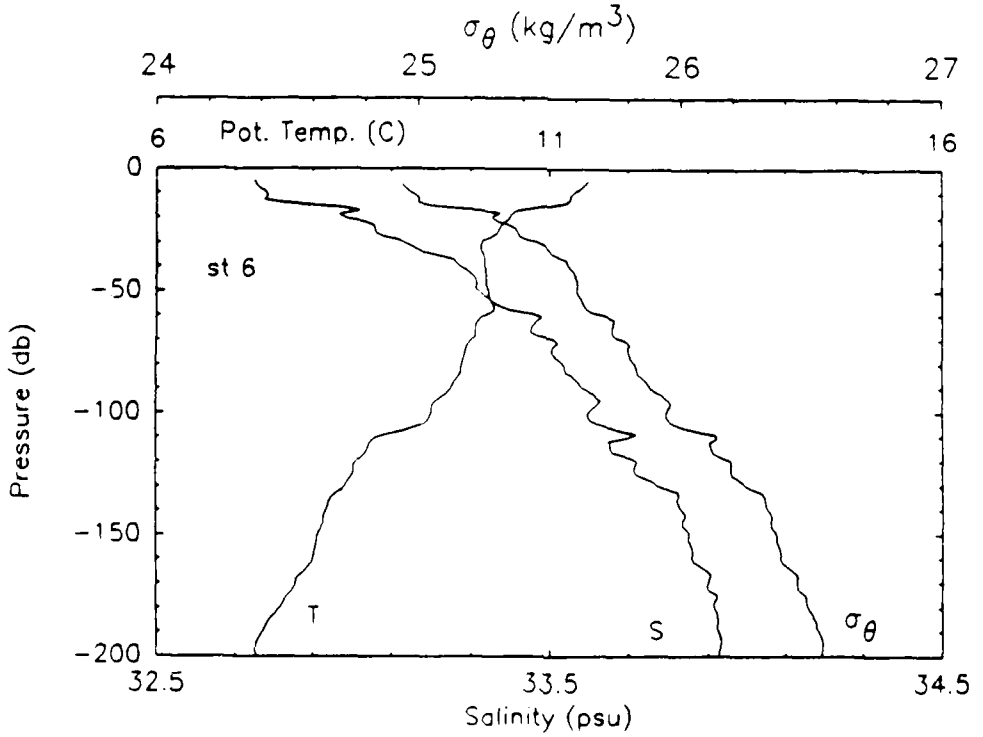
σ_θ (kg/m^3)
24
25
26
27
6
Pot. Temp. (C)
11
16
0
-50
-100
-150
-200
Pressure (db)
st 6
T
S
σ_θ
32.5
33.5
34.5
Salinity (psu)

C.

FIG. 1

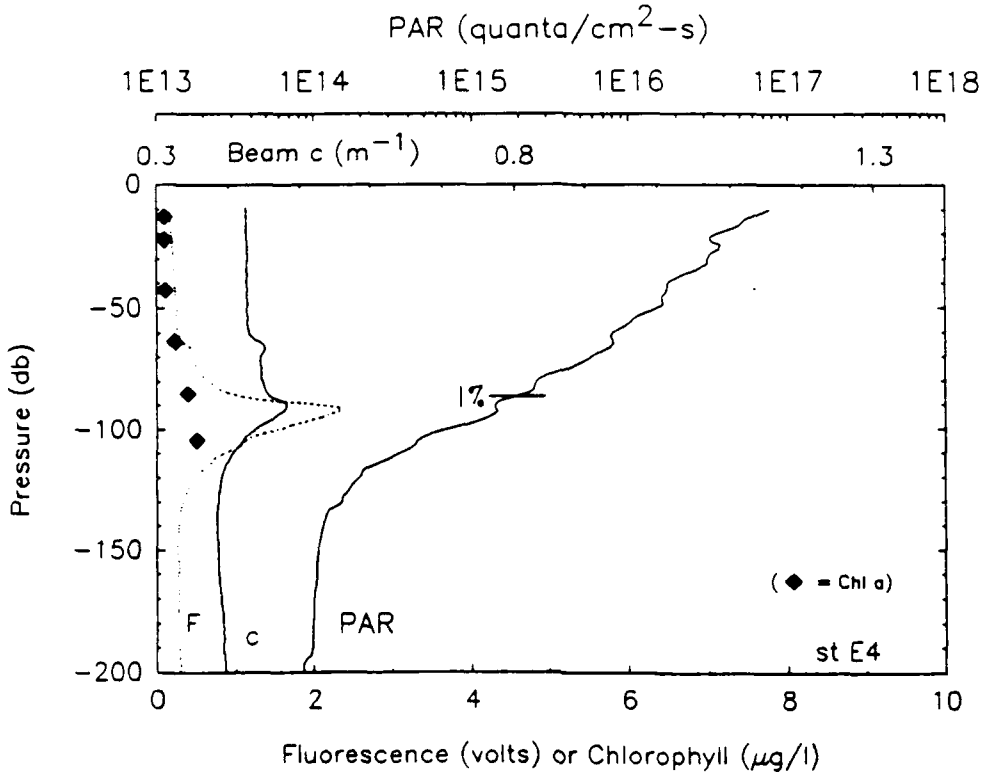
PAR (quanta/cm^2-s)
1E13
1E14
1E15
1E16
1E17
1E18
0.3
Beam c (m^{-1})
0.8
1.3
0
-50
-100
-150
-200
Pressure (db)
1%
(◆ = Chl a)
F
c
PAR
st E4
0
2
4
6
8
10
Fluorescence (volts) or Chlorophyll (μg/l)

A.

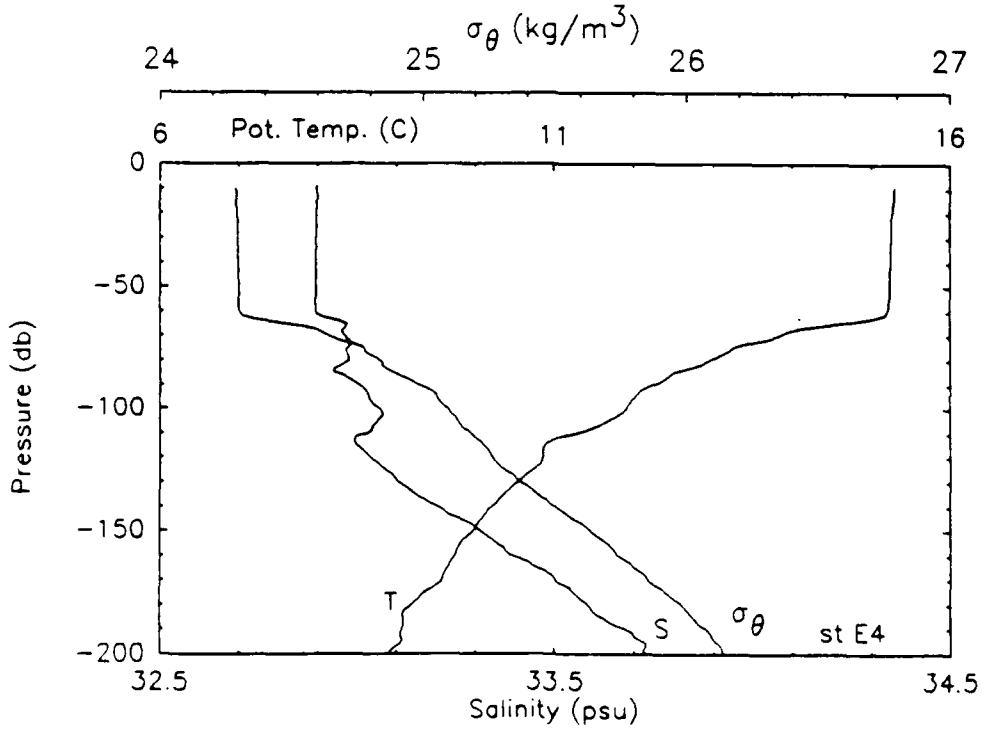
σ_θ (kg/m^3)
24
25
26
27
6
Pot. Temp. (C)
11
16
0
-50
-100
-150
-200
Pressure (db)
T
S
σ_θ
st E4
32.5
33.5
34.5
Salinity (psu)

B.

FIG. 2

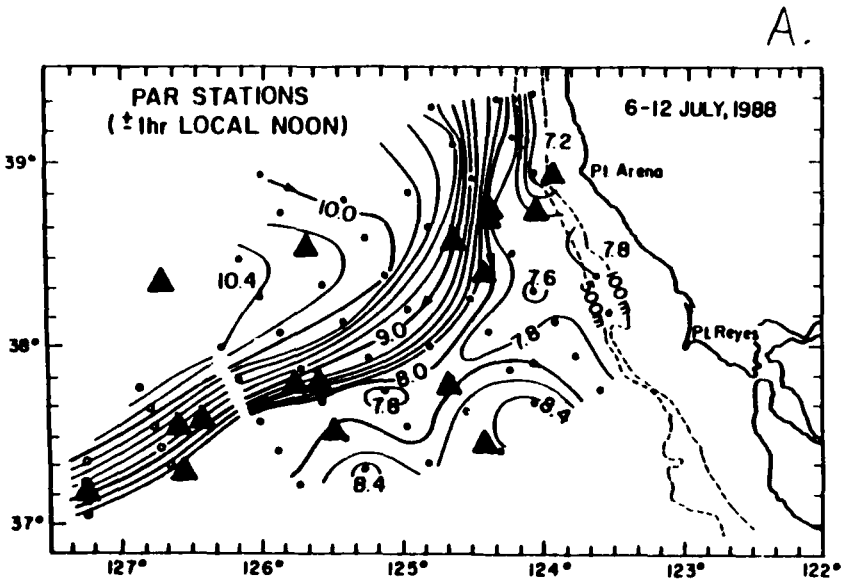
A.
PAR STATIONS
(±1hr LOCAL NOON)
6-12 JULY, 1988
Pt Arena
Pt Reyes
39°
38°
37°
127°
126°
125°
124°
123°
122°
10.0
10.4
9.0
8.0
7.8
7.6
7.2
8.4

FIG. 3

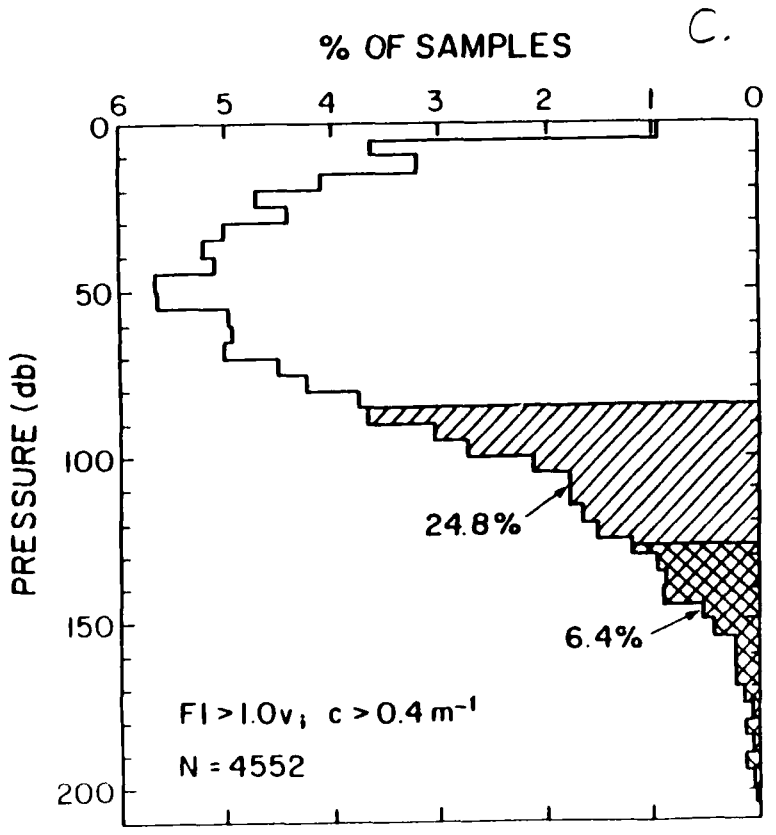
C.
% OF SAMPLES
6 5 4 3 2 1 0
PRESSURE (db)
0
50
100
150
200
24.8%
6.4%
Fl > 1.0v; c > 0.4 m⁻¹
N = 4552

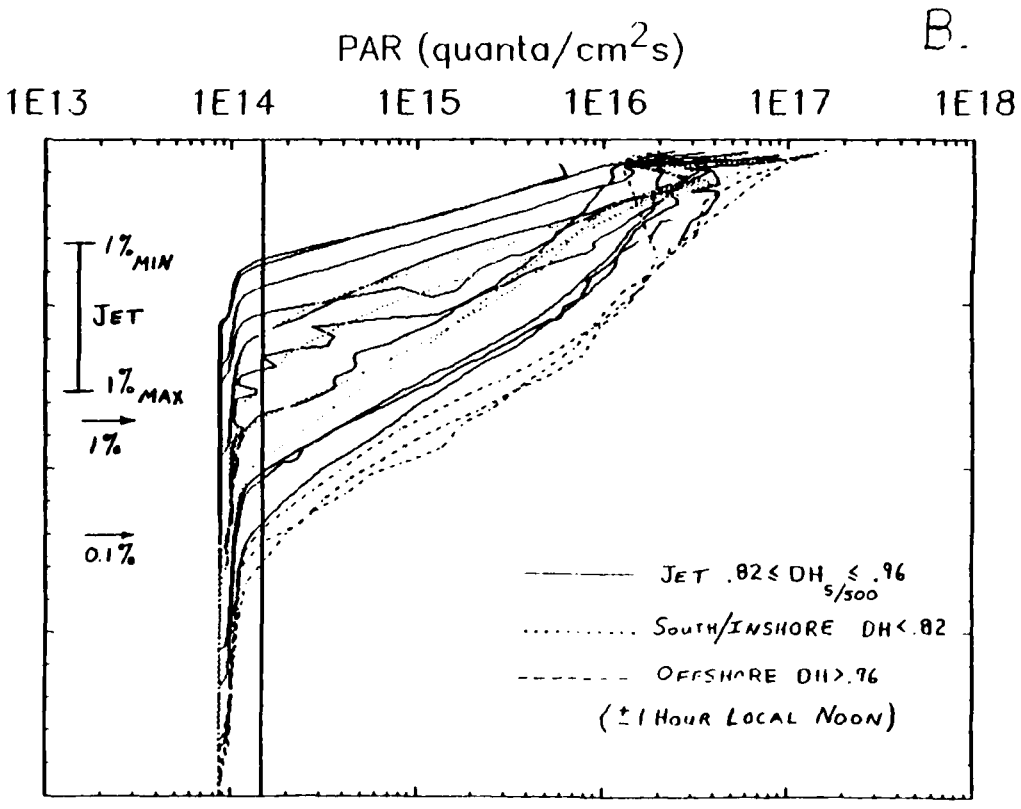
B.
PAR (quanta/cm²s)
1E13
1E14
1E15
1E16
1E17
1E18
1% MIN
JET
1% MAX
1%
0.1%
JET .82 ≤ DH s/500 ≤ .96
SOUTH/INSHORE DH < .82
OFFSHORE DH > .96
(±1 HOUR LOCAL NOON)

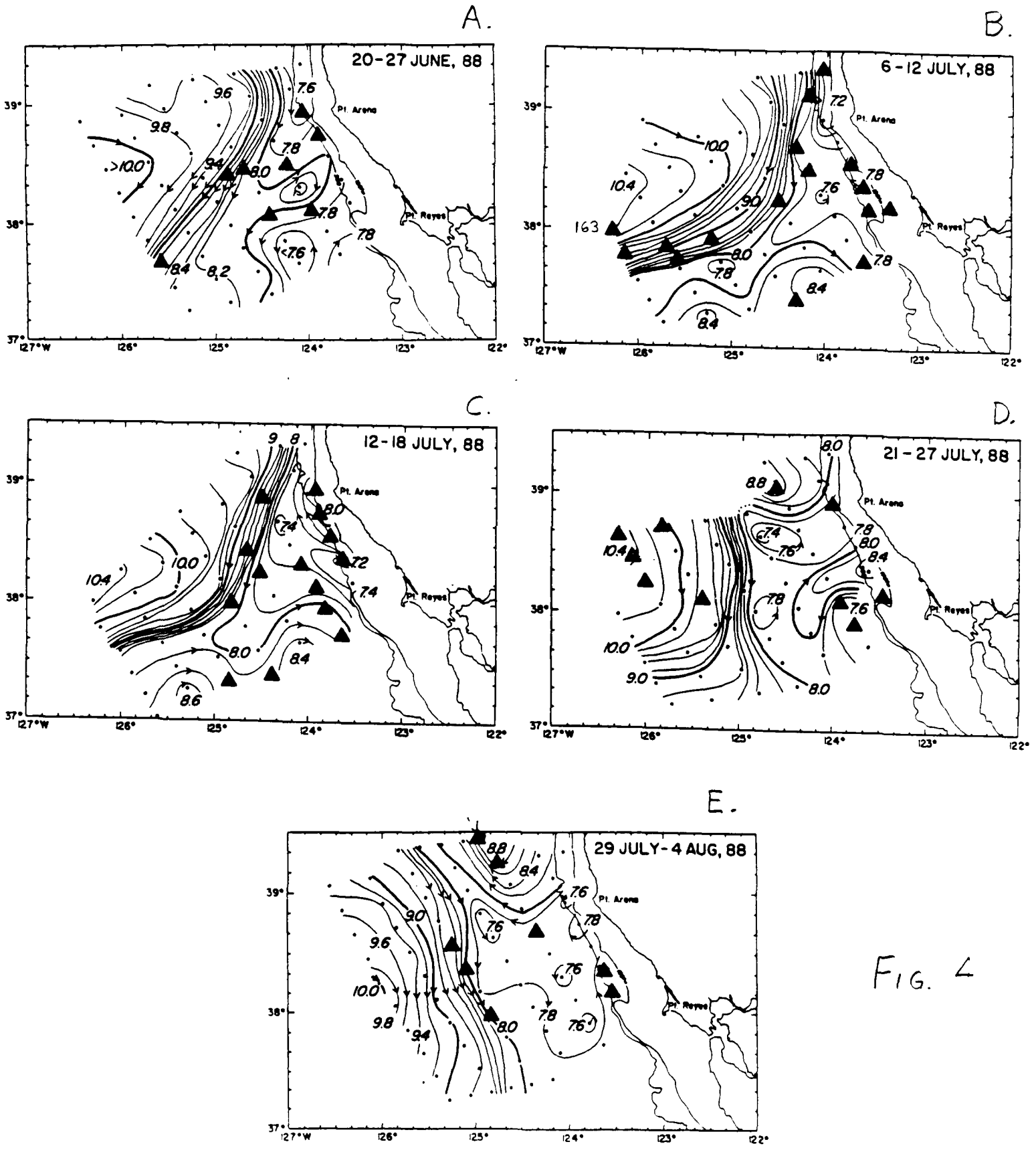
A.
20-27 JUNE, 88
B.
6-12 JULY, 88
C.
12-18 JULY, 88
D.
21-27 JULY, 88
E.
29 JULY-4 AUG, 88
Pt. Arena
Pt. Reyes
39°
38°
37°
127°W
126°
125°
124°
123°
122°

FIG. 4

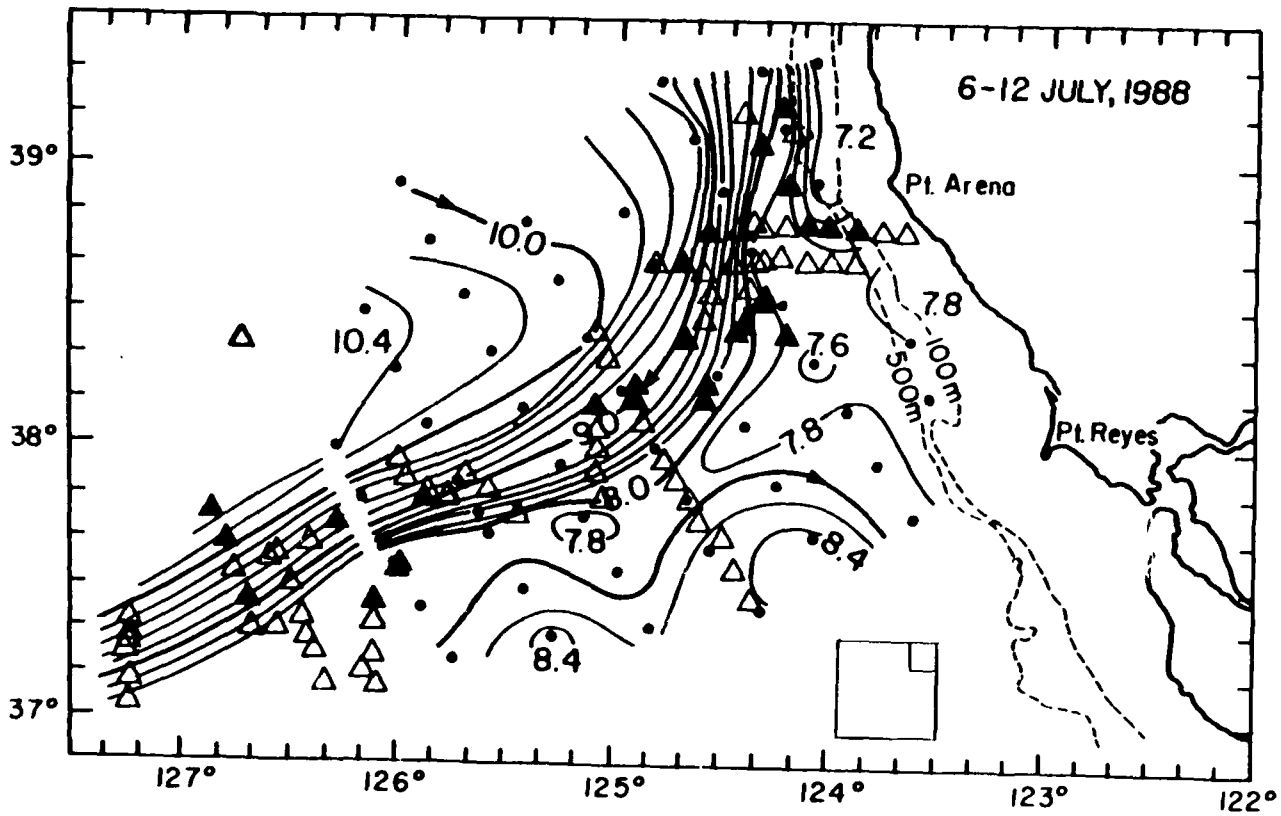
6-12 JULY, 1988
39°
38°
37°
127°
126°
125°
124°
123°
122°
Pt. Arena
Pt. Reyes
10.0
10.4
9.0
8.0
7.8
7.6
7.2
8.4
100m
500m

FIG. 5

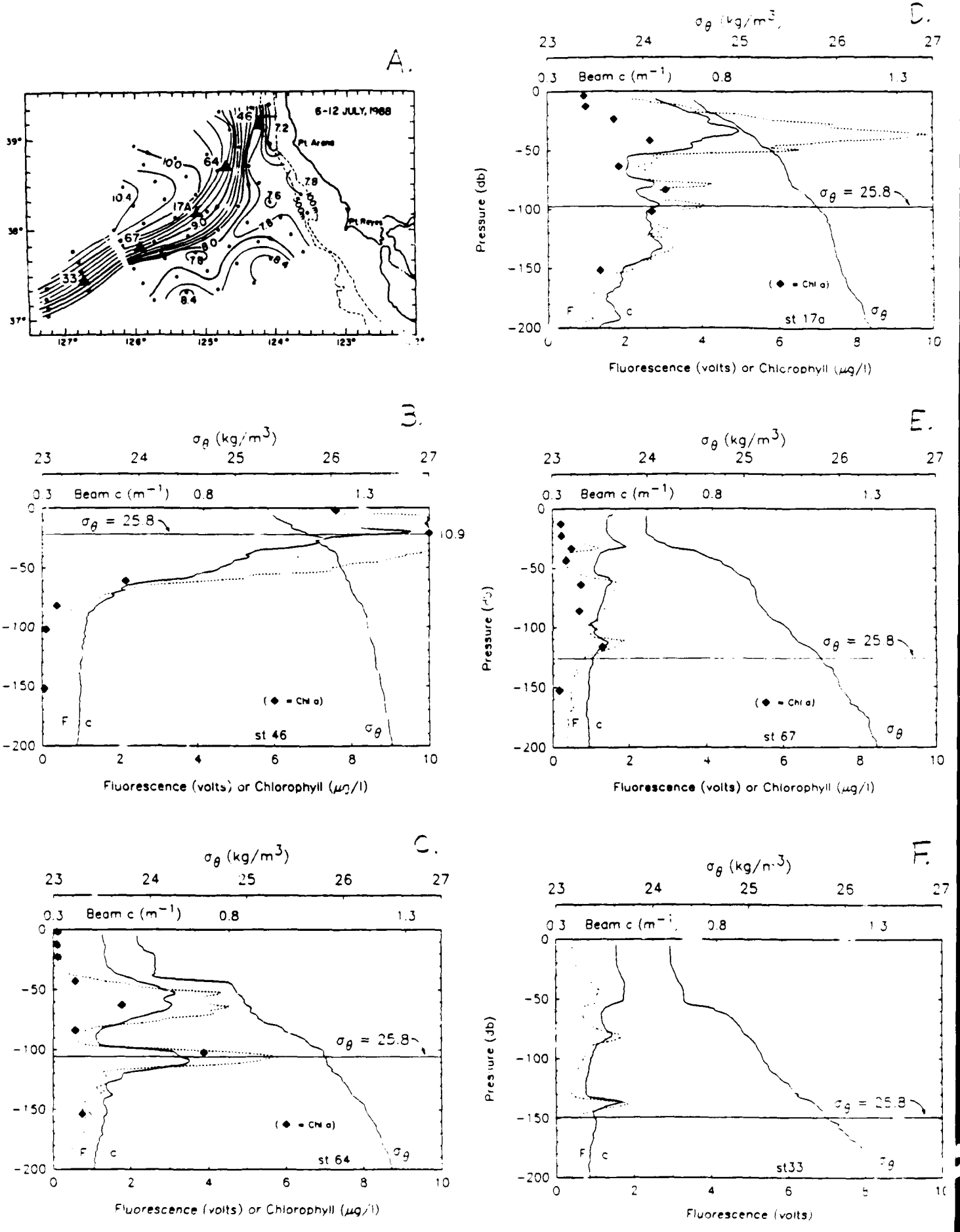
A.
6-12 JULY, 1988
Pt Arena
Pt Reyes
46
7.2
100
64
10.4
17A
67
33
8.4
7.8
7.6
7.0
1.8
39°
38°
37°
127°
126°
125°
124°
123°
B.
σθ (kg/m3)
23
24
25
26
27
0.3
Beam c (m−1)
0.8
1.3
σθ = 25.8
10.9
Pressure (db)
0
−50
−100
−150
−200
F
c
(◆ = Chl a)
st 46
σθ
0
2
4
6
8
10
Fluorescence (volts) or Chlorophyll (μg/l)
C.
σθ (kg/m3)
23
24
25
26
27
0.3
Beam c (m−1)
0.8
1.3
σθ = 25.8
Pressure (db)
0
−50
−100
−150
−200
F
c
(◆ = Chl a)
st 64
σθ
0
2
4
6
8
10
Fluorescence (volts) or Chlorophyll (μg/l)
D.
σθ (kg/m3)
23
24
25
26
27
0.3
Beam c (m−1)
0.8
1.3
σθ = 25.8
Pressure (db)
0
−50
−100
−150
−200
F
c
(◆ = Chl a)
st 17a
σθ
0
2
4
6
8
10
Fluorescence (volts) or Chlorophyll (μg/l)
E.
σθ (kg/m3)
23
24
25
26
27
0.3
Beam c (m−1)
0.8
1.3
σθ = 25.8
Pressure (db)
0
−50
−100
−150
−200
F
c
(◆ = Chl a)
st 67
σθ
0
2
4
6
8
10
Fluorescence (volts) or Chlorophyll (μg/l)
F.
σθ (kg/m3)
23
24
25
26
27
0.3
Beam c (m−1)
0.8
1.3
σθ = 25.8
Pressure (db)
0
−50
−100
−150
−200
F
c
st33
σθ
0
2
4
6
8
10
Fluorescence (volts)

FIG. 6

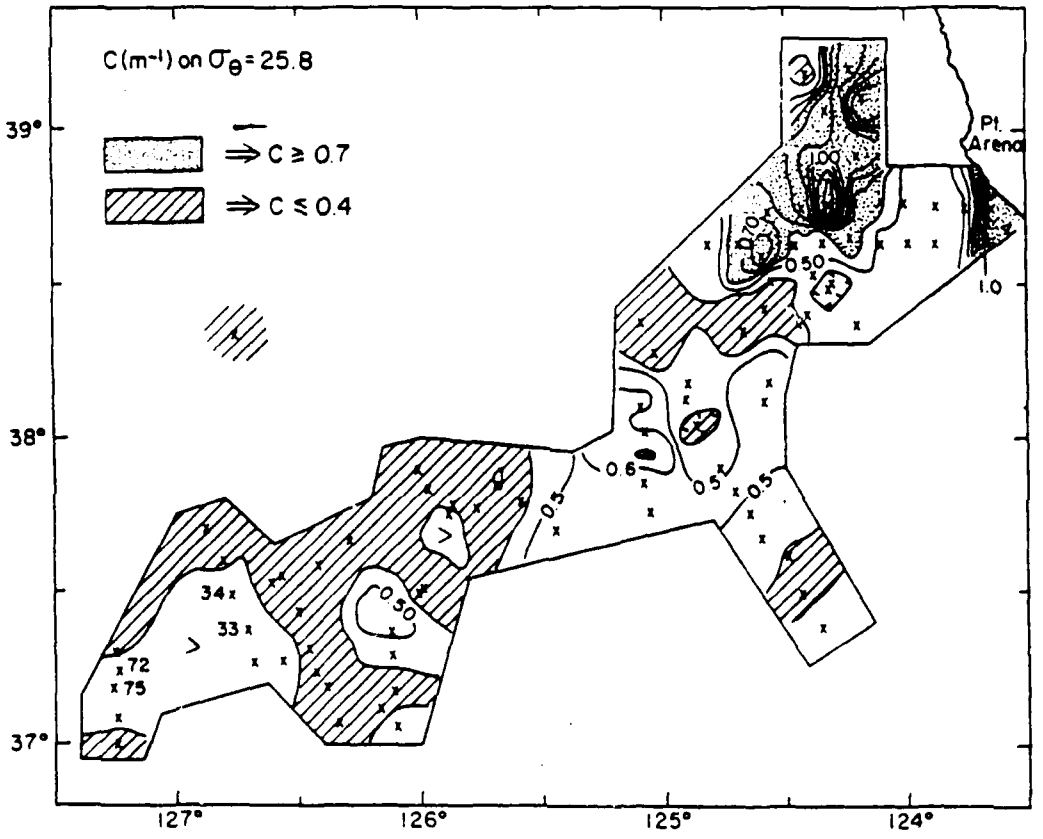
C(m⁻¹) on σθ = 25.8
⇒ C ≥ 0.7
⇒ C ≤ 0.4
Pt. Arena
39°
38°
37°
127°
126°
125°
124°
1.0
0.70
0.50
0.6
0.5
0.5
0.5
0.50
34
33
72
75

A.

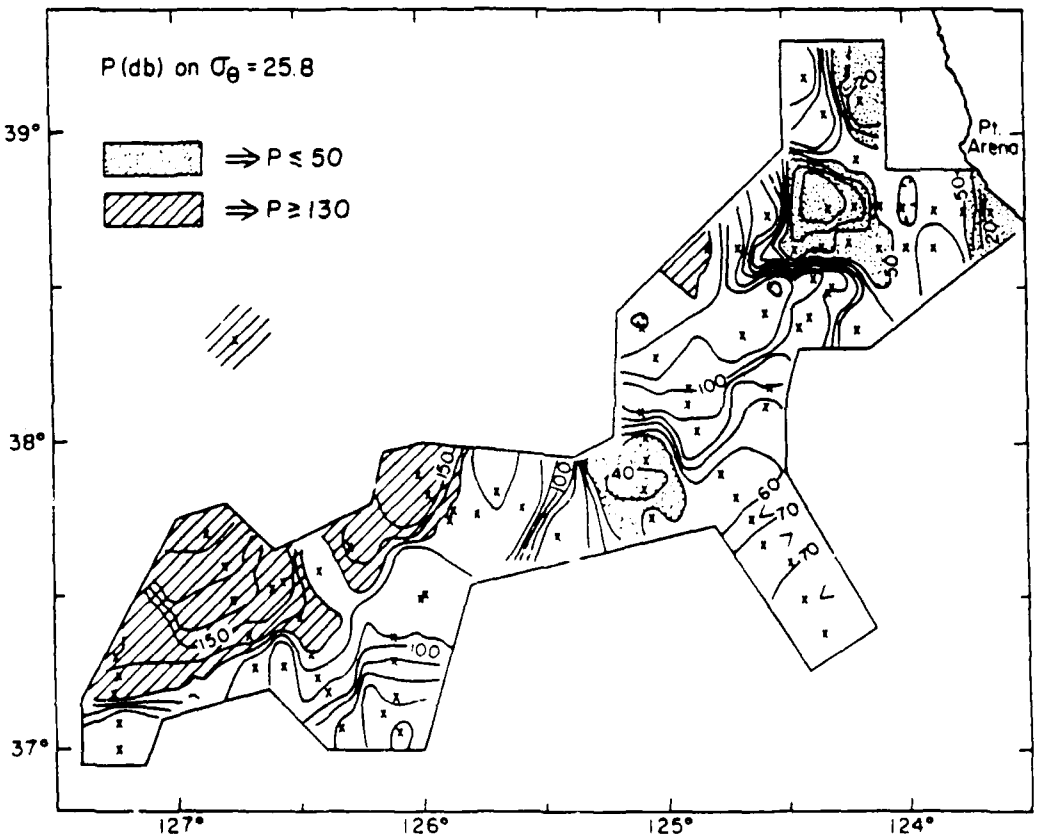
P (db) on σθ = 25.8
⇒ P ≤ 50
⇒ P ≥ 130
Pt. Arena
39°
38°
37°
127°
126°
125°
124°
150
100
40
60
70
70
150
100
100
50
50
20

B.

Fig. 7

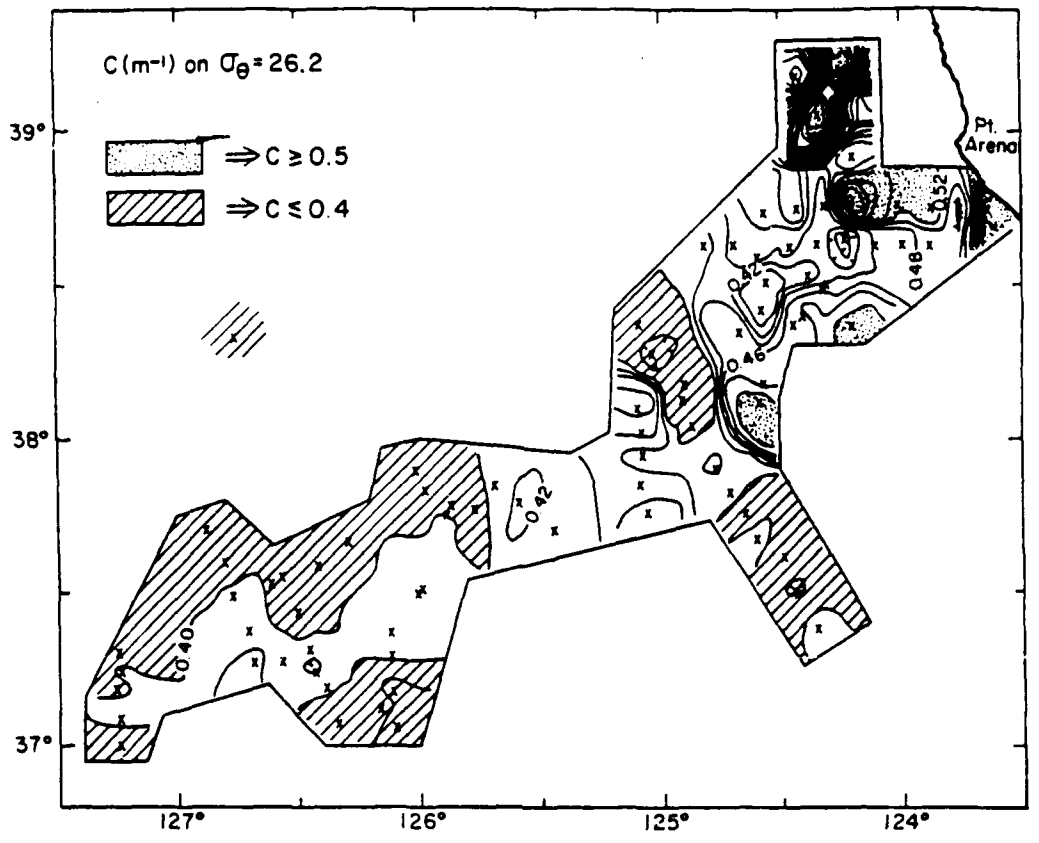
C(m⁻¹) on σ_θ = 26.2
⇒ C ≥ 0.5
⇒ C ≤ 0.4
39°
38°
37°
127°
126°
125°
124°
Pt. Arena
0.52
0.48
0.46
0.42
0.40

A.

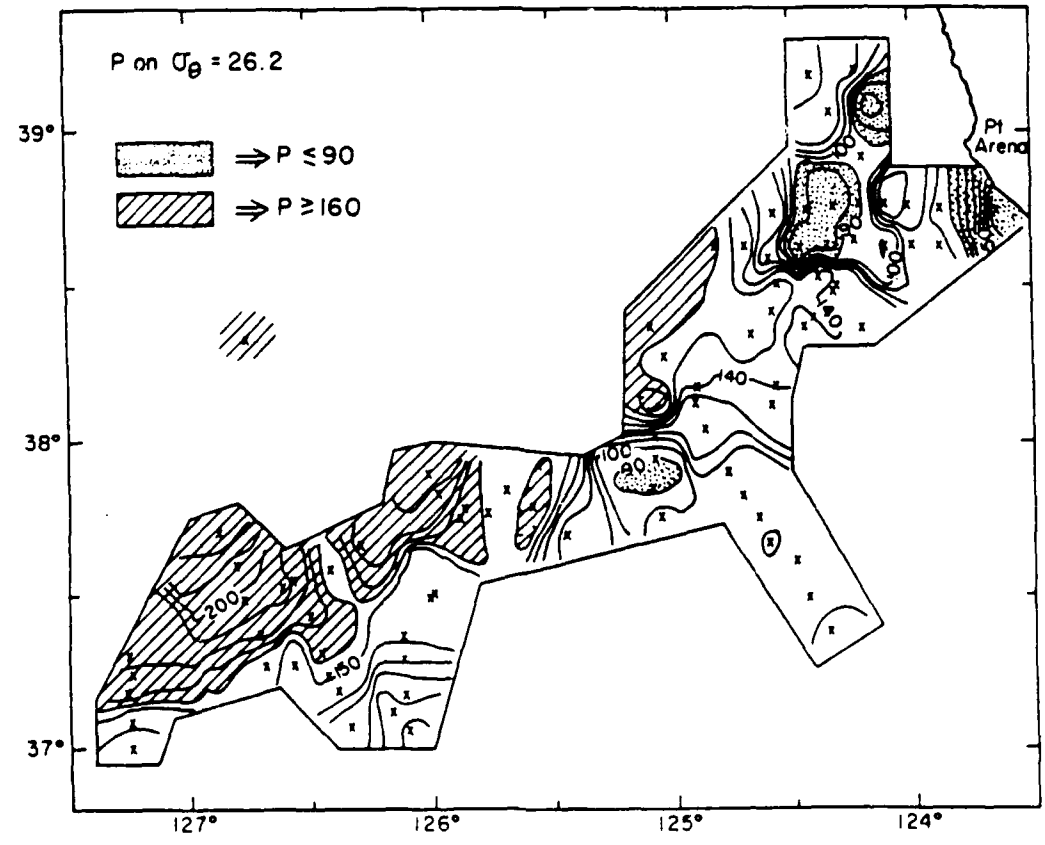
P on σ_θ = 26.2
⇒ P ≤ 90
⇒ P ≥ 160
39°
38°
37°
127°
126°
125°
124°
Pt Arena
90
100
140
150
200

B

Fig 3

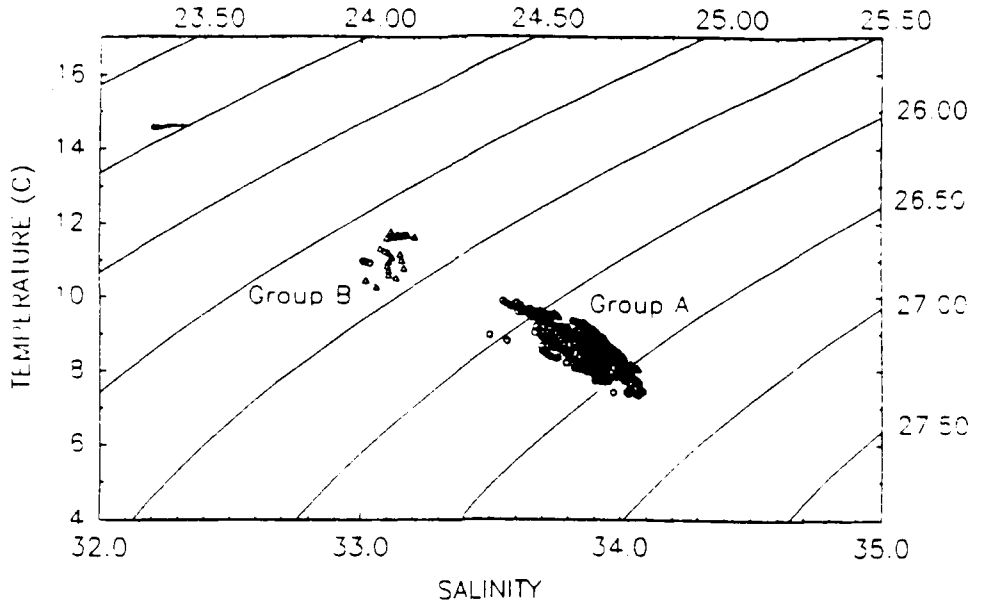
23.50
24.00
24.50
25.00
25.50
16
14
12
10
8
6
4
TEMPERATURE (C)
26.00
26.50
27.00
27.50
Group B
Group A
32.0
33.0
34.0
35.0
SALINITY

A.

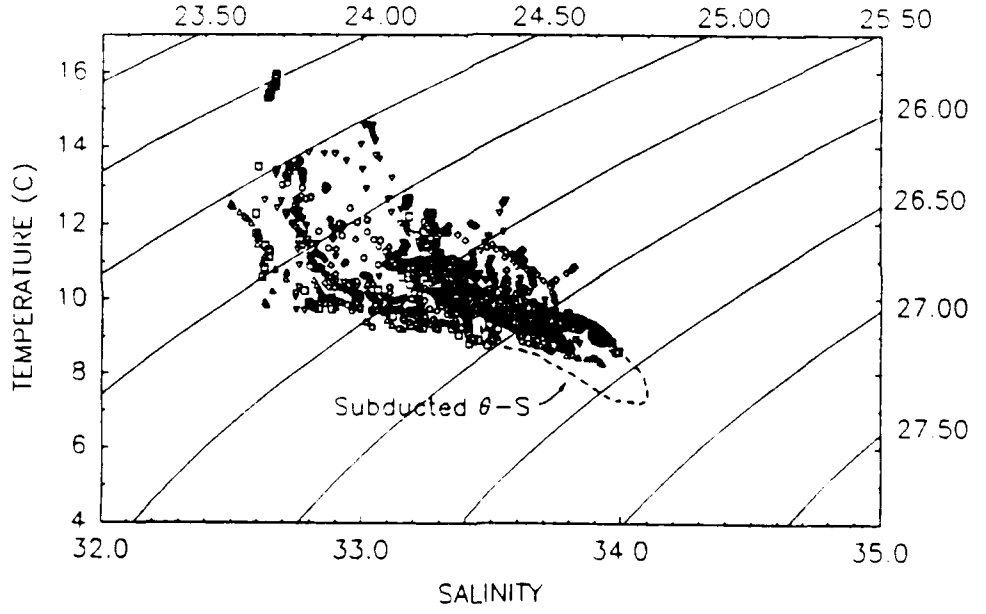
23.50
24.00
24.50
25.00
25.50
16
14
12
10
8
6
4
TEMPERATURE (C)
26.00
26.50
27.00
27.50
Subducted θ–S
32.0
33.0
34.0
35.0
SALINITY

B.

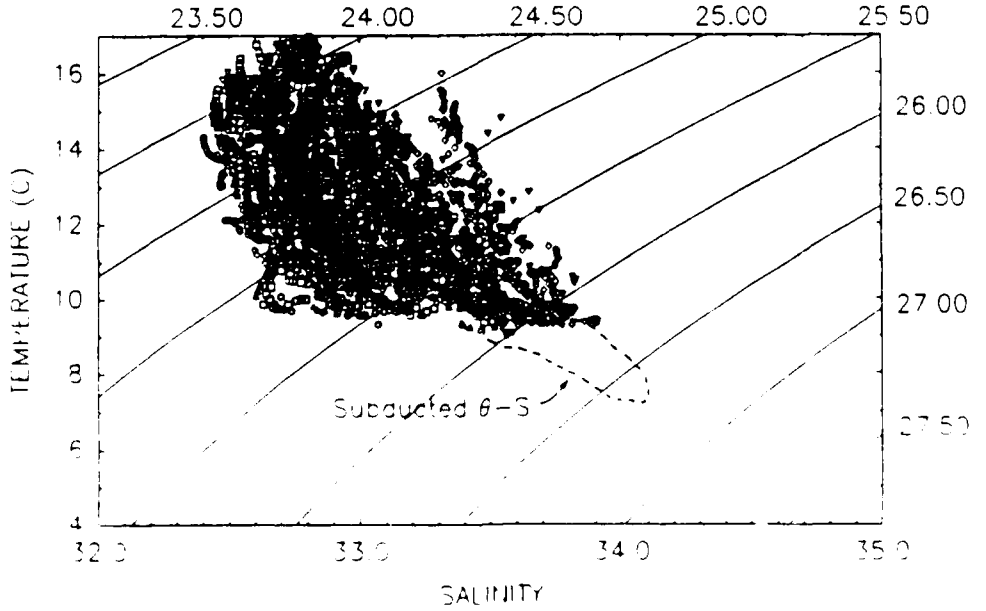
23.50
24.00
24.50
25.00
25.50
16
14
12
10
8
6
4
TEMPERATURE (C)
26.00
26.50
27.00
Subducted θ–S
32.0
33.0
34.0
35.0
SALINITY

C.

FIG. 9

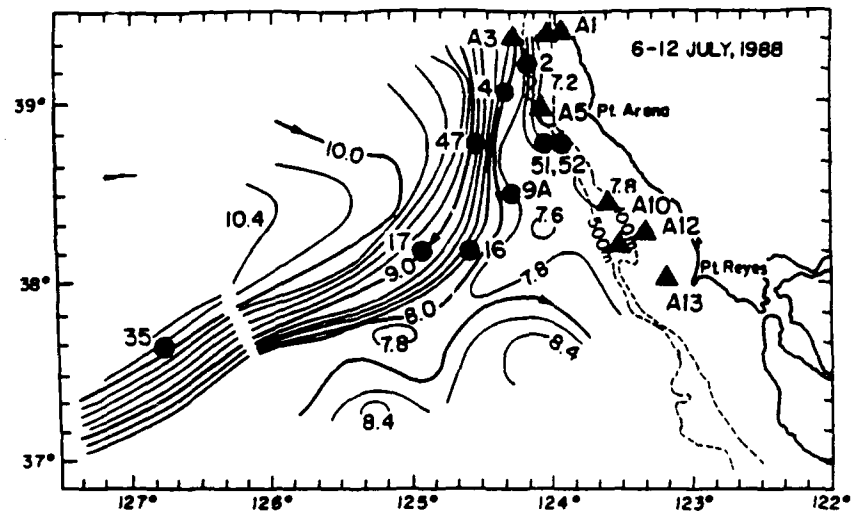
6-12 JULY, 1988
A1
A3
2
4
7.2
A5
Pt. Arena
47
10.0
51,52
9A
7.8
A10
A12
10.4
7.6
17
16
9.0
7.8
Pt. Reyes
A13
35
8.0
7.8
8.4
8.4
39°
38°
37°
127°
126°
125°
124°
123°
122°

A.

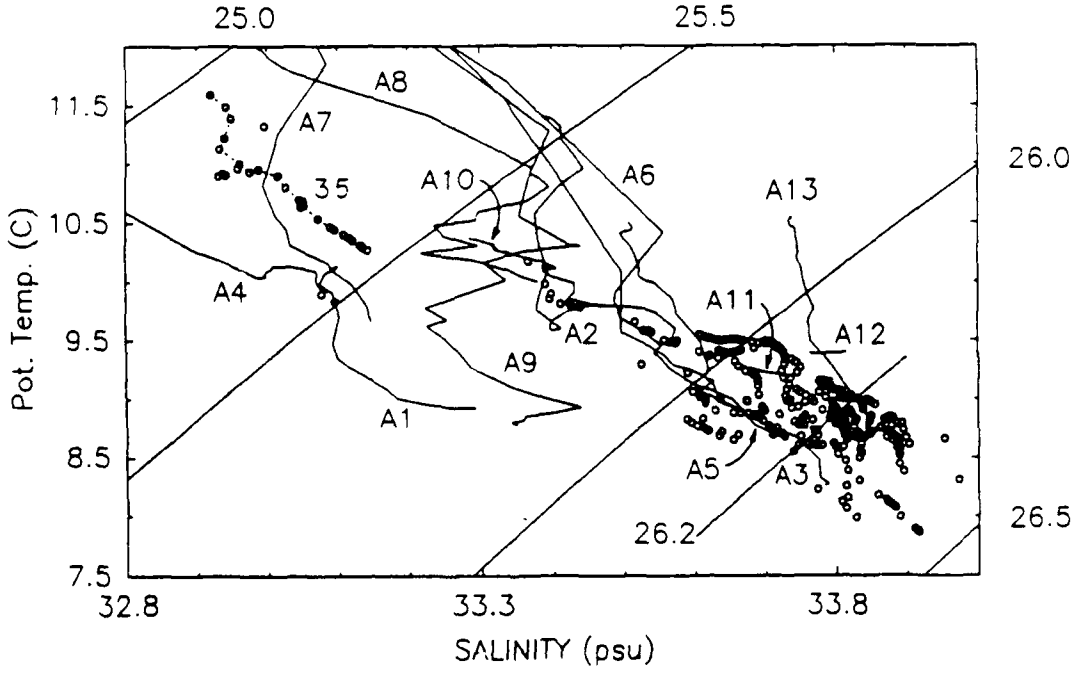
25.0
25.5
A8
A7
11.5
A10
A6
A13
26.0
35
10.5
A4
A11
A2
A12
A9
9.5
A1
A5
A3
8.5
26.2
26.5
7.5
32.8
33.3
33.8
Pot. Temp. (C)
SALINITY (psu)

B.

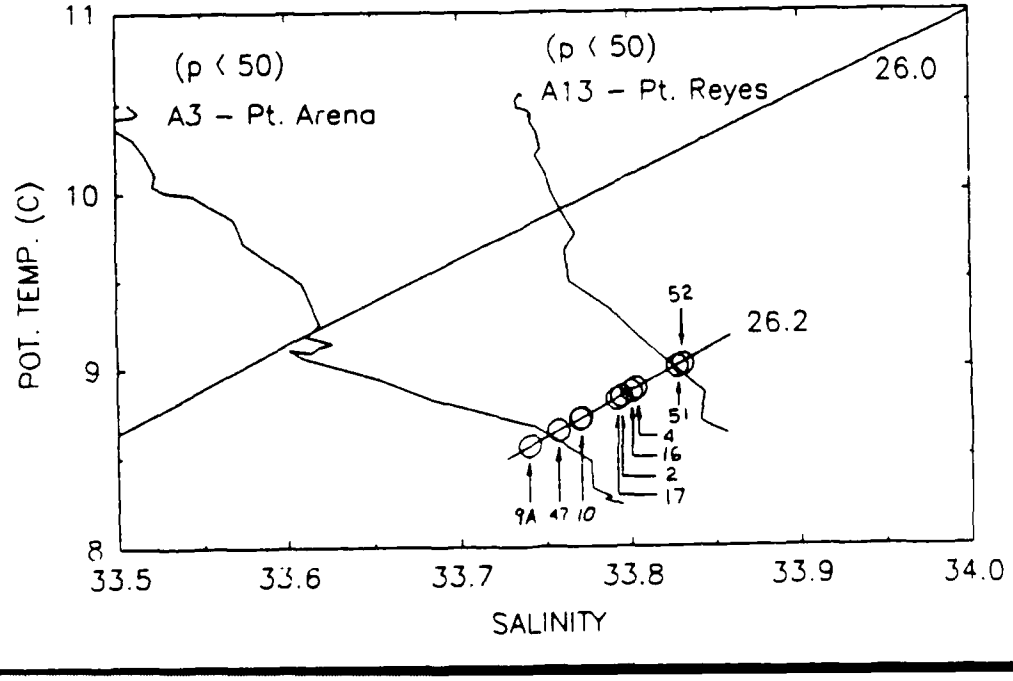
11
(p < 50)
A3 – Pt. Arena
(p < 50)
A13 – Pt. Reyes
26.0
10
52
26.2
9
51
4
16
2
17
9A
47
10
8
33.5
33.6
33.7
33.8
33.9
34.0
POT. TEMP. (C)
SALINITY

C.

Fig. 10

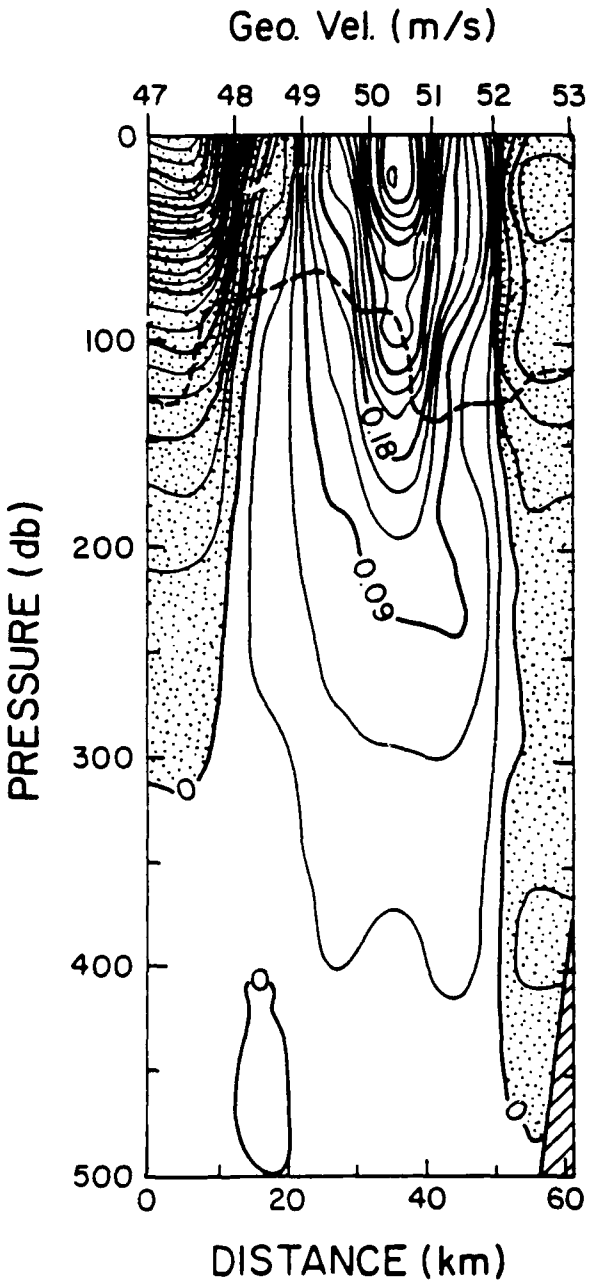
Geo. Vel. (m/s)
47
48
49
50
51
52
53
0
100
200
300
400
500
PRESSURE (db)
0.18
0.09
0
0
0
0
20
40
60
DISTANCE (km)

FIG 11

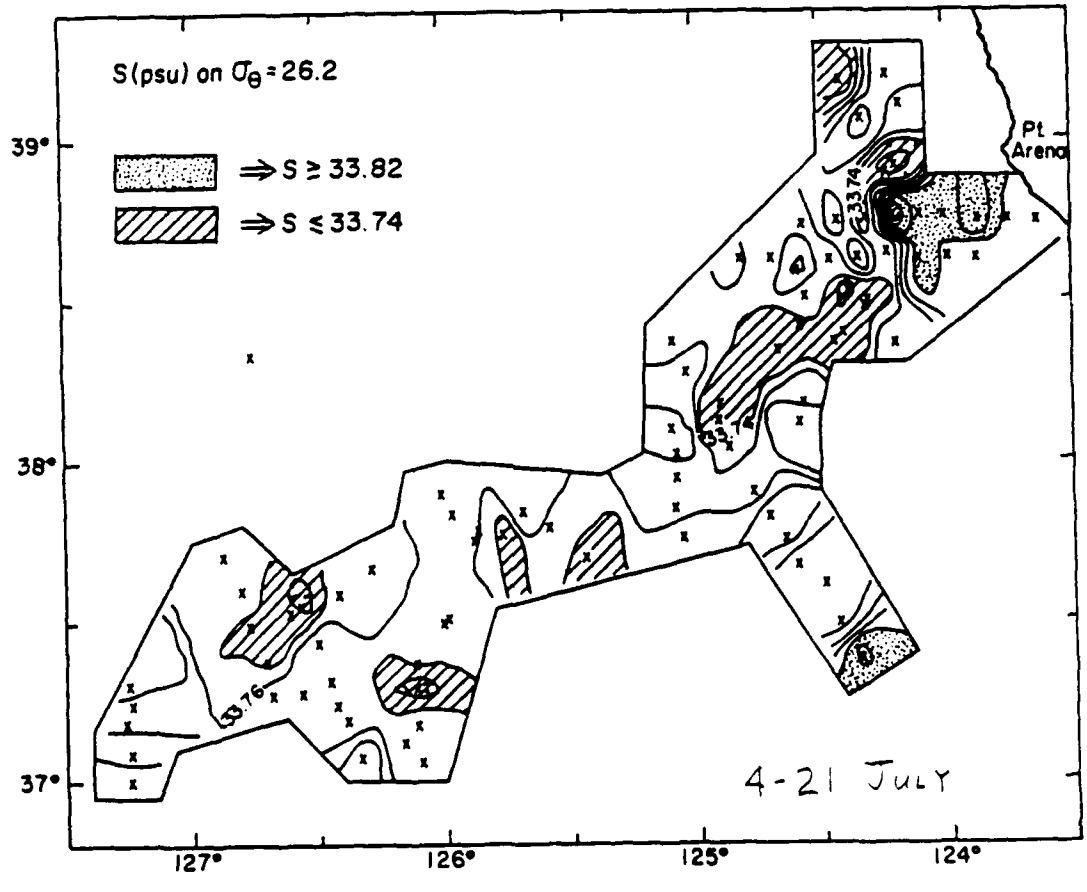
S(psu) on σ_θ = 26.2
⇒ S ≥ 33.82
⇒ S ≤ 33.74
Pt Arena
33.74
33.74
33.76
39°
38°
37°
127°
126°
125°
124°
4-21 JULY

FIG. 12

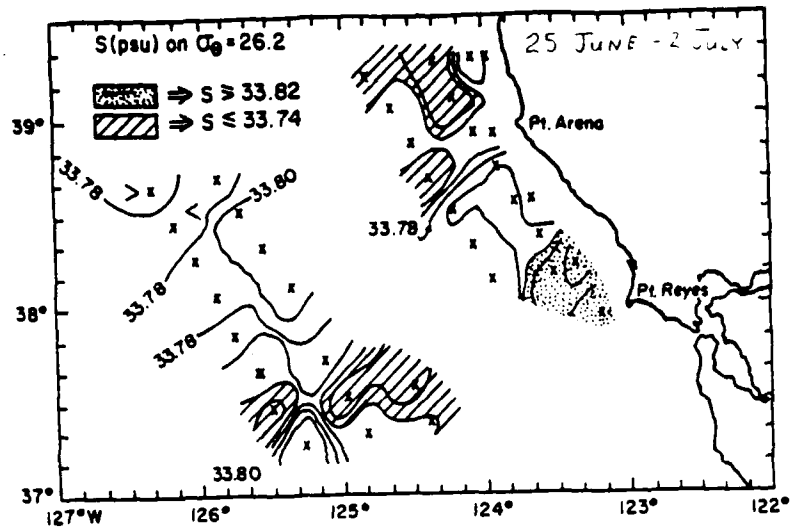
S(psu) on σ_θ = 26.2
⇒ S ≥ 33.82
⇒ S ≤ 33.74
25 JUNE - 2 JULY
Pt. Arena
Pt. Reyes
33.78
33.80
39°
38°
37°
127°W
126°
125°
124°
123°
122°

A.

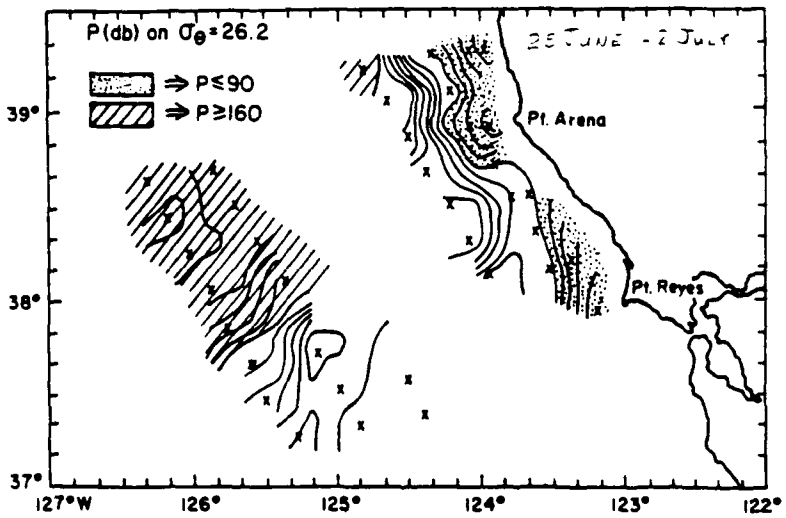
P(db) on σ_θ = 26.2
⇒ P ≤ 90
⇒ P ≥ 160
25 JUNE - 2 JULY
Pt. Arena
Pt. Reyes
39°
38°
37°
127°W
126°
125°
124°
123°
122°

B.

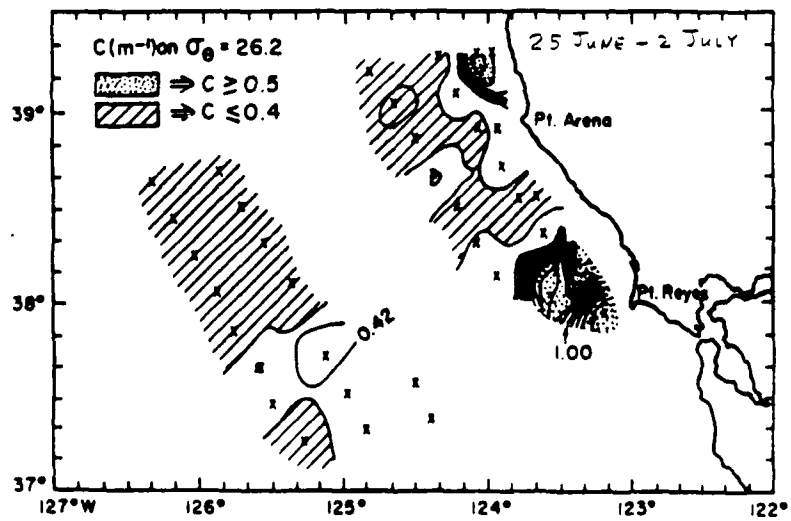
C(m⁻¹) on σ_θ = 26.2
⇒ C ≥ 0.5
⇒ C ≤ 0.4
25 JUNE - 2 JULY
Pt. Arena
Pt. Reyes
0.42
1.00
39°
38°
37°
127°W
126°
125°
124°
123°
122°

C.

FIG. 12

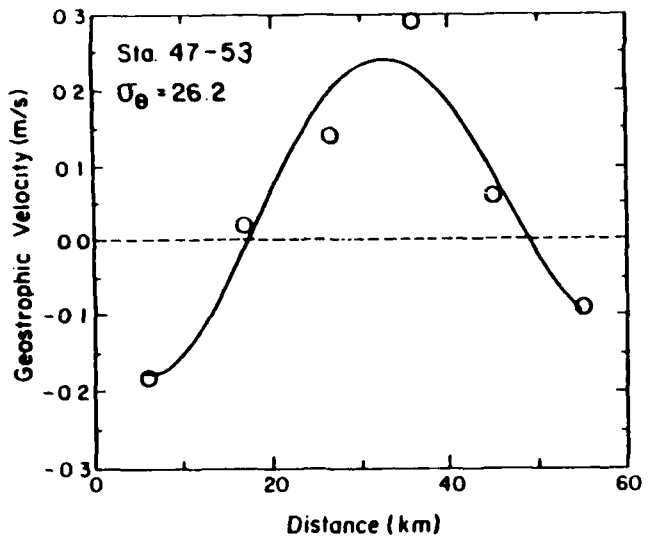
B.
Sta. 47-53
σ_θ = 26.2
Geostrophic Velocity (m/s)
Distance (km)

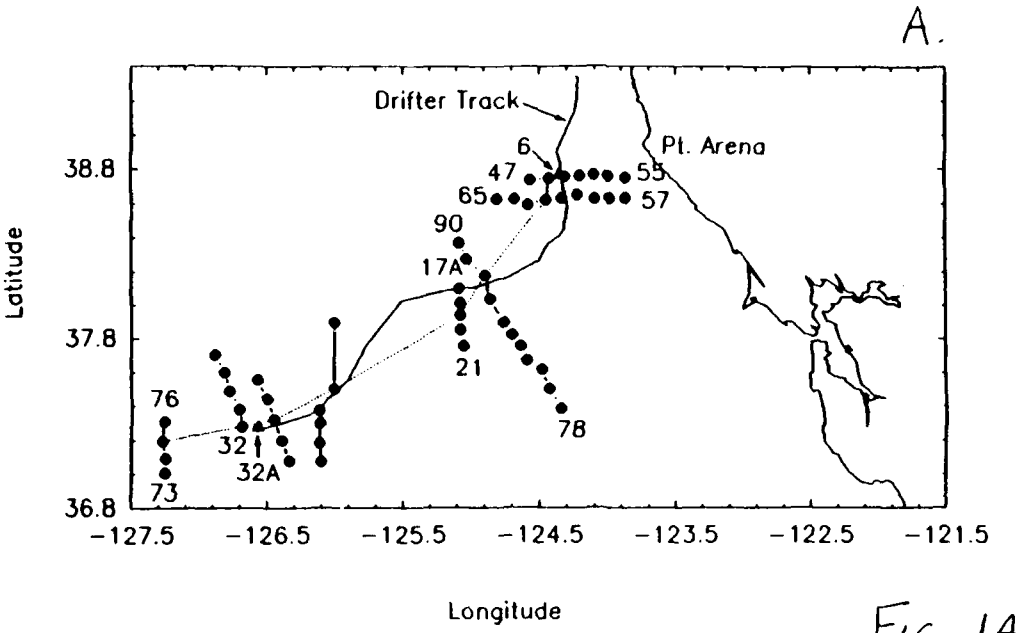
A.
Drifter Track
Pt. Arena
6
47
55
65
57
90
17A
21
76
78
32
32A
73
Latitude
Longitude

FIG. 14

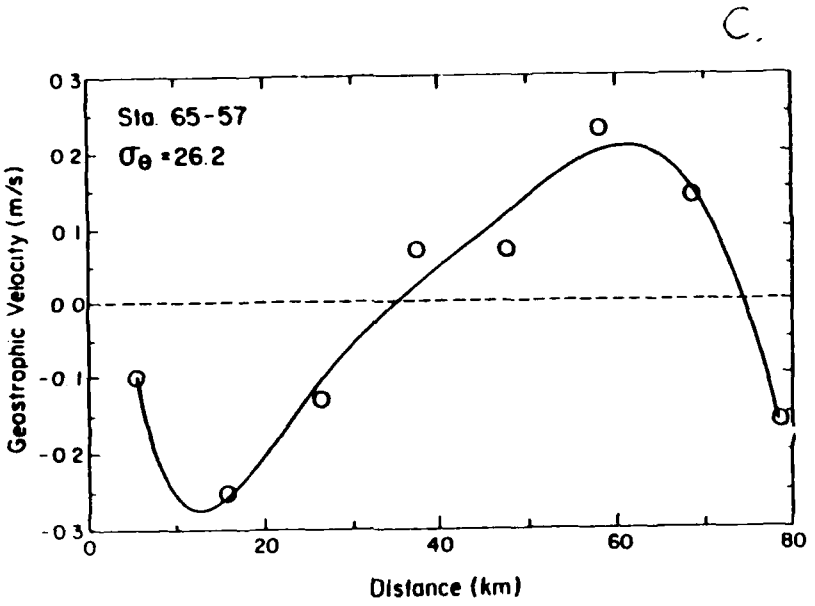
C.
Sta. 65-57
σ_θ = 26.2
Geostrophic Velocity (m/s)
Distance (km)

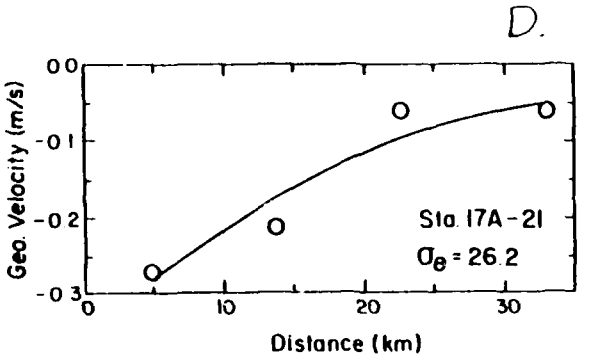
D.
Sta. 17A-21
σ_θ = 26.2
Geo. Velocity (m/s)
Distance (km)

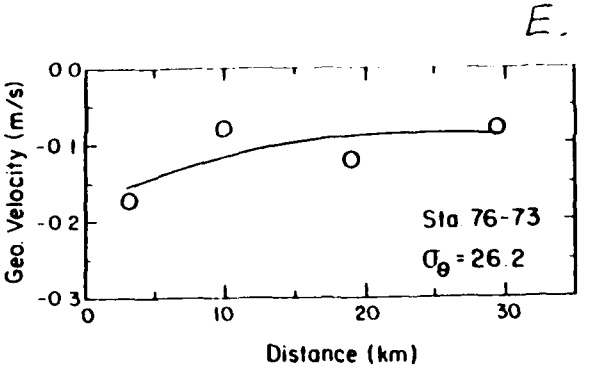
E.
Sta. 76-73
σ_θ = 26.2
Geo. Velocity (m/s)
Distance (km)

Evidence of Subduction Within Cold Filaments of the N. California Coastal Transition Zone

David C. Kadko[1], Libe Washburn[2] and Burton Jones[3]

1. College of Oceanography
Oregon State University
Corvallis, OR. 97331

2. Center for Earth Sciences
University of Southern California
University Park
Los Angeles, CA 90089-0740

3. Hancock Institute for Marine Studies
University of Southern California
Los Angeles, CA 90089-0371

April, 1990

ABSTRACT

Profiles of ^{222}Rn, chlorophyll, nutrients, oxygen, temperature and salinity taken within a cold filament observed in satellite images of the N. California Coastal Transition Zone provide evidence that there is strong vertical transport out of the surface layer by subduction processes occuring within these features. Layers of chlorophyll found below the euphotic zone have associated with them other characteristics of water that at one time had been in contact with the sea-surface including: deficiencies of ^{222}Rn with respect to ^{226}Ra, elevated oxygen concentrations, and warm water on plots of temperature and salinity. The data indicate that the subsurface maxima in chlorophyll are derived from subducted surface layers and are not produced by in-situ phytoplankton growth nor derived by particle settling. The presence of a ^{222}Rn deficiency at depth further suggests that the subducted water had been in contact with the surface within the past week, and indicates that the rate of vertical transport is approximately 25 m/d. This has important implications for the fate of the filaments and for the high primary productivity within them.

Introduction

Satellite imagery has revealed the presence of seaward oriented filaments of cold water which extend 100 - 300 km off northern California. Shipboard investigations have indicated that these features contain cold, often salty, upwelled water that have been carried well beyond the continental shelf (Flament et al, 1985; Kosro and Huyer, 1986; Rienecker and Mooers, 1989). They are associated with surface intensified cross shelf currents which attain speeds as high as 80 cm/s and extend to a depth of at least 100 m.

The coherence between temperature, nutrient, and pigment structure shown by Coastal Zone Color Scanner (CZCS) data and in-situ observations (Traganza et al, 1980; 1981; 1983) indicates that these features may be a significant factor in the transport of related features such as planktonic forms, nutrients, and other chemical tracers of coastal water into the open ocean. To assess the importance of this mode of offshore transport in the heat and mass budget, it is necessary to understand the source of these cold filaments and the fate of water within them. As part of the Coastal Transition Zone (CTZ) Program, whose aim was to investigate the nature, structure and biological processes within the cold filaments seen in satellite images of sea surface temperature, several chemical species such as ^{222}Rn, ^{226}Ra, chlorophyll, nutrients, and oxygen were measured (The Coastal Transition Zone Group, 1988). In this paper, we will describe how profiles of these constituents provide evidence that subsidence, or subduction, of surface water may be occurring within these filaments and that their circulation may therefore not be entirely horizontal. This will have important implications for the fate of the filaments, the primary and secondary production within them, and for the transport of coastal signals to the open ocean.

Background

Radon-222 is a chemically inert, radioactive gas with a half-life of 3.83 days. It is produced by decay of its parent ^{226}Ra ($T_{1/2}$= 1622 yr) within sediments and diffuses in excess of ^{226}Ra across the sediment-water interface into the bottom water. From there, this ^{222}Rn surplus travels vertically and horizontally over distances dictated by the strength of the velocity and eddy field before it decays to a background activity equal to the dissolved ^{226}Ra activity in the water column. At the sea surface, the ^{222}Rn is characteristically *deficient* relative to ^{226}Ra because of gas exchange with the atmosphere. Since no other mechanism can cause this deficiency, measurements of ^{222}Rn-^{226}Ra disequilibria in the surface ocean have been used to estimate gas exchange rates (Broecker and Peng, 1971; Broecker and Peng, 1974; Peng et al 1979). The presence of a ^{222}Rn deficiency deeper in the water column would therefore suggest sinking of water which previously had been in contact with the surface, and which has resided in the deeper water for less than about a week (the time required for ^{222}Rn to regain equilibrium with ^{226}Ra). Associated with deficiencies of ^{222}Rn would be other tracers of water derived from the surface, including chlorophyll in areas of significant productivity, high oxygen, and warm water on plots of temperature and salinity. Relative to the rate of ^{222}Rn re-equilibration, the persistence of the surface derived signal in chlorophyll would depend on the rates of phytoplankton sinking, grazing, respiration and death, and in oxygen on the rate of net community respiration.

Preliminary measurements, as part of a pilot study, were made in 1987. During the period 15 June - 28 June 1987 on the R/V Pt. Sur enhanced levels of fluorescence and chlorophyll, and low ^{222}Rn activities, were measured as deep as 100 m below the sea surface. Unfortunately, the ^{222}Rn and chlorophyll measurements were performed on separate casts, but the data in total suggested the possibility that surface water, characteristically rich in chlorophyll and deficient in ^{222}Rn, was in some instances subsiding within the filament. The pilot program was followed by a much larger field experiment in 1988 which concentrated on a region near Point Arena (Fig 1). It involved three ships and included mapping of the current, hydrographic, nutrient and particle fields from late June through August. Additionally, Lagrangian drifters were deployed in filaments so that parcels of water could be followed and aging processes within the features monitored. This paper will describe sampling that occurred during these operations on the R/V Washington from June 24 - July 23 1988.

Methods

Samples for ^{222}Rn analysis were drawn into 20-liter evacuated glass carboys. The radon is removed from seawater by bubbling helium through the sample and is collected on activated charcoal columns immersed in a dry ice/1-propanol bath (-78°C). The column is then heated and the radon is transferred into an evacuated scintillation cell which is then placed into a photomultiplier tube counting system (Mathieu et al.1988). The largest uncertainty in the analysis is the efficiency of the counting cell which is calibrated against known ^{226}Ra standards. This uncertainty along with statistical counting errors result in a total analytical uncertainty of 8%. The ^{222}Rn, temperature-salinity, and nutrient data, along with chorophyll and O_2 analyses (provided by Dr.T. Hayward, Scripps) are shown in Table 1. Several samples were acidified after the ^{222}Rn analysis and stored for later transport to the OSU laboratory for determination of the ^{226}Ra activity (Table 2). This is accomplished by successive milkings and counting of the ingrown daughter ^{222}Rn from which the ^{226}Ra activity can be calculated.

Results and Discussion

Radium-226

To evaluate ^{222}Rn profiles for the presence of deficiencies resulting from gas exchange, it is necessary to define the activity of ^{226}Ra, which would be the equilibrium activity of ^{222}Rn were there no loss to the atmosphere. Typically, studies of air-sea interaction using ^{222}Rn are confined to the mixed layer because deficiencies in this short lived isotope cannot be mixed deeper than the upper thermocline barrier. In these cases, a single value of ^{226}Ra can be used to define the equilibrium activity because chemical properties are fairly uniform within the mixed layer.

To derive the equilibrium ^{222}Rn activity in their study of gas exchange, Peng et al (1979) established empirical ^{226}Ra-Si relationships for upper thermocline waters from GEOSECS data to estimate the ^{226}Ra activity of the surface mixed layer. The ^{226}Ra activities of submixed layer water with higher Si were simply normalized to the low, *uniform* Si concentration of the mixed layer (< 1mM) and this result served as the mixed layer equilibrium ^{222}Rn activity for the stations where ^{226}Ra was not measured.

In an area such as the CTZ site however, a mixed layer may not be well developed within freshly upwelled waters and therefore intense temperature and chemical gradients often exist quite close to the sea surface. In this highly productive region, enhanced chemical scavenging associated with a

large particle flux (cf Bishop, 1988a) likely contributes to such gradients. Therefore, a single value of ^{226}Ra cannot represent the equilibrium ^{222}Rn activity and vertical profiles of ^{226}Ra with which the ^{222}Rn measurements can be compared must be ascertained. In this work, we therefore established an empirical ^{226}Ra-nutrient relationship and derived ^{226}Ra profiles from the nutrient measurements for those stations where ^{226}Ra was not directly analyzed.

In figure 2 ^{226}Ra is plotted against NO_3, SiO_4 and salinity. These samples were taken from several different stations in 1987 and 1988 and all were collected within the upper 200 m of the surface (Table 2). The large variability of chemical properties among stations is apparent. The horizontal variability and significant vertical gradient in chemical properties from this area within the upper 200 m is further illustrated by the example shown in Figure 3, where chemical profiles from two stations occupied across a filament transect are plotted.

The ^{226}Ra-Si plot of figure 2 shows a great deal of scatter (as did the plots of Peng et al, 1979). The ^{226}Ra-NO_3 relationship is far better. This might indicate that ^{226}Ra uptake and removal from surface waters is associated not with opal tests but rather with soft part debris. Additionally, the ^{226}Ra-nutrient pattern in Figure 2 is similar to that observed for Ba, which is a chemical analog of ^{226}Ra (Collier and Edmond, 1984). As with ^{226}Ra in this study, dissolved Ba concentrations in surface waters have been shown to be in excess of values which would be predicted by correlations with nutrients established for deeper water. It has been suggested therefore that Ba is removed from the upper ocean *below* the zone of nutrient depletion by a mechanism involving barite formation in decomposing organic material (Chow and Goldberg, 1960; Collier and Edmond, 1984; Bishop,1988b). The observation that suspended particulate matter display subsurface enrichments in Ba supports the notion that uptake of this element occurs below the depth of nutricline establishment.

In the CTZ area, the ^{226}Ra correlates well with NO_3 for most samples but is in excess of NO_3 for surface waters which are characterized by low density (< 25.2), low salinity (<33.0), and low Si and NO_3 concentrations (<1μM) more typical of open ocean surface waters that display higher Ba for a given nutrient concentration (Collier and Edmond, 1984). This is apparent at Station 86 where in the upper 40 m the measured ^{226}Ra is much higher than that predicted by the NO_3 concentration (Fig.3). Below 40 m however, the ^{226}Ra and NO_3 are well correlated where the density > 25.2, salinity >33.0 and NO_3> 8 μM. In some instances, water with these properties outcrops in the CTZ and the ^{226}Ra-NO_3 relationship appears to hold all the way to the surface. For example, station 83 (Fig 3), south of the filament, and station 59 (Fig. 4), in the northward flowing section of an anticyclonic eddy adjacent to the filament feature, had surface salinities > 33.2 and NO_3 concentrations > 5 μM. The ^{226}Ra profiles derived from the NO_3 coincide almost exactly with the ^{222}Rn profiles indicating that little gas exchange has occurred. This is particularly true for station 59, where in addition, the relatively limited degree of oxygen supersaturation and a relatively small near-surface chlorophyll maximum imply that the water had only recently been upwelled. Under these circumstances low surface ^{222}Rn is strictly the result of the ^{226}Ra gradient and not gas exchange. Neglecting to account for the ^{226}Ra gradient would in fact suggest an apparent loss of ^{222}Rn and lead to an overestimate of the gas exchange rate. Subduction of water with these characteristics would therefore be manifested by a ^{222}Rn

minimum (but no deficiency). Other examples of this will be illustrated in the following sections.

Water mass characteristics

Figure 5 shows the map of surface salinity for the CTZ study area during the period 6-12 July. The high velocity feature is marked by a broad salinity minimum of <32.6 (Huyer et al, in prep). The ^{226}Ra-NO_3 relationship established here holds for water with S >33.0, NO_3> 8 µM, and density >25.2 found *below* this low salinity layer. The ^{226}Ra-NO_3 correlation is analogous to that observed between Ba (or ^{226}Ra) and Si in submixed layer waters reported elsewhere (Collier and Edmond, 1984; Peng et al 1979). The lower salinity water which characterizes the filament surface (eg station 86, Fig.3) represents another end-member and has very low NO_3 concentrations, a density < 25.2 and is marked by high ^{226}Ra/nutrient and ^{226}Ra/S ratios. Figure 6 shows various property-property plots within the upper 200 m from stations collected while following a drifter along the filament (discussed below) during this time period. It is apparent that the properties display a change in slope at the same salinity and density where the ^{226}Ra-NO_3 relationship terminates. Where the low salinity filament surface water overides the higher salinity water ^{222}Rn values may actuall, increase to the surface (again, see station 86) because of the high ^{226}Ra values. This is contrary to the more typical situation where, because of gas exchange, low ^{222}Rn values are observed.

The thickness of the low salinity, low density surface layer is not uniform in this area. Figure 5b shows that the underlying high salinity water outcrops near the coast in the zone of upwelling. Figure 5d further shows that the depth of the 25.8 density surface, which is in the center of the σ_θ range for which the ^{226}Ra-NO_3 relationship is defined, is also quite shallow near shore (< 20 m) and deepens steeply through the filament feature.

Drifter stations

As part of the R/V Washington experiment, we collected water sample profiles while following an instrumented drifter (which was drogued at 5 m) along a filament path during the period 4-10 July, 1988. The drifter initially followed a southward course, but on July 6 the drift changed to a more southwestward direction (Drifter #1 in Figs.1 and 5). Because of significant vertical shear in the jets (Kosro and Huyer, 1986) the surface drifter is not tracking the movement of a vertically coherent water mass but rather the direction of the surface flow; the "age" of surface water is most likely different from that of deeper water.

In figure 7a-h, vertical profiles of chlorophyll, ^{222}Rn, ^{226}Ra (derived from the NO_3 profile using the least squares fit of Figure 2a), O_2, fluorescence, T and S are plotted for the drifter stations 2,4,11A, 6A, 17A, 15, 22A and 27A respectively. The T-S plot for each station is aiso shown. Stations 2, 4, and 11A along the southward segment of the drifter track show layers of fluorescence and chlorophyll as deep as 150 m which is well below the euphotic zone in this environment, as defined by the 1% light level determined by a PAR (Photosynthetically Available Radiation) sensor (Table 3). In each case, there is a corresponding deficiency of ^{222}Rn with respect to the NO_3-derived ^{226}Ra profile for bottle sample depths above 110 m which were within the range of the ^{226}Ra-NO_3 correlation (S > 33.0 and density > 25.2). Otherwise, the ^{222}Rn is at, or close to equilibrium with the ^{226}Ra activity. For stations 2 and 4, there are also layers of high chlorophyll and fluor-

escence deeper than 110 m, with no corresponding ^{222}Rn deficit. In these latter cases, the water masses have likely been at depth long enough for the ^{222}Rn-^{226}Ra equilibrium to be re-established. Evidently, the persistence time for the phytoplankton (and the corresponding chlorophyll and fluorescence signals) in these deep layers is greater than 1 week. At stations 4 and 11A, an O_2 maximum (O_2 was not measured at station 2) was also observed at the same depth of the ^{222}Rn deficiency and the high chlorophyll feature. Each of these signals are characteristic properties of near surface water. On the T-S plots, this layer appears as a saline, warm feature. It is interpreted as upwelled water which lost ^{222}Rn from gas exchange, gained O_2 from gas exchange and photosynthesis, warmed through solar heating, and gained phytoplankton biomass before sinking within the filament structure. The subducted feature is associated with S >33.2 and density >25.6, with this density horizon deepening seaward from station 2 to 4 then 11A. This is also seen in Figure 5d.

Station 6A, along the southward section of the drifter track, displayed a thin layer of high fluorescence and chlorophyll at about 60 m and density of approximately 25.6 which again corresponded to a warm saline feature on the T-S diagram and to an O_2 maximum. This coincided with a minimum in the ^{222}Rn profile, but not a deficiency relative to the derived ^{226}Ra activity. This might reflect the presence of water which initially was at the surface and has resided at depth for a period greater than the mean life of ^{222}Rn. Alternatively, this could represent sinking of water with the characteristics of station 59 (Fig.4) discussed earlier, where there was insufficient gas exchange to affect a ^{222}Rn deficiency. At a depth of about 155 m, corresponding to density 26.38, a small peak of fluorescence and chlorophyll and a slight ^{222}Rn deficiency was observed which might be indicative of an older parcel of subducted surface water.

The relationships observed at the earlier stations are not as apparent in the stations collected after the drifter turned to the southwest. This might reflect filament aging processes (eg ^{222}Rn ingrowth, phytoplankton loss, turbulent mixing) or different source water (containing different ^{226}Ra-NO_3 and T-S properties, for example). For station 17A the ^{222}Rn generally follows the derived ^{226}Ra profile for densities >25.6. At 150 m, corresponding to density 26.1, a ^{222}Rn deficiency and a slight maximum of O_2 is observed. There is substantial fluorescence at this depth and warming indicated on the T-S diagram (Fig. 7e). This is suggestive of a subducted feature. Station 15, which was slightly off the drifter track displays a very clear peak of deep chlorophyll and fluorescence between 57 and 122 meters which corresponds to a distinct warming trend on the T-S plot. There is the suggestion of an oxygen maximum at this depth but no apparent signal from the radon data. Station 22A shows a broad chlorophyll and fluorescence signal to a depth of approximately 100 m depth which is marked by low nutrients and salinity and appears to be the surficial layer which characterizes the filament. It is quite deep at this station. The 25.8 density horizon is deep, at 126 m, and does not show evidence of recent contact with the sea surface. Station 27A is the most seaward of the drifter #1 stations at which ^{222}Rn data were collected. There is a distinct, deep chlorophyll and fluorescence layer at approximately 120 m which coincides with a warmer saline feature on the T-S diagram at approximately the 25.8 density surface as was observed in the initial drifter profiles. However, this signal is not seen in the oxygen profile and the ^{226}Ra-NO_3 relationship does not appear to hold for this station.

Stations 46-72

A second series of stations were occupied near the axis of the feature as defined by a second drifter deployment starting on July 13 (Fig 1). There was no evidence of subduction at nearshore station 46 (Fig 8a) where the 25.8 density horizon was only about 20 m deep, approximately the depth of the euphotic zone. There was a large chlorophyll maximum at the surface corresponding to a substantial deficiency in ^{222}Rn and to a large (110%) supersaturation in oxygen. Further offshore and down the filament axis at station 62 (Fig 8b), the 25.8 density surface was deeper, at approximately 30 m, and there was a subsurface deficiency of ^{222}Rn. This corresponded to a chlorophyll maximum suggesting a subducted layer, although there was no corresponding maximum in O_2. The surface water of this station is not depleted in NO_3 however and the chlorophyll values are relatively low, suggesting that photosynthetic production of chlorophyll and O_2 were not far along before subduction occurred.

Station 67 was approximately 200 km down the drifter track and the 25.8 density surface, at 126 m, was much deeper than the previous stations (Fig 8c). This horizon corresponded to a deep chlorophyll maximum, to a ^{222}Rn minimum and to a slightly warmer saline feature on the T-S diagram. The ^{222}Rn minimum layer may have been derived from surface water with characteristics described for station 59, that is, manifesting a steep nutrient gradient and no ^{222}Rn deficiency. The subducted feature was overidden by the less saline, nutrient poor layer described earlier. Station 69 (Fig. 8d) was about 250 km down the drifter track and the 25.8 density surface was at 141 m. There was no apparent evidence of a subducted layer at or below that depth. Between 45 and 100 m however, there was a broad salinity minimum within which were a chlorophyll maximum at 76 m and an O_2 maximum at 55 m. This feature was above the range of the ^{226}Ra-NO_3 correlation but ^{226}Ra was measured directly at this station. At the depth of the chlorophyll maximum and at the minimum salinity (32.767) there is a maximum of ^{226}Ra which in effect produces a sharp deficit in ^{222}Rn. An inspection of Figure 2c indicates that low salinity surface water of this region is characterized by high ^{226}Ra. The data suggest therefore that *low* salinity, high ^{226}Ra water had in this case subducted, and that the ^{222}Rn had yet to establish equilibrium. There is no obvious explanation for the lack of correspondence between the O_2 maximum and the ^{226}Ra and chlorophyll maxima however. It appears that station 69 is unique in that subduction of *more* saline waters has been described up to this point. This implies a different source of water for the subducted layer at this particular station.

Summary and Conclusions

Profiles of ^{222}Rn, chlorophyll, oxygen, nutrients, temperature and salinity taken within a cold filament seen in satellite images off Pt. Arena, California provide evidence which suggest that subduction of surface water is occurring within these features. Layers of chlorophyll found below the euphotic zone have associated with them other characteristics of water that at one time had contact with the sea-surface including: deficiencies of ^{222}Rn, elevated oxygen concentrations, and warm water on plots of temperature and salinity. Of these, ^{222}Rn is the least ambiguous indicator of subduction because of its inert nature. However, its application is complicated in the CTZ region because there are substantial activity gradients of its parent ^{226}Ra in the surface water. To our knowledge, this is the first reported instance of such gradients in the surface ocean. It has been suggested that removal of ^{226}Ra from surface waters is enhanced by

scavenging processes associated with high particle flux (Bishop, 1988a). In regions of strong upwelling, where additionally there may be a minimal mixed layer, near surface ^{226}Ra gradients might be common. Failure to recognize this (i.e. assuming a constant ^{226}Ra activity in the upper ocean) would lead to gross overestimates of gas exchange by the $^{222}Rn/^{226}Ra$ disequilibrium method. In order to analyze the ^{222}Rn data we derived a ^{226}Ra - NO_3 relationship which enabled the derivation of vertical profiles of ^{226}Ra for the stations where ^{226}Ra was not directly measured. This procedure appeared to hold for most of the stations that were studied. Uncertainties inherent in the ^{222}Rn measurement and the ^{226}Ra-NO_3 correlation however would preclude establishing the presence of a subducted layer based on a ^{222}Rn deficiency alone. Therefore, deficiencies of ^{222}Rn only in association with anomalies in other measured properties were deemed significant.

In 1982 another filament was surveyed which had several similarities to the feature described in this work (Flament et al, 1985). In both cases, the offshore flow of the filament appeared to originate on the continental shelf to the north of Point Arena (see Fig. 5a). Flament et al, 1985 presented evidence based on T-S characteristics that more saline water to the south of the filament was subducted under this northern, less saline water which comprised the filament surface. The authors of that work further suggested that the subduction was possibly forced by a convergence at the front where the filament and southern water met.

A nearshore source of subducted water in our data is supported by the observation that the subducted layers have high salinities found to outcrop near the coast, and that no ^{222}Rn deficiencies are found at any station seaward of station 17A (with the exception of station 69 which might have a different source). Based on either the maximum or mean geostrophic velocities along the filament, and assuming that subduction out of the surface layer occurs off Pt. Arena, a time scale of 5-10 days is calculated for transport along the 26.1 density surface to where the ^{222}Rn deficiency is noted (Fig 7e, Washburn et al, in prep.). This time scale is consistent with the mean life of ^{222}Rn.

Flament et al 1985 estimated a downwelling velocity of about 9 m/d using assumptions of subducted layer thickness and length of the convergence region. By considering the ^{222}Rn deficit in the deep chlorophyll maxima we can also estimate a downwelling velocity. Using station 17A as an example, we divide the depth of the deep chlorophyll maximum by the mean life of radon : 150 m/ 5.5 d to derive a rate of approximately 27 m/d.

The evidence presented here suggests that the sub-euphotic maxima in chlorophyll are derived from subducted surface layers and not produced by in-situ phytoplankton growth nor derived by particle settling. The occurence of a ^{222}Rn deficiency with these maxima suggest that the water had been in contact with the sea surface within the past week, requiring downwelling velocities much greater than the phytoplankton sinking rates of < 2m/d determined in an upwelling region off of Pt. Conception, California (Bienfang,1985). Subsurface chlorophyll maxima have been observed before in the Northeast Pacific but have been attributed to adaptation of phytoplankton cells to low light by an increase in their chlorophyll content (Anderson, 1969). This has led to the suggestion that a subsurface oxygen maximum near the depth of these chlorophyll layers is the result of deep photosynthesis (Anderson, 1969). Others however have suggested that offshore advection and subsequent sinking of coastal upwelled water, enriched in oxygen by photosynthesis at the surface, may be responsible for

the observed maxima in oxygen (Stefansson and Richards, 1964). It is conceivable that both processes occur, that is, phytoplankton in surface water photosynthetically enriched in oxygen would, upon subduction, respond to lower light by increasing the cellular chlorophyll content and over time contribute to the oxygen maximum by further photosynthesis. However, in the profiles from the CTZ discussed here the ^{222}Rn deficiencies indicate that the subduction must occur rapidly, and consequently the observed oxygen maxima had to have been derived from the surface.

Acknowledgements

The authors wish to thank Dr. T. Hayward for providing the oxygen and chlorophyll data presented here. Dr. J. Huyer kindly provided the maps for Figure 5. This work was supported by the Office of Naval Research.

References

Anderson G.G., Subsurface chlorophyll maximum in the Northeast Pacific Ocean, Limnol. Oceanogr. 14, 386-391, 1969.

Bienfang P., Sedimentation of suspended microparticulate material in the Point Conception upwelling ecosystem, a technical report of research performed during the 1983 OPUS II fieldwork, The Oceanic Institute, Waimanalo, Hawaii, 24pp, 1985.

Bishop J.K., Is the N. Atlantic south of Iceland a particulate matter hot spot?, EOS, 69, 1117, 1988a.

Bishop J.K., The barite-opal-organic carbon association in oceanic particulate matter, Nature, 332, 341-343, 1988b.

Broecker W.S. and T-H. Peng, The vertical distribution of radon in the BOMEX area, Earth Planet. Sci. Lett, 11, 99-108, 1971

Broecker W.S. and T-H. Peng, Gas exchange rates between air and sea, Tellus, 26, 21-35, 1974.

Collier R. and J. Edmond, The trace element geochemistry of marine biogenic particulate matter, Prog. Oceanog., 13, 113-199, 1984.

Chow T.J. and E.D. Goldberg, On the marine geochemistry of barium, Geochim. Cosmo. Acta., 20, 192-198, 1960.

Flament P., L. Armi , and L. Washburn , The evolving structure of an upwelling filament, J. Geophy. Res., 90, 11765-11778, 1985.

Huyer A., J. Fleischbein , P.M. Kosro, S. Ramp, T. Stanton and L. Washburn, T-S characteristics of the Coastal Transition Zone, J. Geophys. Res (in prep)

Kosro P. M. and Huyer A., CTD and velocity surveys of seaward jets off Northern California, July 1981 and 1982, J. Geophys. Res., 91, 7680-7690, 1986.

Mathieu G.G., P.E. Biscaye, R.A. Lupton and D.E. Hammond, System for measurement of ^{222}Rn at low levels in natural waters, Health Phy., 5, 989-992, 1988.

Peng T-H.,W.S. Broecker, G.G Mathieu and Y-H. Li, ^{222}Rn evasion rates in the Atlantic and Pacific oceans as determined during the GEOSECS program, J. Geophys. Res., 84, 2471-2486, 1979.

Rienecker M. M. and Mooers C .N. K., Mesoscale eddies, jets and fronts off Point Arena, California, July 1986, J. Geophys. Res., 94, 12,555-12,569, 1989.

Stefansson, U. and Richards F.A., Distributions of dissolved oxygen, density and nutrients off the Washington and Oregon Coasts, Deep Sea Res., 11, 355-380, 1964.

The Coastal Transition Zone Group. The Coastal Transition Zone Program, EOS, 69, 698-699, 704-707, 1988.

Traganza E.D., Nestor D.A. and McDonald A. K., Satellite observations of a nutrient upwelling off the coast of California, J. Geophys. Res., 85, 4101-4106, 1980

Traganza E.D., J. C. Conrad and L. C. Breaker, Satellite observations of a cyclonic upwelling system and giant plume in the California Current, in Coastal Upwelling, F.A. Richards ed American Geophysical Union, Washington D.C. 229-241, 1981

Traganza E.D., Silva V.M., Austin D.M., Hanson W.L., and Bronsink, S.H., Nutrient mapping and recurrence of coastal upwelling centers by satellite remote sensing: its implication to primary production and the sediment record, in Coastal Upwelling Part A, E. Suess and J. Thiede ed, Plenum Press, New York, 61-83, 1983.

Washburn L., D.C. Kadko and B. Jones, Water mass subduction in a coastal upwelling system, J. Geophy. Res. (in prep).

TABLE 1
Analytical Data for ^{222}Rn Stations

TATION	PRESSURE (db)	CHLOR. (µg/L)	Salinity (psu)	Pot.Temp (°C)	Sig.Theta Potential Density	SiO4 (µM)	NO3 (µM)	Rn222 (dpm/100L)	O_2 (ml/L)	O_2 (% Sat
2	1.9	6.948	32.966	10.680	25.248	1.83	4.86	NA		
	7.0	9.241	33.104	10.331	25.416	2.14	9.36	NA		
	12.6	8.894	33.151	10.184	25.478	2.54	10.61	7.08		
	21.6	5.663	33.149	9.985	25.510	4.00	12.56	7.25		
	42.6	9.888	33.528	9.950	25.812	4.54	15.78	6.62		
	61.6	6.288	33.660	9.389	26.007	6.17	18.36	7.09		
	82.6	6.254	33.684	9.185	26.058	7.49	19.74	6.80		
	102.6	9.485	33.776	8.878	26.179	8.72	20.90	9.56		
	132.6	11.536	33.813	8.728	26.232	10.32	22.01	10.30		
	205.6	0.057	34.005	7.365	26.584	19.02	31.85	10.53		
4	1.6	6.097	32.748	11.037	25.017	0.61	3.08	NA		
	12.6	5.768	32.752	10.915	25.041	0.54	3.78	7.22	6.59	105.0
	23.6	4.834	32.758	10.406	25.134	1.65	5.91	8.10	6.6	104.4
	41.6	4.614	33.274	9.917	25.619	4.79	15.25	9.30	6.25	98.5
	61.6	7.636	33.467	10.031	25.750	4.77	16.77	8.37	5.53	86.2
	82.6	7.031	33.554	9.834	25.851	5.64	17.99	8.02	5.84	91.6
	102.6	6.702	33.626	9.445	25.971	7.52	20.26	9.00	5.74	89.7
	126.6	6.152	33.781	8.986	26.166	9.54	22.60	9.41	5.23	81.0
	202.6	0.046	33.718	7.276	26.371	18.49	32.99	11.20	5.07	77.3
	502.6	0.020	34.156	5.160	26.988	37.77	46.01	NA	2.93	43.2
									0.57	8.0
6A	1.9	6.043	32.878	11.303	25.070	0.01	4.64	NA	6.64	107.2
	12.6	6.207	32.909	11.016	25.145	0.27	5.82	6.89	6.56	105.2
	23.6	6.372	32.915	10.700	25.206	0.65	6.96	7.55	6.37	101.0
	43.6	4.152	33.037	10.133	25.397	2.45	10.72	13.30	5.88	92.5
	62.6	10.712	33.337	10.399	25.586	1.15	12.55	8.20	6.37	100.7
	81.6	4.152	33.312	9.541	25.710	5.41	17.65	8.64	5.17	79.8
	102.6	0.080	33.536	8.941	25.981	9.18	23.37	9.58	3.97	60.9
	155.6	0.203	33.859	7.963	26.384	16.33	30.72	9.67	3.46	52.2
	201.6	0.054	33.952	7.363	26.543	17.24	31.77	10.88	3.01	44.6
	503.6	0.064	34.152	5.204	26.979	36.89	45.05	NA	0.67	9.5
11A	2.5	3.648	32.715	11.609	24.887	1.52	2.13	NA	6.62	106.9
	12.6	3.474	32.718	11.562	24.898	1.46	2.18	8.67	6.64	106.7
	21.6	3.891	32.771	11.186	25.008	1.49	2.96	8.32	6.61	105.2
	43.6	5.493	32.844	10.722	25.146	1.74	5.60	6.80	6.37	101.1
	62.6*									
	80.6	0.130	33.242	9.784	25.616	6.48	16.51	8.63	4.72	73.4
	109.6	2.554	33.550	9.313	25.933	7.71	19.80	8.08	4.96	76.2
	150.6	0.240	33.842	8.355	26.312	12.90	27.88	10.10	3.23	48.9
	202.6	0.068	33.977	7.602	26.529	15.91	30.24	11.09	3.11	46.4
	505.6	0.054	34.223	5.713	26.975	32.49	42.93	NA	0.52	7.4

TABLE 1 (Cont.)

ATION	PRESSURE (db)	CHLOR. (ug/L)	Salinity (psu)	Pot.Temp (°C)	Sig.Theta Potential Density	SiO4 (uM)	NO3 (uM)	Rn222 (dpm/100l)	O2 (ml/l)	O2 (% Sat)
15	2.6	2.43	32.799			0.51	2.15	NA	6.42	103.2
	12.6	2.52	32.766			0.53	2.13	7.98	6.64	106.7
	22.6	3.283	32.825			0.31	2.69	8.96	6.53	104.4
	42.6	5.713	33.105			1.95	9.64	8.50	5.91	93.7
	62.6	2.015	33.437			5.67	15.72	NA	5.55	86.7
	83.6	2.328	33.503			6.35	17.24	8.46	5.41	84.5
	103.6	2.536	33.539			6.69	17.52	9.24	5.29	82.4
	153.6	0.769	33.808			12.81	26.87	9.60	3.33	50.6
	202.6	0.302	33.963			15.53	29.14	11.83	2.76	41.4
	503.5	0.029	34.151			33.72	40.87	NA	0.64	9.1
17A	3.6	0.950	32.660	13.320	24.518	0.61	0.22	NA		
	12.6	0.994	32.659	13.308	24.520	0.56	0.28	5.34	6.31	
	23.6	1.737	32.727	11.851	24.853	0.49	1.11	4.89	6.32	104.6
	41.6	2.675	32.842	10.501	25.183	1.93	6.72	9.03	6.51	104.9
	63.6	1.859	33.161	10.428	25.444	2.58	10.15	7.84	6.12	96.5
	83.6	3.075	33.272	10.250	25.561	4.19	13.93	7.52	6	94.6
	101.6	2.710	33.552	9.797	25.856	8.04	19.59	9.84	5.63	88.4
	151.6	1.355	33.754	9.233	26.106	11.16	24.25	8.33	5.18	80.9
	202.6	0.319	33.956	7.984	26.457	16.04	30.88	10.70	4.78	74.1
	500.6	0.024	34.166	5.451	26.961	35.62	44.13	NA	2.85	43.0
22A	2.3	1.219	32.684	13.280	24.544	0.54	0.30	NA	0.63	8.9
	12.6	1.143	32.684	13.293	24.542	0.61	0.21	5.55		
	23.6	1.038	32.690	12.928	24.619	0.61	0.24	6.25		
	43.6	1.338	32.703	11.248	24.944	0.89	1.50	8.96		
	63.6	1.187	32.737	10.785	25.052	1.78	3.79	9.10		
	80.6	1.633	32.797	10.596	25.132	1.99	5.35	9.00		
	104.6	0.125	33.210	10.282	25.507	5.39	14.29	10.39		
	151.6	0.013	33.754	8.487	26.222	12.15	26.48	10.07		
	202.6	0.066	33.993	7.979	26.486	16.71	31.78	10.94		
	504.6	0.049	34.135	5.147	26.973	36.99	44.34	NA		
27A	3.2	0.676	32.685	13.284	24.545	0.43	0.30	NA	6.35	106.4
	13.6	0.703	32.678	13.252	24.545	0.19	0.03	6.16	6.36	106.6
	23.6	0.764	32.643	12.416	24.681	0.15	0.01	7.67	6.5	107.8
	44.6	0.939	32.647	11.732	24.812	0.34	0.21	9.00	6.56	107.2
	64.6	0.262	32.972	11.093	25.181	NA	NA	NA	2.1	33.7
	84.6	0.912	33.242	10.167	25.552	4.11	12.81	9.08	5.6	88.1
	110.6	2.223	33.531	9.782	25.841	8.03	19.66	9.51	4.94	77.9
	150.6	0.202	33.818	8.455	26.278	13.19	28.52	9.43	3.07	46.7
	203.6	0.076	33.993	7.765	26.517	16.60	31.44	9.68	2.48	37.1
	504.6	0.038	34.211	5.397	27.004	34.41	42.78	NA	0.48	6.8
46	2.5	7.609	33.418	12.005	25.360	1.05	9.08	NA	6.96	112.8
	13.6	9.971	33.480	10.790	25.630	1.52	11.13	4.86	6.83	109.1
	21.6	10.877	33.576	10.099	25.824	2.34	13.72	6.60	6.41	101.4
	42.6	6.670	33.747	9.167	26.111	7.02	20.97	7.34	4.96	76.7
	61.6	2.154	33.765	8.756	26.190	11.48	25.69	9.26	3.96	60.5
	82.6	0.379	33.851	8.361	26.317	14.74	29.83	10.95	3.12	47.3
	102.6	0.102	33.897	8.084	26.396	16.00	31.74	10.45	2.81	42.4
	152.6	0.050	34.042	7.908	26.536	19.08	32.99	10.62	2.03	30.5
	203.6	0.050	34.033	7.333	26.611	20.31	33.23	11.60	2.3	34.1
	463.6	0.026	34.206	6.072	26.916	33.16	41.32	NA	0.61	8.8

TABLE 1 (Cont.)

ATION	PRESSURE (db)	CHLOR. (ug/L)	Salinity (psu)	Pot.Temp (°C)	Sig.Theta Potential Density	SiO4 (uM)	NO3 (uM)	Rn222 (dpm/kg)	O2 (ml/L)	O_2 (%sat)
59	2.78	2.345	33.284	12.333	25.194	0.58	8.71	NA	6.5	106.9
	22.58	4.152	33.352	11.165	25.463	0.71	9.54	6.96	6.43	103.4
	42.81	1.099	33.456	10.050	25.738	6.23	16.99	8.70	5.17	81.2
	62.95	0.747	33.692	9.403	26.029	10.39	22.93	8.77	4.68	72.4
	79.34	0.533	33.772	9.170	26.130	11.71	24.81	9.50	4.44	68.3
	104.38	0.439	33.843	8.963	26.218	12.82	26.36	9.93	4.22	64.8
	154.62	0.302	33.912	8.574	26.333	14.67	28.82	10.98	3.37	51.4
	205.83	0.165	34.039	8.050	26.512	17.97	32.88	11.34	2.04	30.7
	507.68	NA	34.213	5.707	26.968	31.87	41.47	13.60	0.53	NA
62	11.60	0.476	33.213	12.456	25.115	0.54	4.34	7.21	6.44	107.1
	21.60	NA	33.319	11.057	25.457	1.46	7.32	7.49	6.14	NA
	42.60	1.372	33.663	9.195	26.040	8.11	18.98	6.66	4.72	73.1
	62.60	0.516	33.752	8.746	26.181	12.06	24.12	10.06	3.86	58.8
	82.60	0.478	33.803	8.642	26.237	12.37	25.52	9.20	3.7	56.4
	102.60	0.357	33.850	8.451	26.303	13.81	27.15	10.66	3.49	53.0
	152.60	0.163	33.926	7.597	26.489	16.48	28.45	11.71	3.12	46.5
	202.60	0.099	33.962	7.086	26.590	19.05	30.37	11.53	2.93	43.1
	502.60	0.069	34.189	5.121	27.018	37.21	42.97	NA	0.43	6.1
67	12.60	0.212	32.633	15.729	23.989	2.09	0.08	NA	5.92	104.1
	22.60	0.241	32.632	15.655	24.005	2.09	0.14	4.10	5.95	104.0
	33.60	0.494	32.618	14.273	24.291	1.99	0.09	6.44	6.33	107.5
	43.60	0.353	32.832	12.905	24.733	2.09	0.11	8.99	6.4	105.9
	63.60	0.742	32.864	11.363	25.048	2.26	0.31	9.39	6.44	103.2
	85.60	0.698	32.837	10.592	25.163	2.95	3.17	8.46	6.16	97.0
	116.60	1.302	33.266	9.924	25.611	6.13	13.37	7.23	5.44	85.0
	152.60	0.167	33.604	9.011	26.024	11.59	23.26	10.54	3.69	56.7
	202.60	0.096	33.897	8.112	26.391	16.99	29.46	10.97	2.82	42.5
	502.60	0.030	34.110	5.170	26.950	35.81	41.31	NA	0.94	13.2
69	0.90	0.292	32.638	15.473	24.049	1.03	0.00	NA	5.96	NA
	17.60	0.285	32.639	15.481	24.048	1.04	0.00	4.84	5.96	104.6
	32.60	0.278	32.660	15.420	24.078	1.02	0.08	5.50	5.96	104.5
	54.60	0.198	32.834	13.122	24.692	1.07	0.00	7.40	6.35	109.9
	75.60	0.928	32.767	10.468	25.130	1.91	2.86	8.08	6.29	103.0
	92.60	0.360	32.885	10.195	25.268	3.17	7.25	8.14	5.76	90.7
	115.60	0.280	33.125	9.663	25.544	6.41	15.23	10.24	4.89	76.8
	153.60	0.030	33.629	8.973	26.050	10.47	23.89	10.35	3.69	56.7
	202.60	0.054	33.916	8.083	26.411	15.15	29.56	9.60	2.87	43.4
	503.60	0.027	34.159	5.530	26.947	34.44	42.63	NA	0.63	9.0
83	12.71	0.670	33.209	13.376	24.932	0.34	5.31	5.19	6.33	107.6
	22.71	1.176	33.237	12.774	25.072	0.31	5.99	6.98	6.36	105.6
	40.48	3.822	33.305	11.397	25.385	1.03	8.83	7.08	6.19	100.7
	61.98	0.725	33.664	9.195	26.042	9.89	22.19	8.80	4.41	68.4
	82.61	0.390	33.688	8.878	26.110	10.27	22.84	8.42	4.19	64.5
	102.51*									
	153.80	0.059	33.965	7.943	26.470	15.86	29.30	9.77	2.92	43.8
	202.57	0.061	33.977	7.204	26.585	18.03	30.03	10.76*	3.15	46.6
	511.80	NA	34.228	5.306	27.027	NA	NA	NA	NA	NA

TABLE 1 (Cont.)

ATION	PRESSURE (db)	CHLOR. (ug/L)	Salinity (psu)	Pot.Temp (C)	Sig.Theta Potential Density	SiO4 (uM)	NO3 (uM)	Rn222 (dpm/100L)	O2 (ml/L)	O_2 (% Sat.
36	12.60	0.764	32.689	12.328	24.734	1.36	0.71	9.30	6.56	109.
	29.60	0.725	32.861	10.832	25.140	1.96	2.74	NA	6.17	97.
	42.60	0.632	33.071	10.904	25.291	2.93	8.64	7.22	6.05	96.
	62.60	0.478	33.266	10.536	25.507	3.53	11.65	8.35	5.85	92.
	83.60	0.054	33.361	9.180	25.807	8.57	19.70	NA	4.37	67.
	102.60	0.027	33.536	8.831	25.999	10.34	23.15	8.67	3.95	60.
	130.60	0.146	33.770	8.551	26.225	12.77	26.75	9.24	3.55	53.
	202.60	0.032	33.969	7.508	26.536	17.40	30.68	12.25+	2.97	44.
	502.60	NA	34.140	5.023	26.991	NA	NA	NA	NA	NA

*bottle mistrip
NA=not analyzed
+uncertainty >8%

TABLE 2

^{226}Ra Data - N. California CTZ

	sample	depth (m)	^{226}Ra (dpm/100l)	S	T (°C)	DENSITY	Si (µM)	NO3 (µM)
987	1-19	25	5.7 ± .2	33.2	11.88	25.15	0	3.4
	14-Rn9	20	10.4 ± .4	33.385	10.43	25.62	27.2	25.4
	23-19	20	9.3 ± .3	33.08	11.28	25.23	8.4	9.1
	31-Rn9	20	5.1 ± .3	32.546	13.39	24.4	0.3	0
	56-19	20	7.5 ± .2	33.84	9.67	26.1	20.3	19
	826-4	80	8.0 ± .3	33.435	9.855	25.755	16.1	16.9
	826-13	100	9.3 ± .3	33.6	8.8	26.05	20.3	19.7
	826-19	125	9.7 ± .3	33.823	8.15	26.33	22.7	20.6
	104-Rn4	65	11.5 ± .5	33.75	9	26.15	25.8	23.7
	104-Rn3	105	10.0 ± .4	33.9	8.4	26.34	32	27.1
988	86-Rn9	12.6	10.6 ± .2	32.689	12.33	24.734	1.36	0.71
	86-13	29.6	8.8 ± .3	32.86	10.83	25.14	1.96	2.74
	86-Rn8	42.6	9.3 ± .3	33.071	10.9	25.291	2.93	8.64
	86-4	62.6	7.3 ± .2	33.266	10.54	25.507	3.53	11.65
	86-Rn12	102.6	8.8 ± .4	33.536	8.83	25.999	10.34	23.15
	86-Rn2	130.6	10.6 ± .7	33.77	8.55	26.225	12.77	26.75
	86-Rn4	202.6	11.0 ± .6	33.969	7.51	26.536	17.4	30.68
	83-Rn12	12.71	6.5 ± .3	33.209	13.38	24.932	0.34	5.34
	83-Rn9	22.71	7.5 ± .3	33.237	12.77	25.07	0.31	5.99
	83-Rn2	40.48	11.8 ± .4	33.305	11.4	25.39	1.03	8.83
	83-19	61.98	10.8 ± .2	33.664	9.195	26.042	9.89	22.19
	83-Rn4	82.61	8.3 ± .3	33.688	8.88	26.11	10.27	22.84
	83-4*	102.51	7.1 ± .2	—	—	—	3.35	11
	83-Rn8	153.8	11.1 ± .6	33.965	7.94	26.47	15.86	29.3
	83-13	202.57	10.6 ± .3	33.765	8.41	26.24	18.03	30.03
	69-Rn9	17.6	8.7 ± .3	32.639	15.481	24.048	1.04	0
	69-Rn4	54.6	8.4 ± .3	32.834	13.122	24.692	1.03	0
	69-Rn2	75.6	11.1 ± .7	32.767	10.468	25.13	1.91	2.86
	69-Rn12	92.6	9.6 ± .2	32.885	10.195	25.27	3.17	7.25
	69-Rn8	115.6	9.8 ± 1.4	33.125	9.663	25.544	6.41	15.23
	69-4	202.6	10.6 ± .5	33.916	8.083	26.411	15.15	29.56

*mistrip, uncertain depth

TABLE 3

EUPHOTIC ZONE DEPTH ESTIMATES

Station	Z (1%) (m)	Z (0.1%) (m)	Station	Z (1%) (m)	Z (0.1%) (m)
2	22	39	46	16	25
4	28	47	59	33	57
6a	23	37	62	44	74
11a	30	46	67	61	92
17a	37	57	69	64	96
22a	47	73	83	42	61
27a	49	80	86	64	101

Figure Captions

Fig 1. Location of stations occupied by the R/V Washington during the period 4 - 21 July 1988. Stations discussed in this paper are noted by filled circles. The two drifter tracks discussed in the text are also indicated.

Fig 2. Plots of ^{226}Ra versus A) NO_3 B) SiO_4 C) Salinity for stations occupied during the R/V Pt. Sur expedition in 1987 and the R/V Washington cruise in 1988. Samples are from various depths within 200 m of the sea surface. Low salinity, high ^{226}Ra values are indicated and are excluded from the ^{226}Ra-NO_3 regression.

Fig 3. Profiles of chlorophyll, ^{222}Rn, ^{226}Ra (measured), ^{226}Ra (derived from nitrate profile), NO_3 and O_2 (% sat.)
Top: station 86. Note that for the upper 40 m, where S<33, the ^{226}Ra derived from NO_3 diverges from the measured values.
Bottom: station 83.

Fig 4. Top panel: Profiles of chlorophyll, ^{222}Rn, ^{226}Ra (derived), and O_2 (% saturation) for station 59. Middle panel: Profiles of fluorescence, T and S. Bottom panel: T-S diagram for station 59.

Fig 5. (A) Map of dynamic height relative to 500 m (B) Surface salinity (salinity minimum is shaded) (C) Temperature at 0 db (D) depth of the σ_t=25.8 density surface for the study area during the period 6 -12 July, 1988. Drifter #1 stations are shown. Maps courtesy of J. Huyer.

Fig 6. (A) Nitrate vs. salinity (B) Temperature vs. Density (C) Density vs. Salinity (D) Temperature vs. Salinity for the upper 200 m of drifter #1 stations 2,4,6A,11A,17A,22A and 27A. Arrows indicate discontinuity in the slope of each plot.

Fig 7. Top panel: Vertical profiles of chlorophyll, ^{222}Rn, O_2 (% saturation) and derived ^{226}Ra for stations occupied during the 4 - 10 July drifter experiment. The depth of the σ_t=25.8 density surface is indicated. Middle panel: Vertical profiles of temperature, salinity and fluorescence. Deep fluorescence layers corresponding to warm water on the T-S diagram are hatchured. Bottom panel: T-S plot with hatchured areas indicating the depth interval of warm water corresponding to the high fluorescence features.

Fig 8. Top panel: Vertical profiles of chlorophyll, ^{222}Rn, O_2 (% saturation) and derived ^{226}Ra for stations occupied during the 13-18 July drifter experiment. The depth of the σ_t=25.8 density surface is indicated. Middle panel: Vertical profiles of temperature, salinity and fluorescence. Deep fluorescence layers corresponding to warm water on the T-S diagram are hatchured. Bottom panel: T-S plot with hatchured areas indicating the depth interval of warm water corresponding to the high fluorescence features. Measured ^{226}Ra values are shown for station 69.

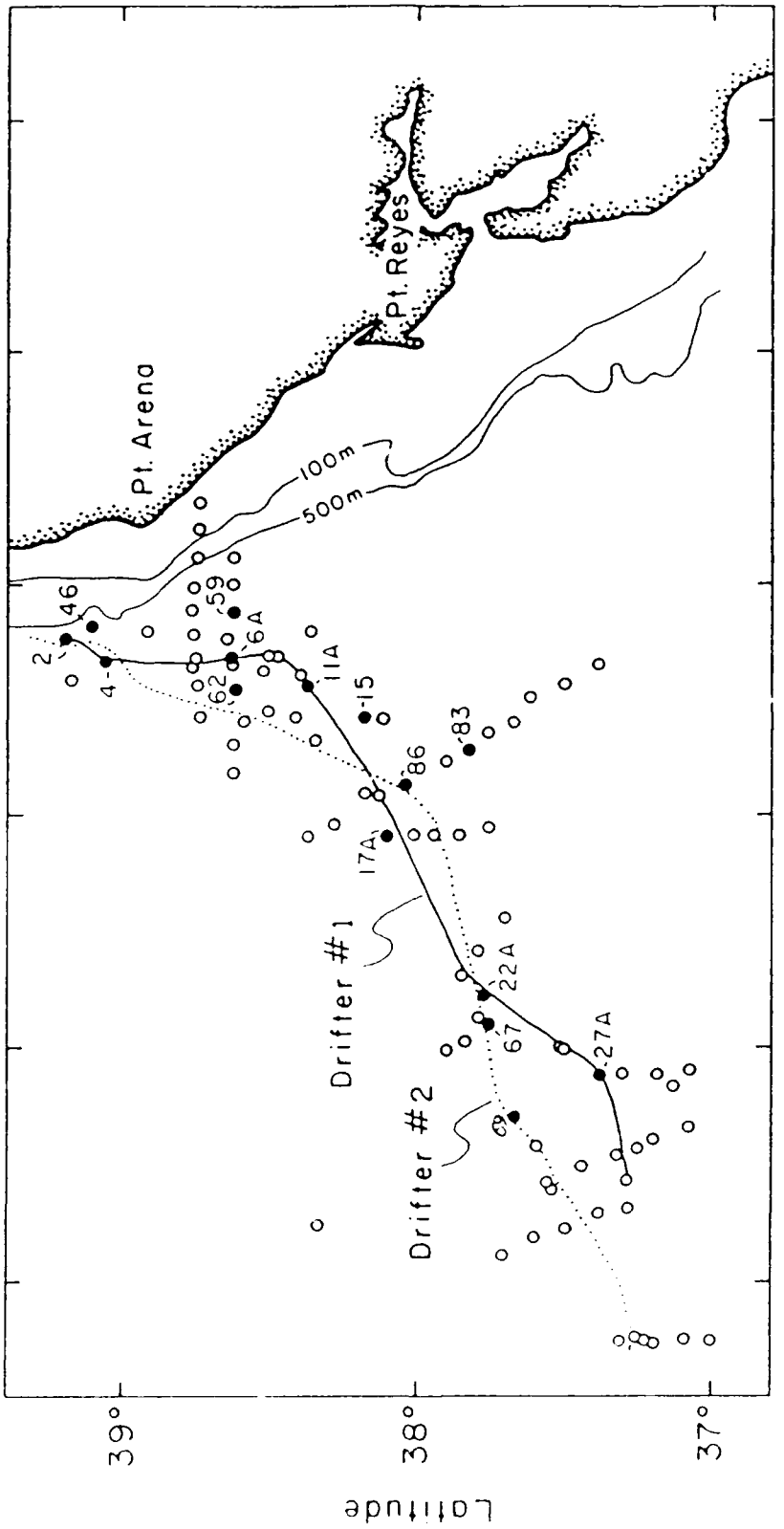
Pt. Arena
Pt. Reyes
100m
500m
Drifter #1
Drifter #2
2
4
46
59
6A
62
11A
15
83
86
17A
22A
67
27A
39°
38°
37°
127°
126°
125°
124°
123°
122°
Latitude
Longitude

Fig 2

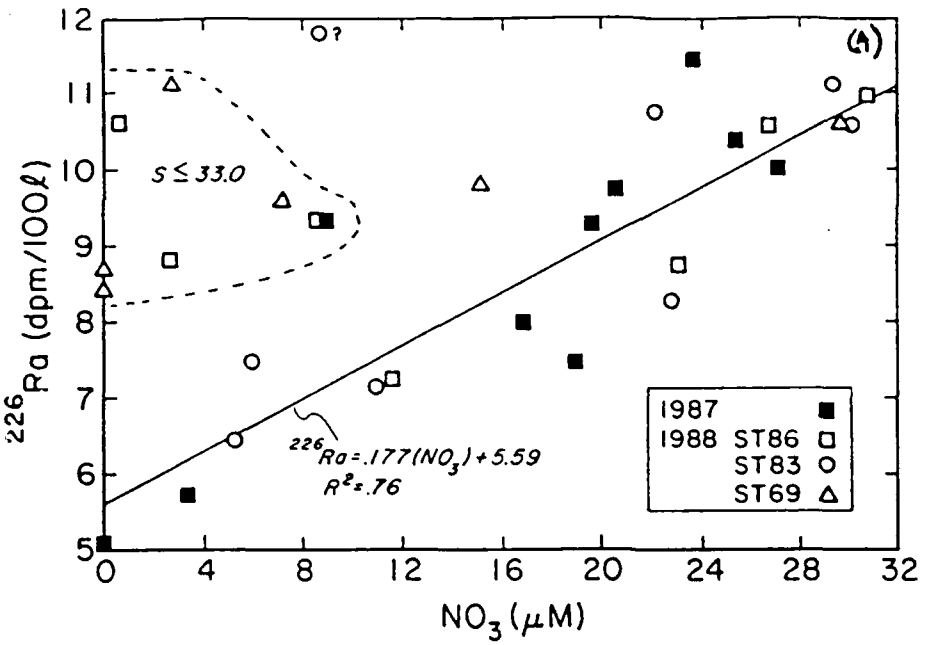
(A)
^{226}Ra (dpm/100ℓ)
NO_3 (μM)
S ≤ 33.0
$^{226}Ra = .177(NO_3) + 5.59$
$R^2 = .76$
1987
1988 ST86
ST83
ST69

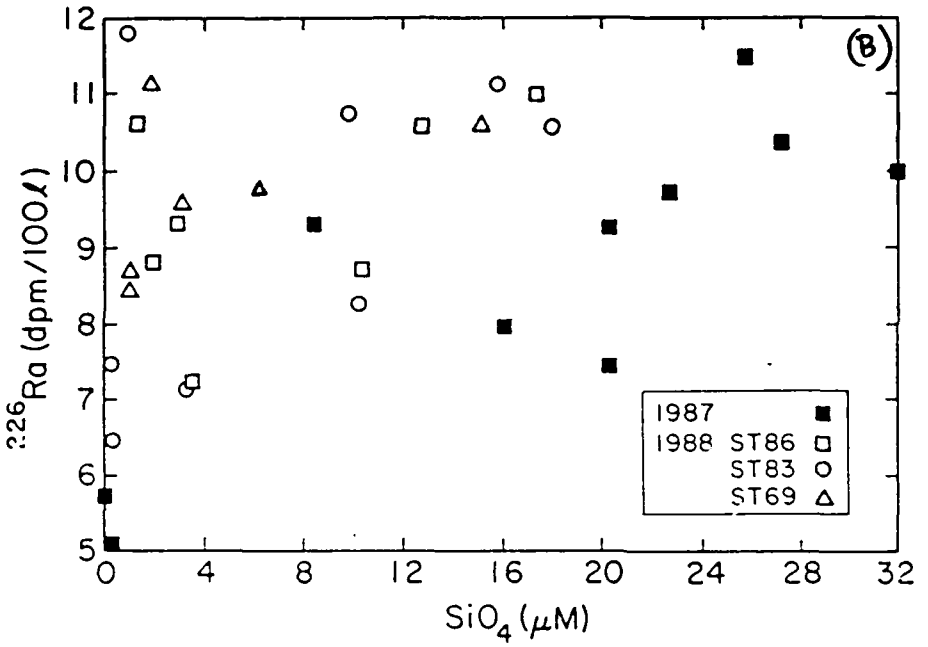
(B)
^{226}Ra (dpm/100ℓ)
SiO_4 (μM)
1987
1988 ST86
ST83
ST69

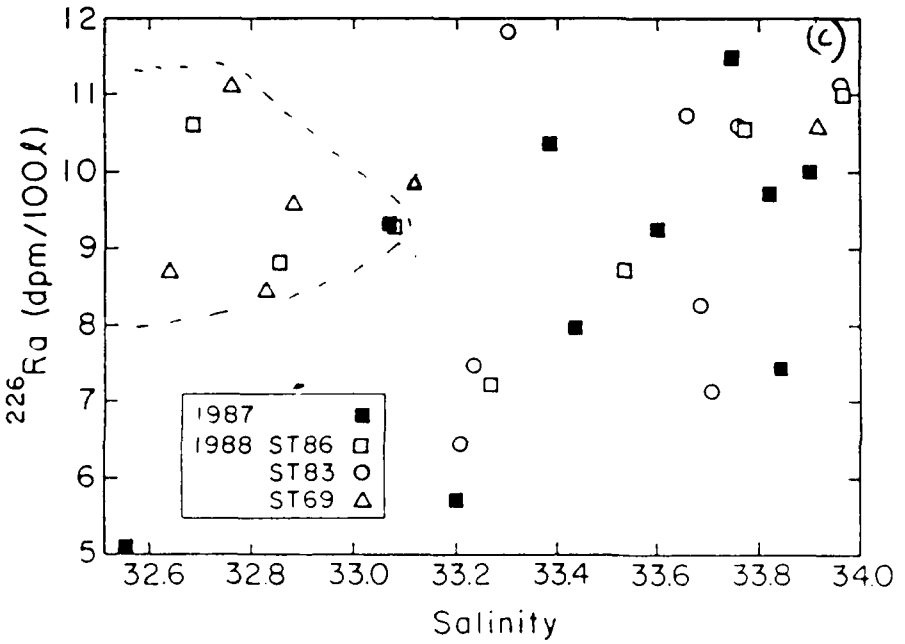
(C)
^{226}Ra (dpm/100ℓ)
Salinity
1987
1988 ST86
ST83
ST69

Fig 3

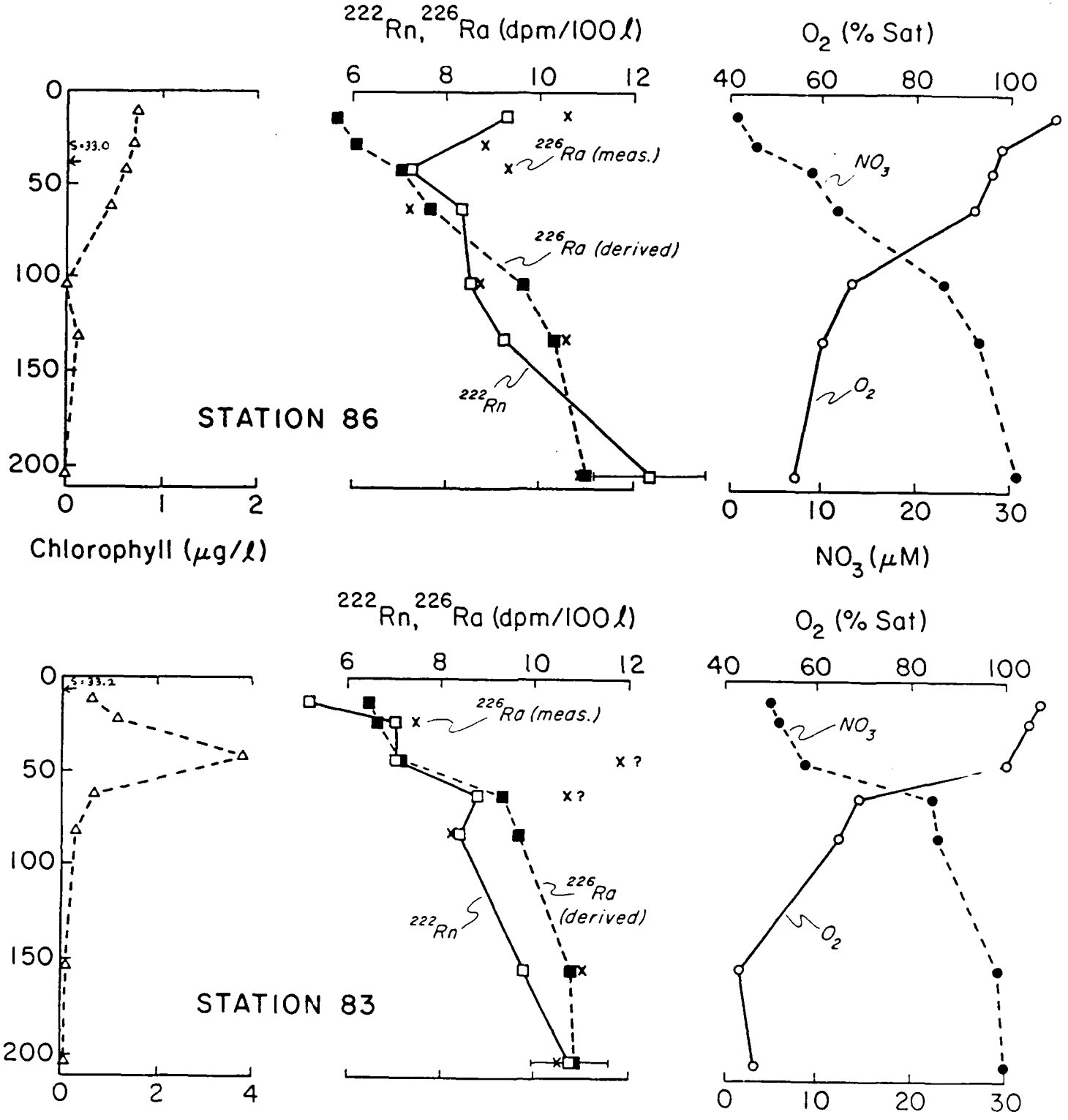
^{222}Rn, ^{226}Ra (dpm/100 ℓ)
O_2 (% Sat)
S=33.0
^{226}Ra (meas.)
^{226}Ra (derived)
^{222}Rn
NO_3
O_2
STATION 86
Chlorophyll (μg/ℓ)
NO_3 (μM)
S=33.2
STATION 83

Fig 4

STATION 59

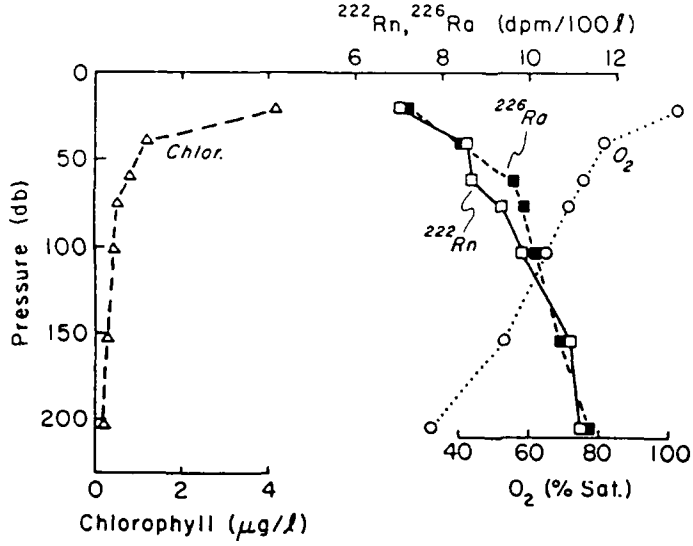

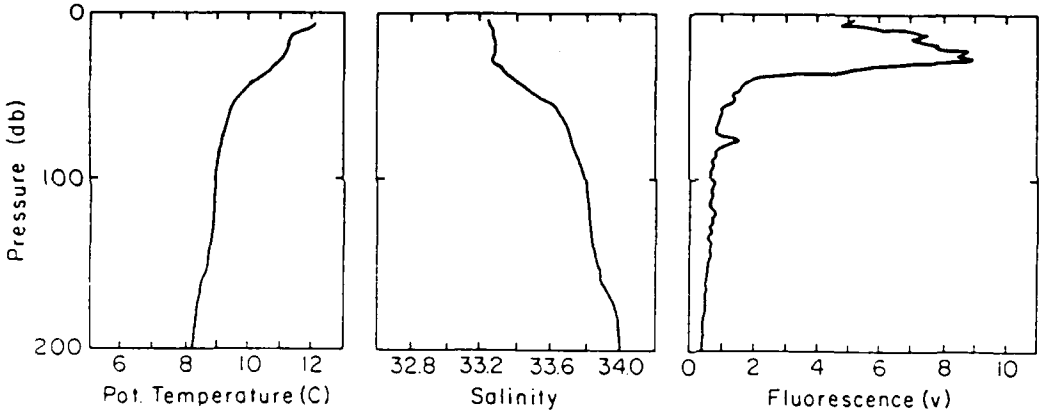

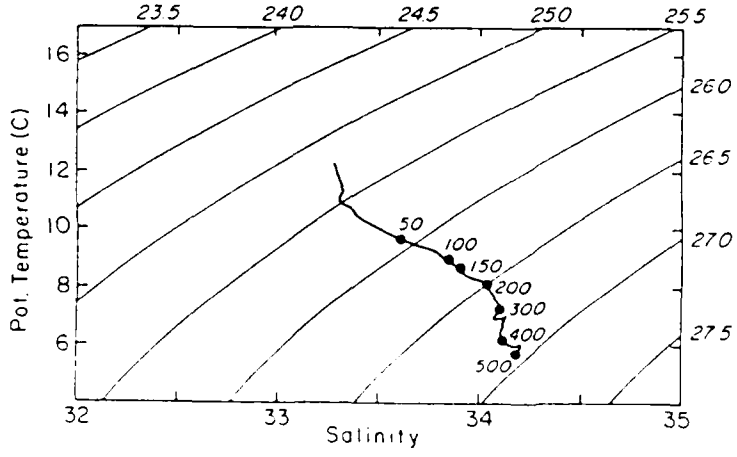

Fig 5

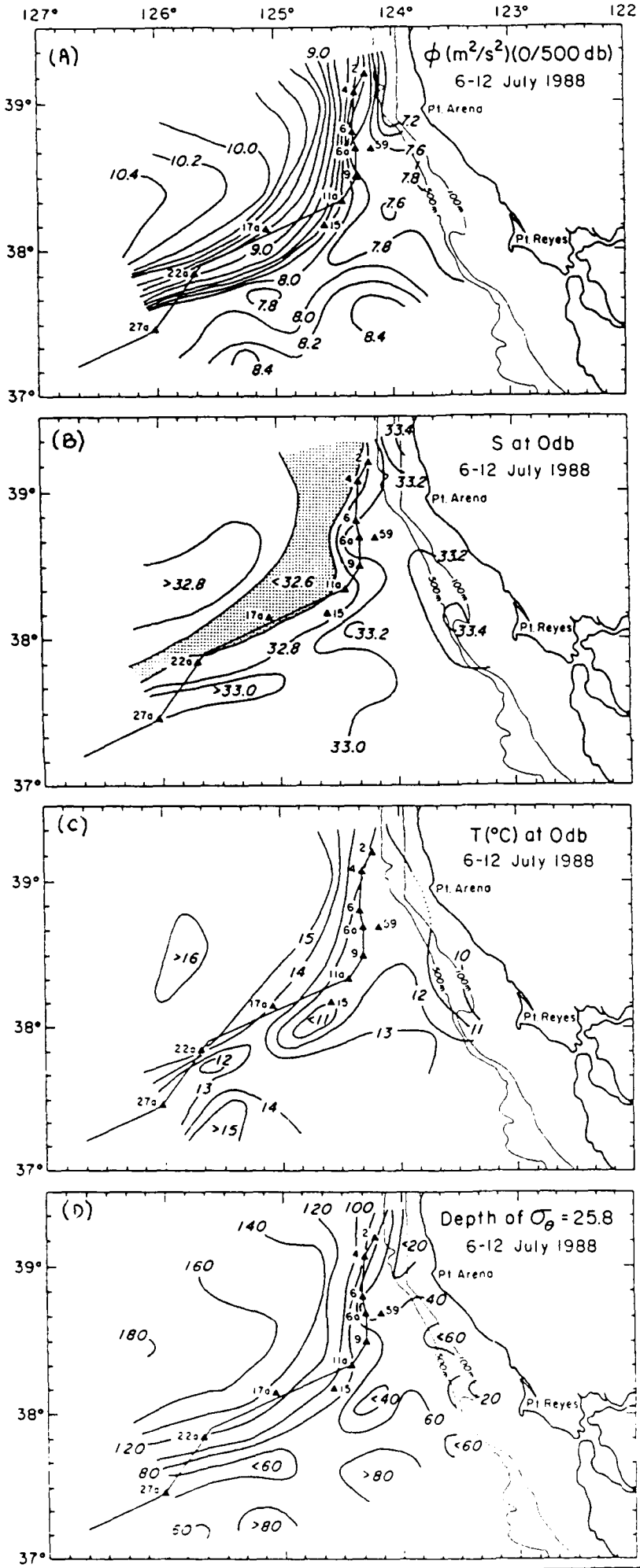
127°
126°
125°
124°
123°
122
(A)
ϕ (m^2/s^2)(0/500 db)
6-12 July 1988
Pt. Arena
Pt. Reyes
39°
38°
37°
(B)
S at 0db
6-12 July 1988
Pt. Arena
Pt. Reyes
>32.8
<32.6
>33.0
33.0
(C)
T(°C) at 0db
6-12 July 1988
Pt. Arena
Pt. Reyes
>16
>15
(D)
Depth of σ_θ = 25.8
6-12 July 1988
Pt. Arena
Pt. Reyes
<20
<40
<60
>80

DRIFTER 1 0-200 m.

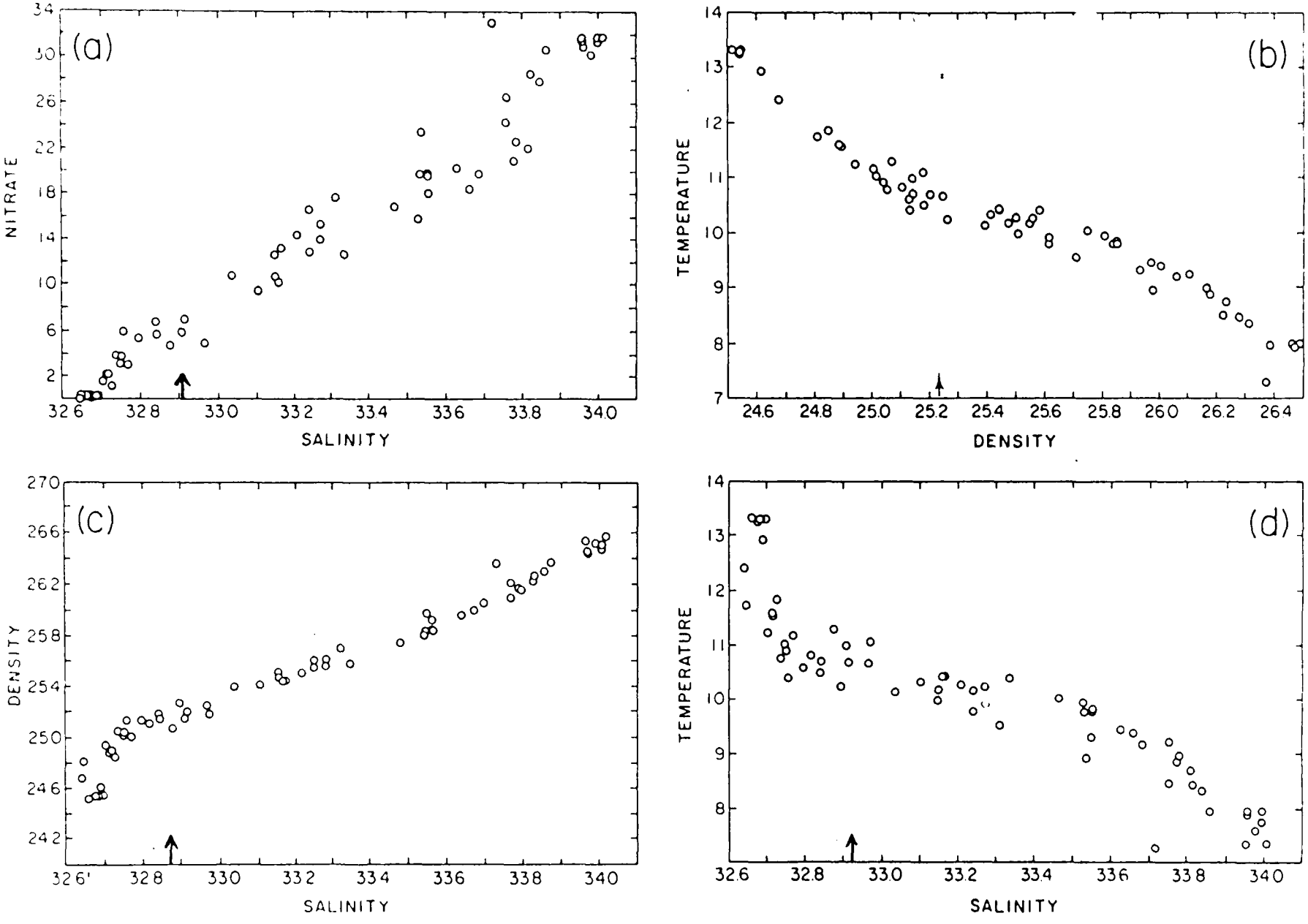

STATION 2

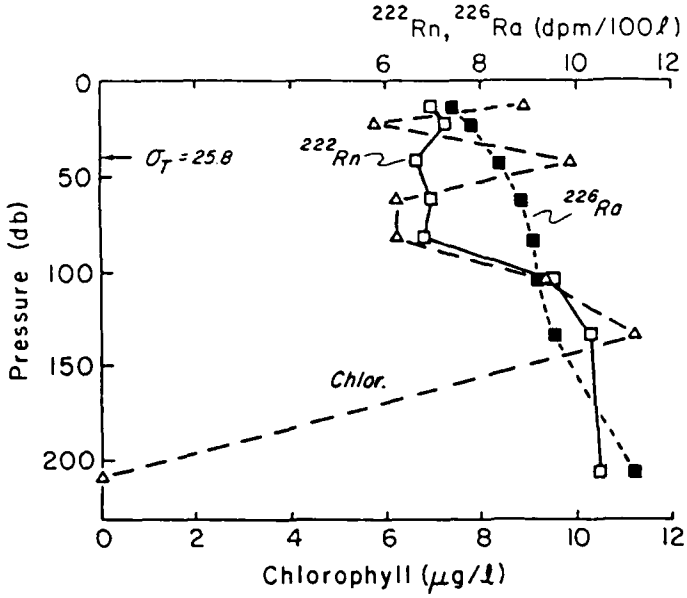
222Rn, 226Ra (dpm/100ℓ)
6
8
10
12
0
50
100
150
200
Pressure (db)
σT = 25.8
222Rn
226Ra
Chlor.
0
2
4
6
8
10
12
Chlorophyll (μg/ℓ)

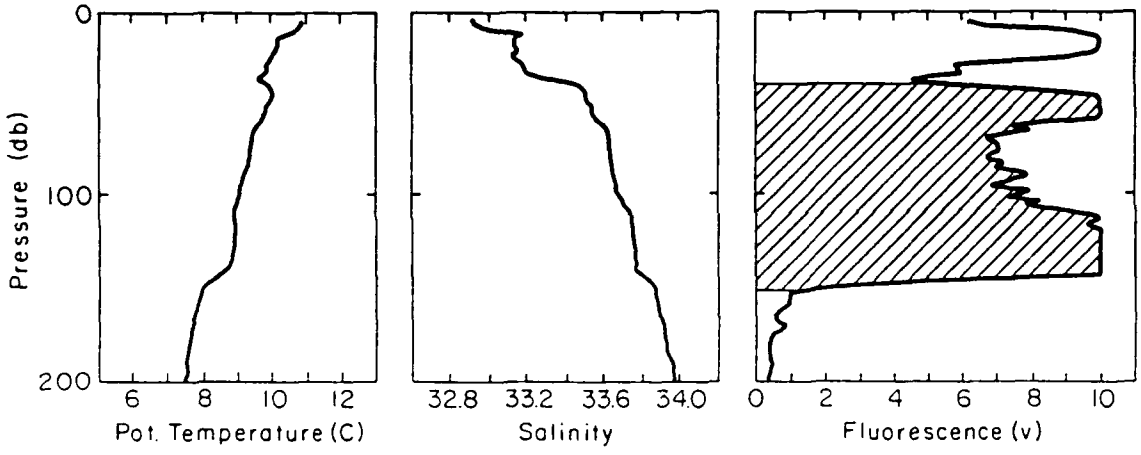
0
100
200
Pressure (db)
6
8
10
12
Pot. Temperature (C)
32.8
33.2
33.6
34.0
Salinity
0
2
4
6
8
10
Fluorescence (v)

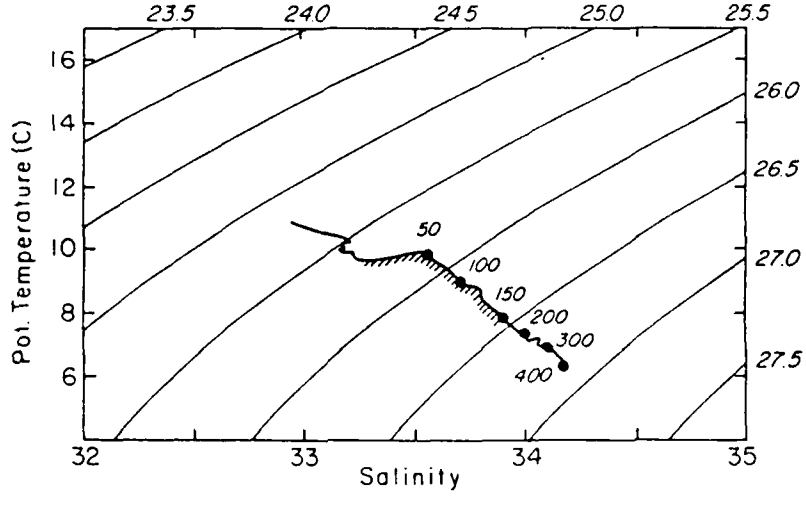
23.5
24.0
24.5
25.0
25.5
26.0
26.5
27.0
27.5
16
14
12
10
8
6
Pot. Temperature (C)
50
100
150
200
300
400
32
33
34
35
Salinity

STATION 4

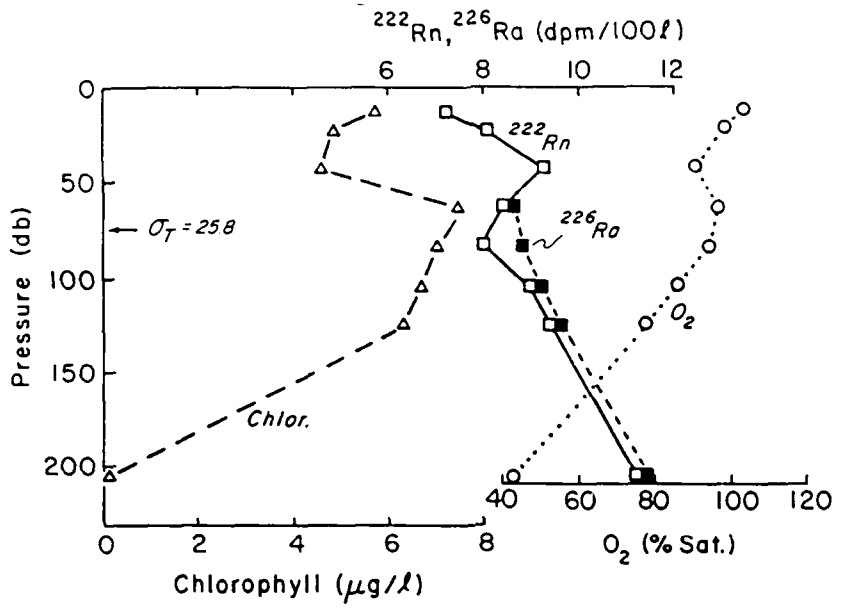
^{222}Rn, ^{226}Ra (dpm/100ℓ)
6 8 10 12
0
50
100
150
200
Pressure (db)
σ_T = 25.8
^{222}Rn
^{226}Ra
O_2
Chlor.
0 2 4 6 8
Chlorophyll (μg/ℓ)
40 60 80 100 120
O_2 (% Sat.)

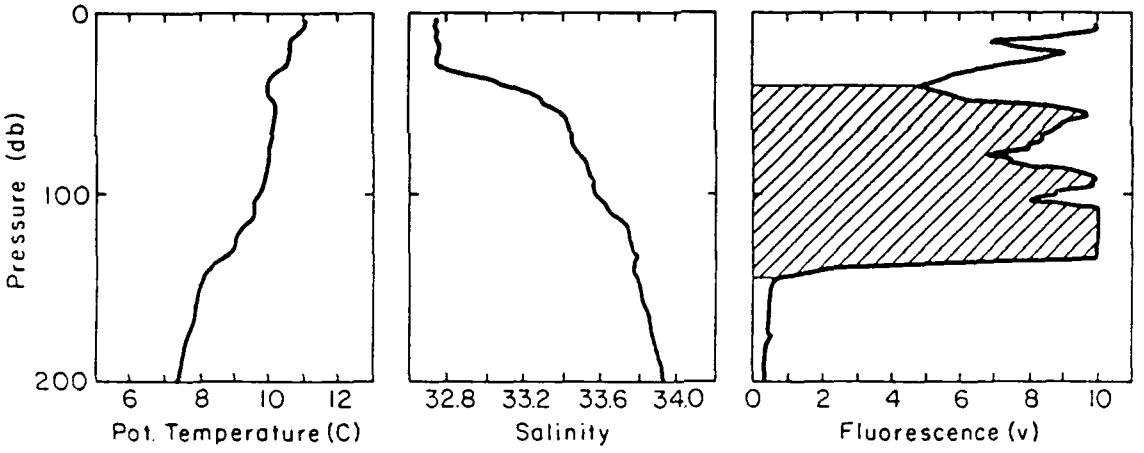
0
100
200
Pressure (db)
6 8 10 12
Pot. Temperature (C)
32.8 33.2 33.6 34.0
Salinity
0 2 4 6 8 10
Fluorescence (v)

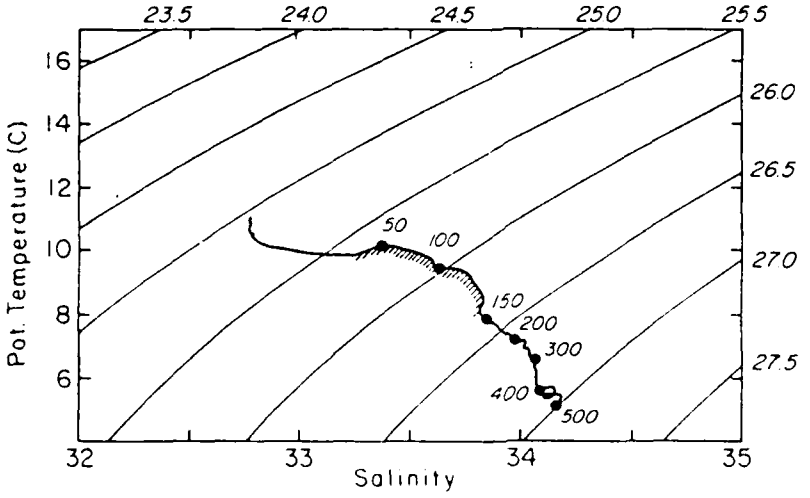
23.5 24.0 24.5 25.0 25.5
26.0
26.5
27.0
27.5
16
14
12
10
8
6
Pot. Temperature (C)
50
100
150
200
300
400
500
32 33 34 35
Salinity

STATION 11A

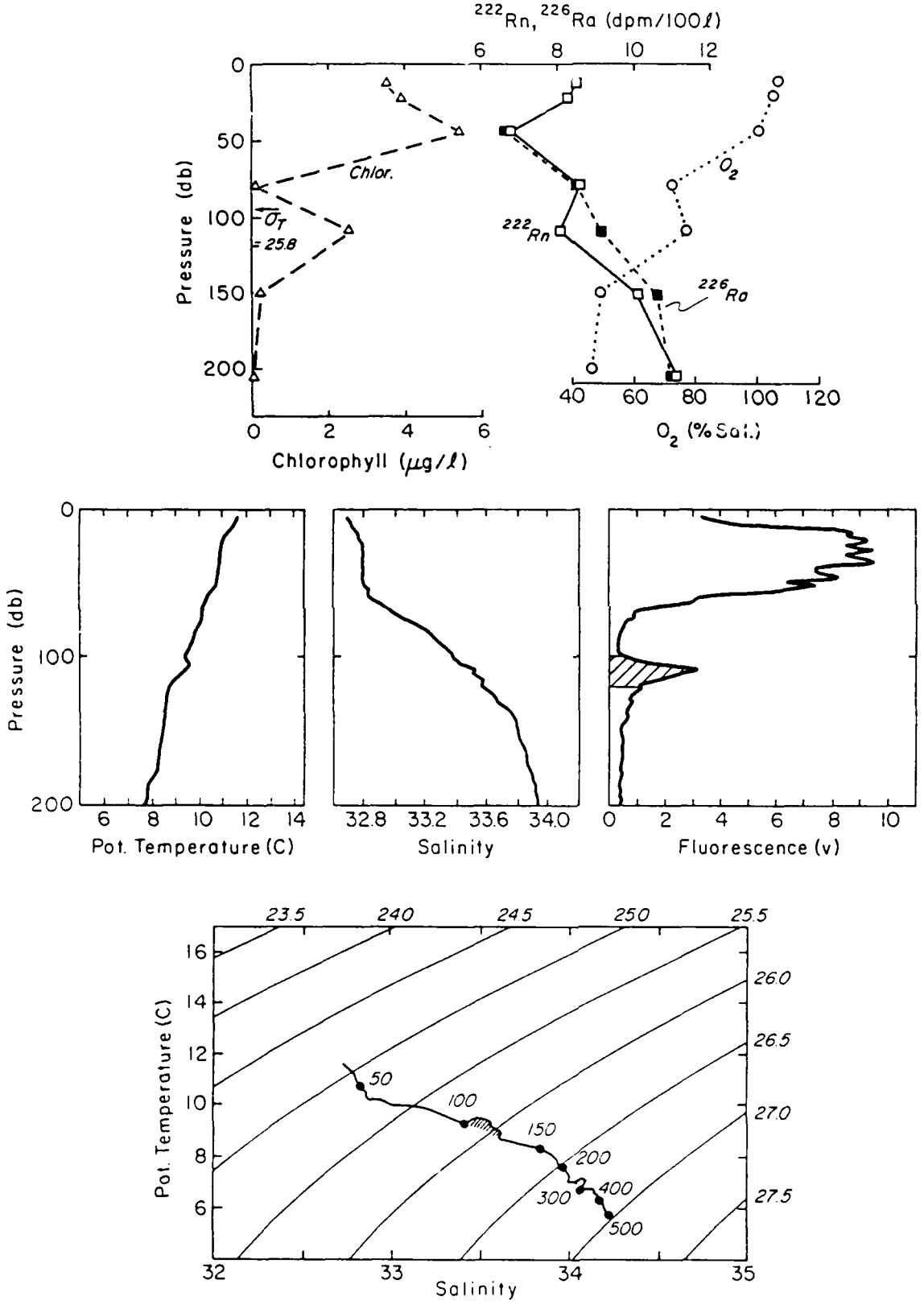
222Rn, 226Ra (dpm/100ℓ)
6 8 10 12
0
50
100
150
200
Pressure (db)
Chlor.
$\overline{\sigma_T}$ = 25.8
222Rn
226Ra
O2
0 2 4 6
Chlorophyll (μg/ℓ)
40 60 80 100 120
O2 (% Sat.)
0
100
200
Pressure (db)
6 8 10 12 14
Pot. Temperature (C)
32.8 33.2 33.6 34.0
Salinity
0 2 4 6 8 10
Fluorescence (v)
23.5 24.0 24.5 25.0 25.5
26.0
26.5
27.0
27.5
16
14
12
10
8
6
Pot. Temperature (C)
50
100
150
200
300
400
500
32 33 34 35
Salinity

STATION 6A

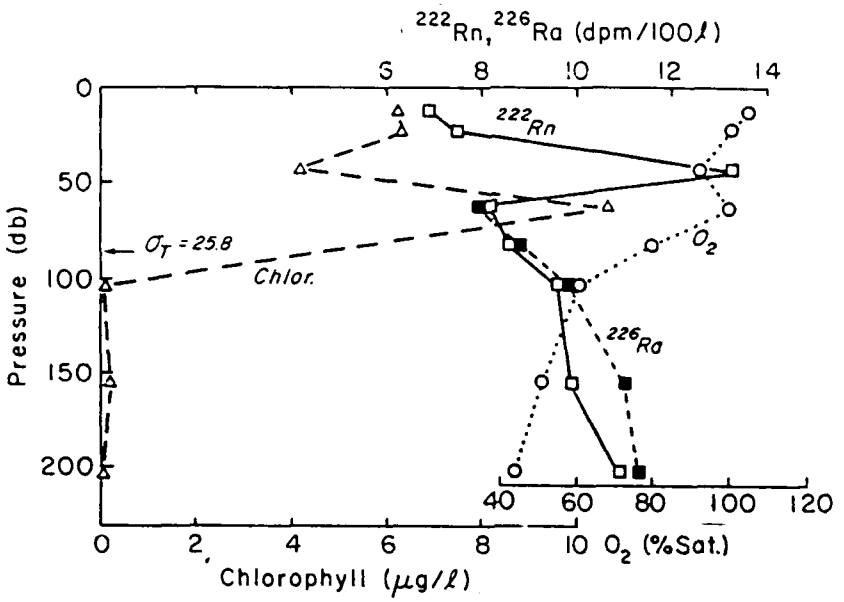
$^{222}Rn, ^{226}Ra$ (dpm/100ℓ)
5 8 10 12 14
0
50
100
150
200
Pressure (db)
^{222}Rn
$\sigma_T = 25.8$
Chlor.
O_2
^{226}Ra
40 60 80 100 120
0 2 4 6 8 10
Chlorophyll (μg/ℓ)
O_2 (%Sat.)

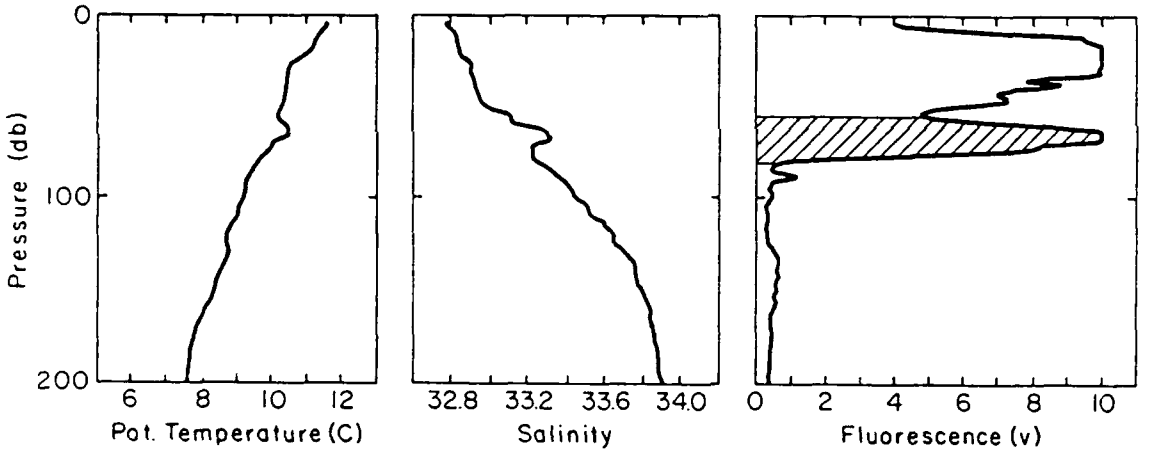
0
100
200
Pressure (db)
6 8 10 12
Pot. Temperature (C)
32.8 33.2 33.6 34.0
Salinity
0 2 4 6 8 10
Fluorescence (v)

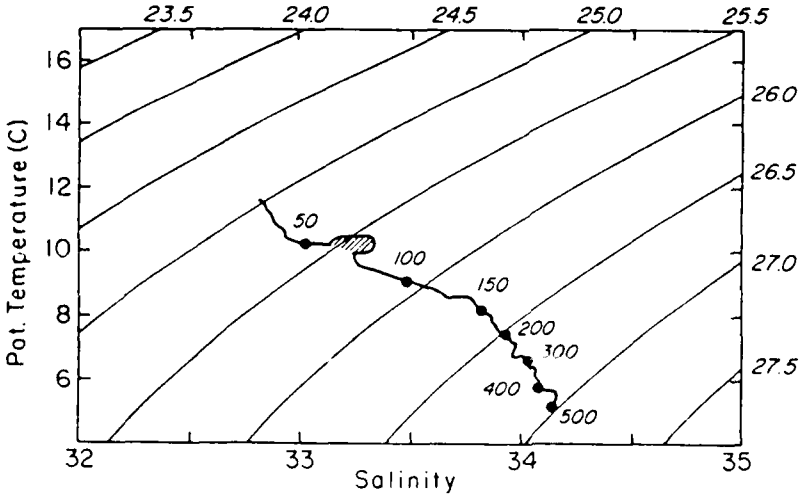
23.5
24.0
24.5
25.0
25.5
26.0
26.5
27.0
27.5
16
14
12
10
8
6
Pot. Temperature (C)
50
100
150
200
300
400
500
32
33
34
35
Salinity

STATION 17A

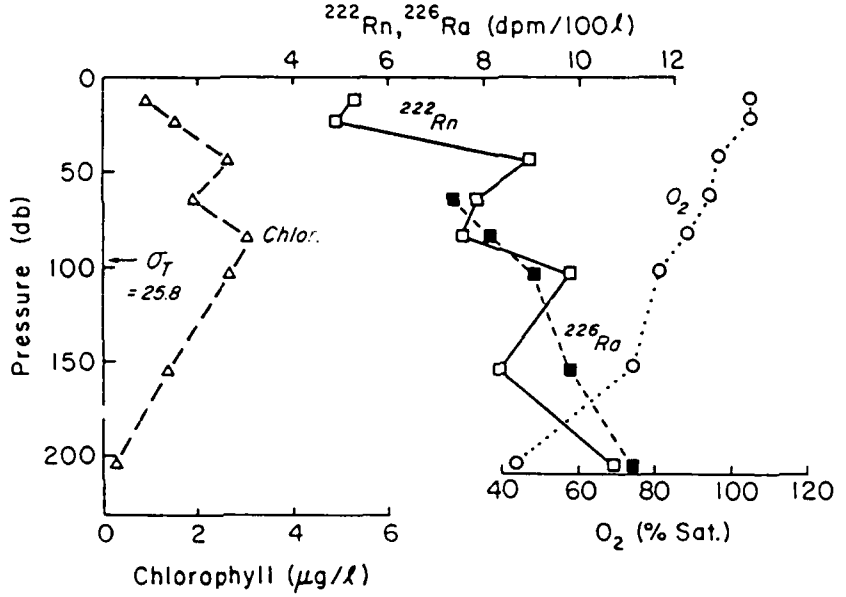
^{222}Rn, ^{226}Ra (dpm/100ℓ)
4 6 8 10 12
0
50
100
150
200
Pressure (db)
^{222}Rn
Chlor.
σ_T = 25.8
^{226}Ra
O_2
0 2 4 6
Chlorophyll (μg/ℓ)
40 60 80 100 120
O_2 (% Sat.)

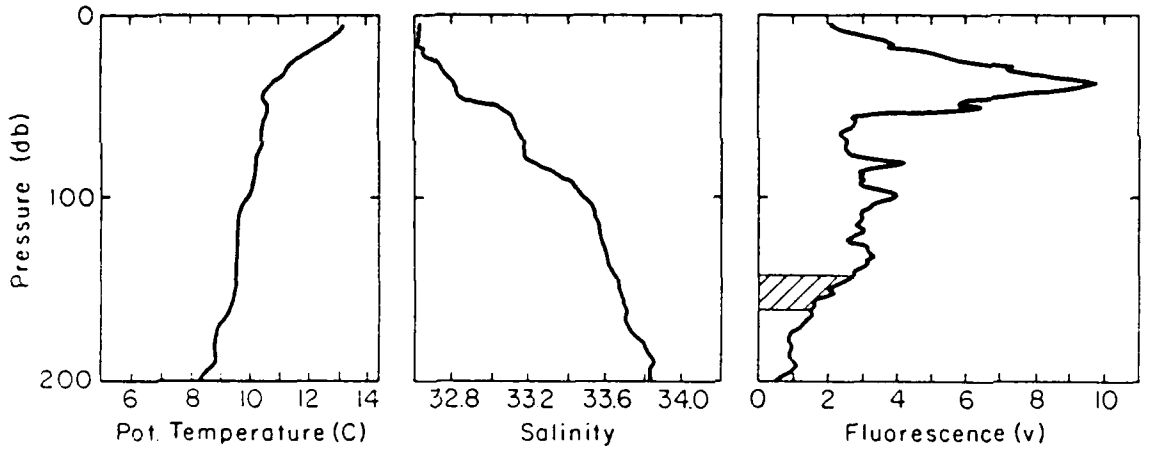
0
100
200
Pressure (db)
6 8 10 12 14
Pot. Temperature (C)
32.8 33.2 33.6 34.0
Salinity
0 2 4 6 8 10
Fluorescence (v)

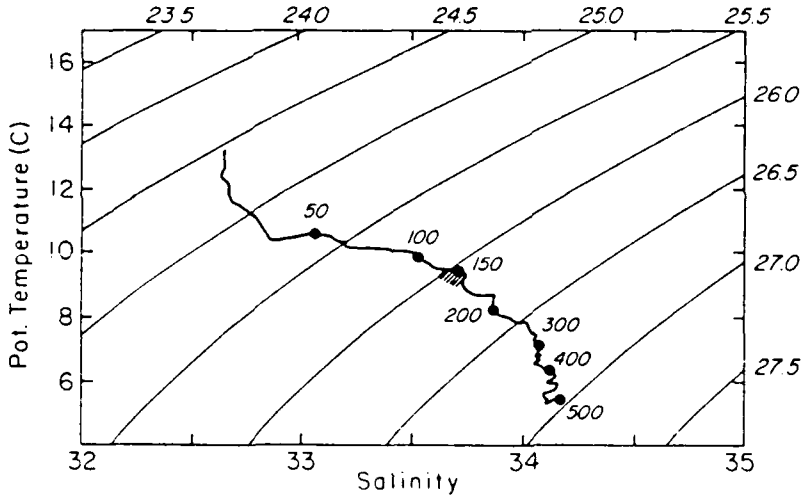
23.5
24.0
24.5
25.0
25.5
26.0
26.5
27.0
27.5
16
14
12
10
8
6
Pot. Temperature (C)
50
100
150
200
300
400
500
32
33
34
35
Salinity

STATION 15

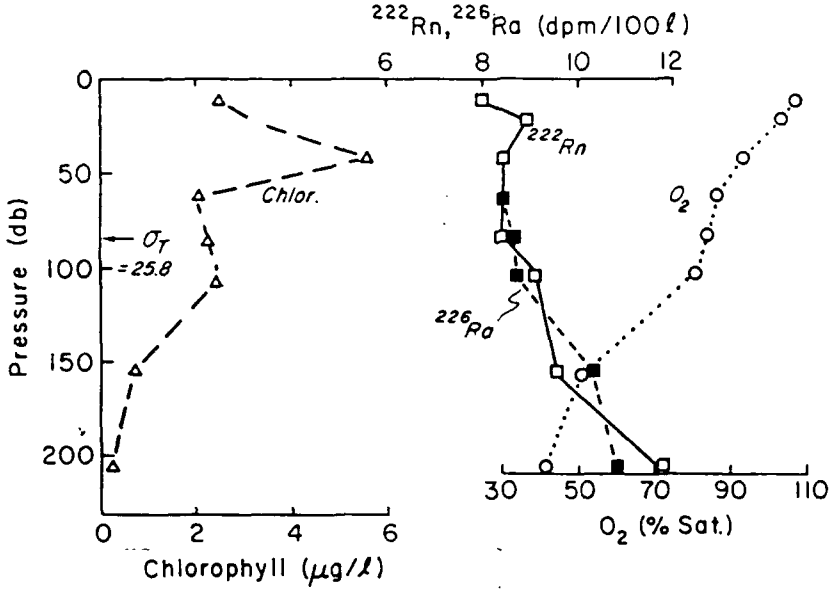
^{222}Rn, ^{226}Ra (dpm/100 ℓ)
6 8 10 12
0
50
100
150
200
Pressure (db)
σ_T = 25.8
Chlor.
^{222}Rn
^{226}Ra
O_2
0 2 4 6
Chlorophyll (μg/ℓ)
30 50 70 90 110
O_2 (% Sat.)

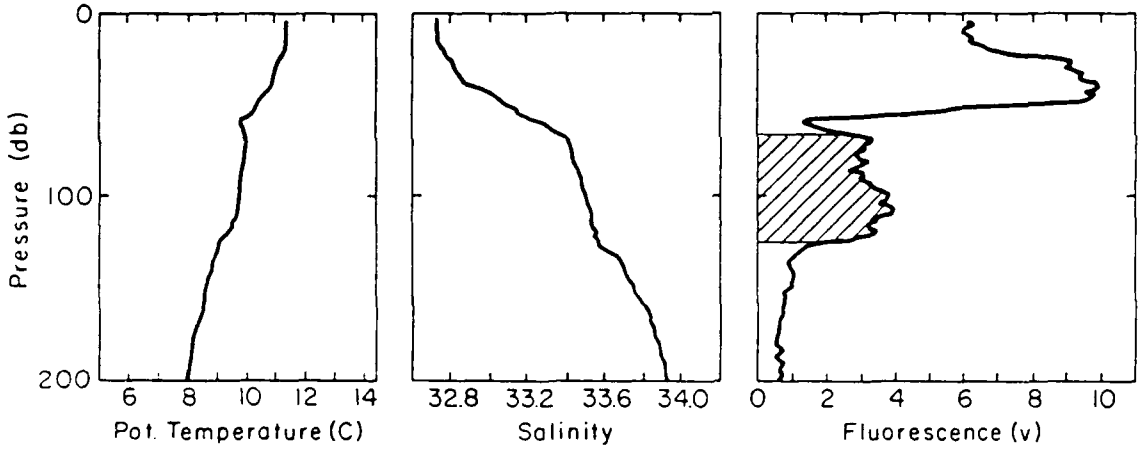
0
100
200
Pressure (db)
6 8 10 12 14
Pot. Temperature (C)
32.8 33.2 33.6 34.0
Salinity
0 2 4 6 8 10
Fluorescence (v)

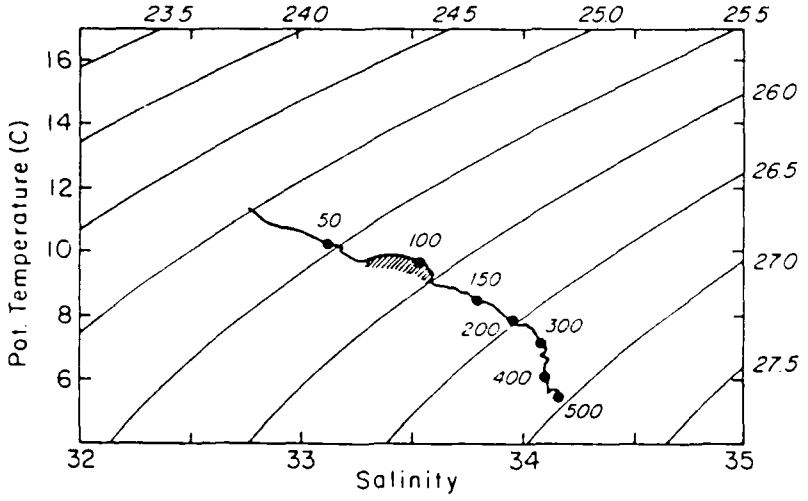
23.5 24.0 24.5 25.0 25.5
16
14
12
10
8
6
Pot. Temperature (C)
26.0
26.5
27.0
27.5
50
100
150
200
300
400
500
32 33 34 35
Salinity

STATION 22A

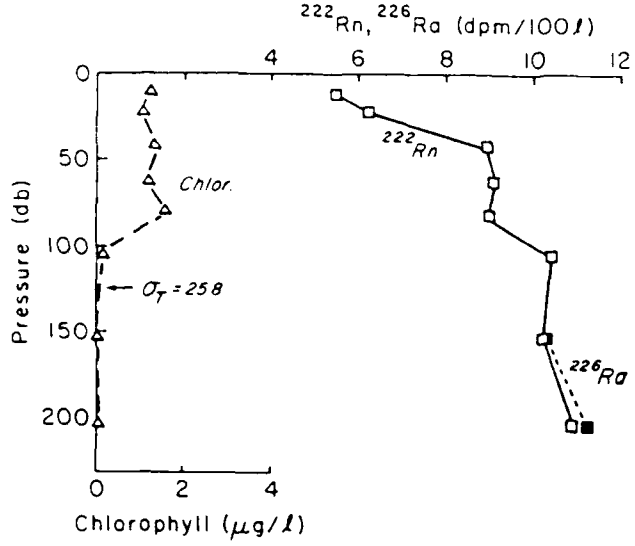
^{222}Rn, ^{226}Ra (dpm/100 l)
4
6
8
10
12
0
50
100
150
200
Pressure (db)
Chlor.
$\sigma_T = 25.8$
^{222}Rn
^{226}Ra
0
2
4
Chlorophyll ($\mu g/l$)

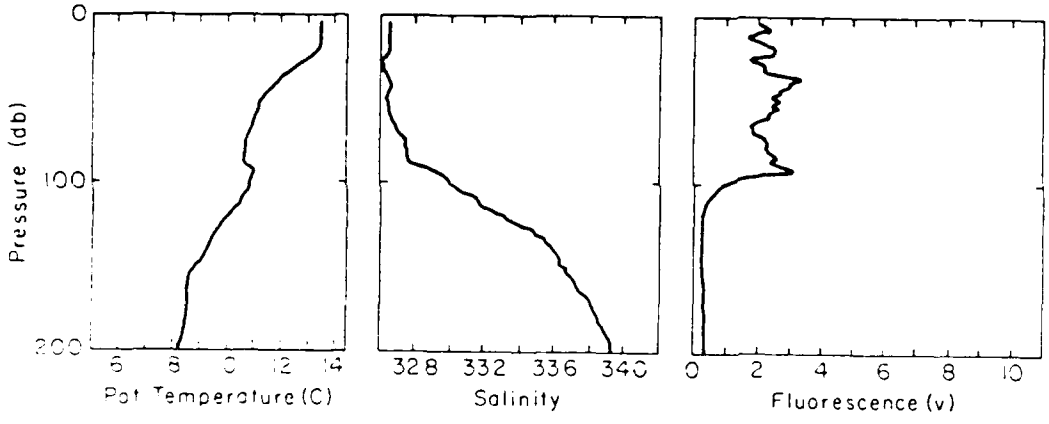
0
100
200
Pressure (db)
6
8
10
12
14
Pot Temperature (C)
328
332
336
340
Salinity
0
2
4
6
8
10
Fluorescence (v)

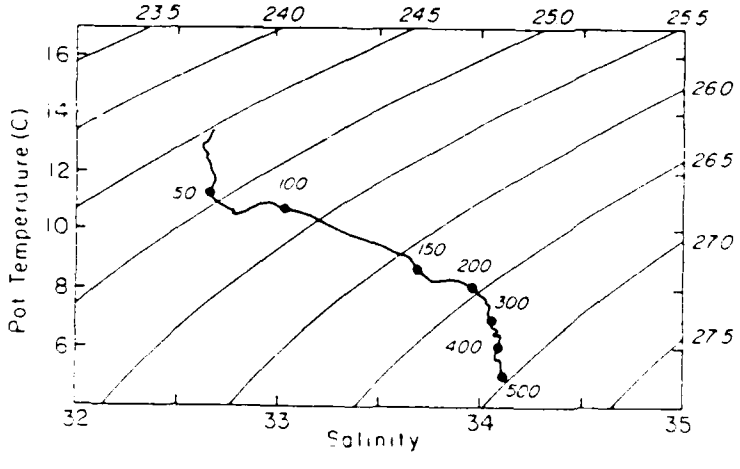
235
240
245
250
255
260
265
270
275
16
14
12
10
8
6
Pot Temperature (C)
50
100
150
200
300
400
500
32
33
34
35
Salinity

STATION 27A

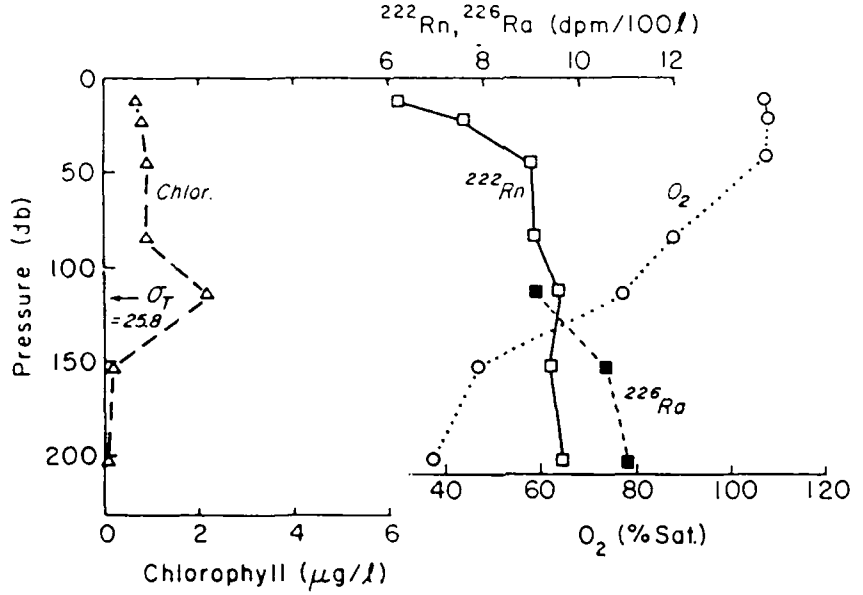
222Rn, 226Ra (dpm/100ℓ)
6
8
10
12
0
50
100
150
200
Pressure (db)
Chlor.
σT = 25.8
222Rn
O2
226Ra
0
2
4
6
Chlorophyll (μg/ℓ)
40
60
80
100
120
O2 (% Sat.)

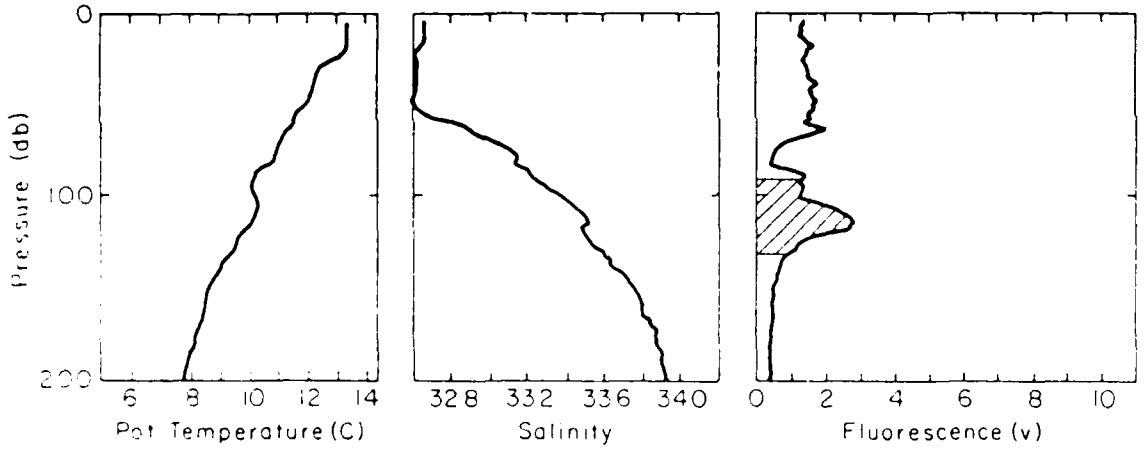
0
100
200
Pressure (db)
6
8
10
12
14
Pot Temperature (C)
328
332
336
340
Salinity
0
2
4
6
8
10
Fluorescence (v)

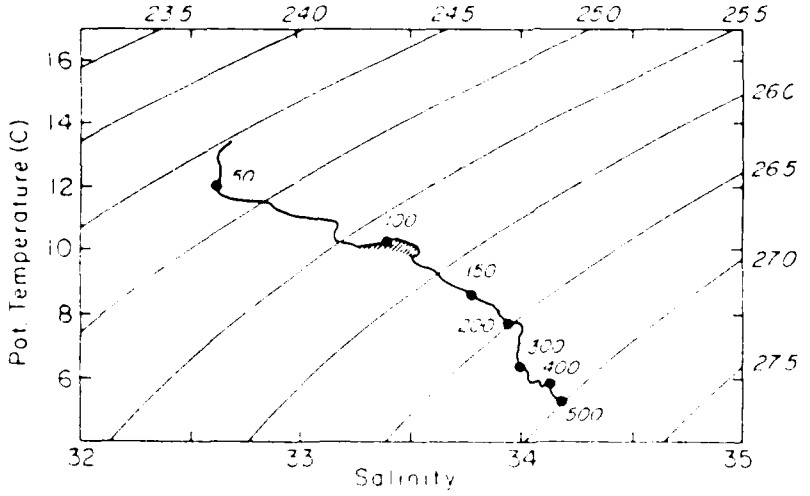
235
240
245
250
255
16
14
12
10
8
6
Pot. Temperature (C)
26C
265
270
275
50
100
150
200
300
400
500
32
33
34
35
Salinity

STATION 46

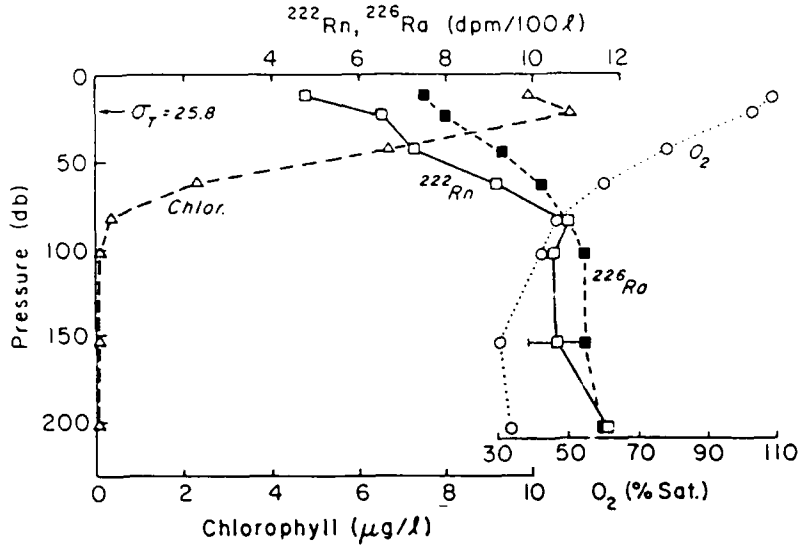
^{222}Rn, ^{226}Ra (dpm/100ℓ)
4 6 8 10 12
0
50
100
150
200
Pressure (db)
σ_T = 25.8
Chlor.
^{222}Rn
^{226}Ra
O_2
30 50 70 90 110
O_2 (% Sat.)
0 2 4 6 8 10
Chlorophyll (μg/ℓ)

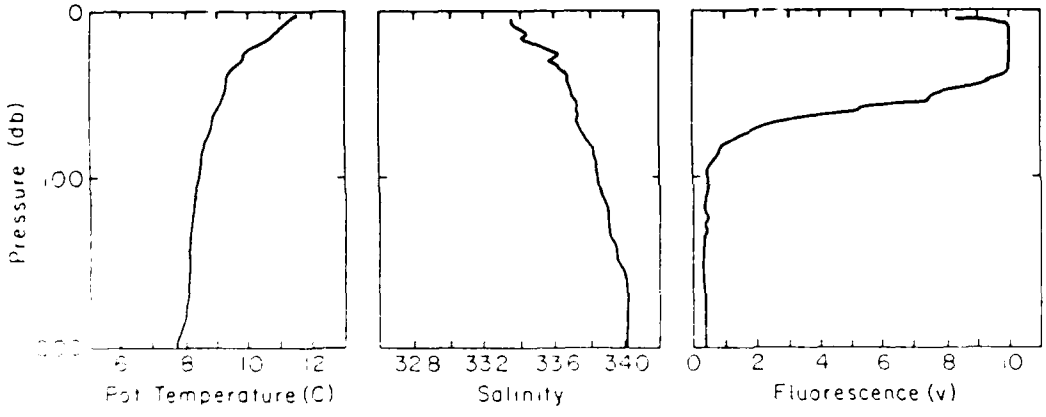
0
100
Pressure (db)
8 10 12
Pot Temperature (C)
328 332 336 340
Salinity
0 2 4 6 8 10
Fluorescence (v)

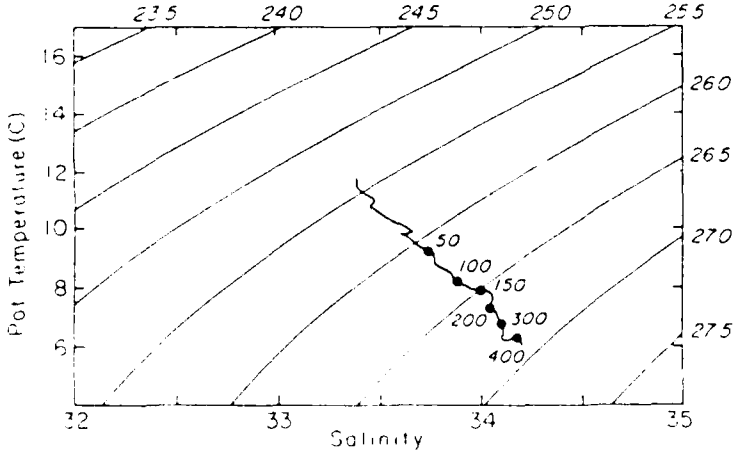
235
240
245
250
255
260
265
270
275
16
14
12
10
8
6
Pot Temperature (C)
50
100
150
200
300
400
32 33 34 35
Salinity

STATION 62

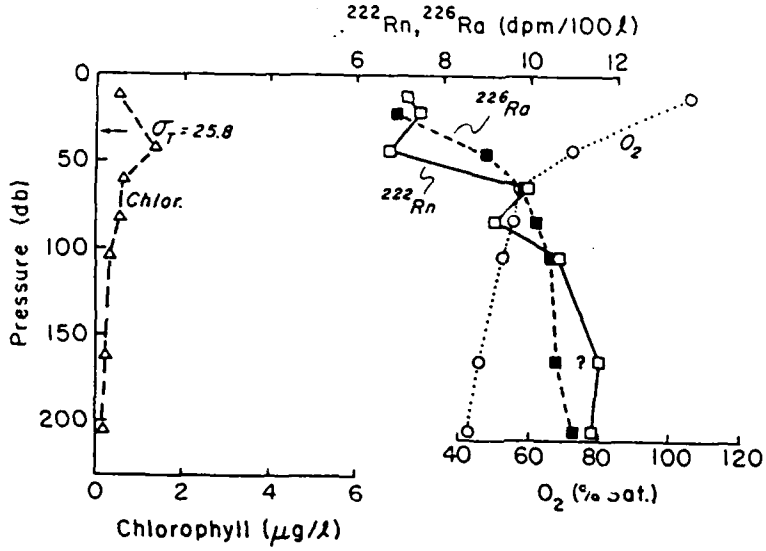
^{222}Rn, ^{226}Ra (dpm/100 ℓ)
6 8 10 12
0
50
100
150
200
Pressure (db)
σ_T = 25.8
Chlor.
^{226}Ra
O_2
^{222}Rn
?
0 2 4 6
Chlorophyll (μg/ℓ)
40 60 80 100 120
O_2 (% sat.)

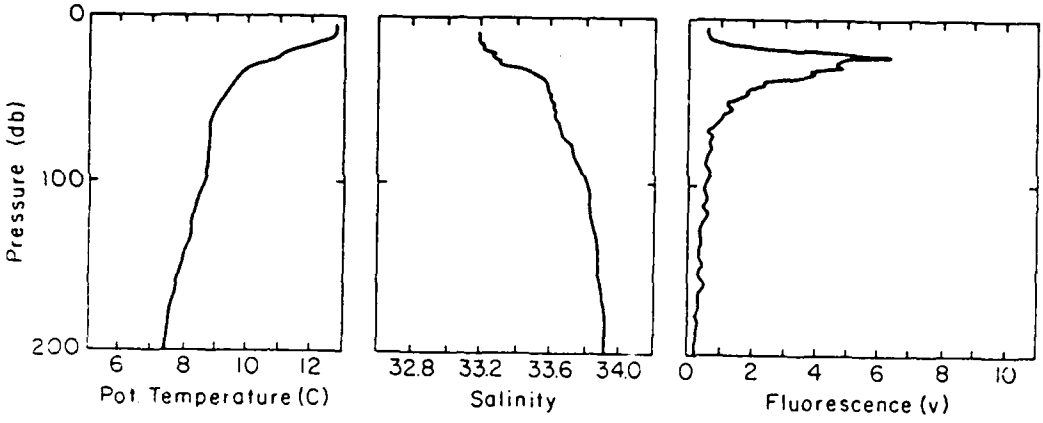
0
100
200
Pressure (db)
6 8 10 12
Pot. Temperature (C)
32.8 33.2 33.6 34.0
Salinity
0 2 4 6 8 10
Fluorescence (v)

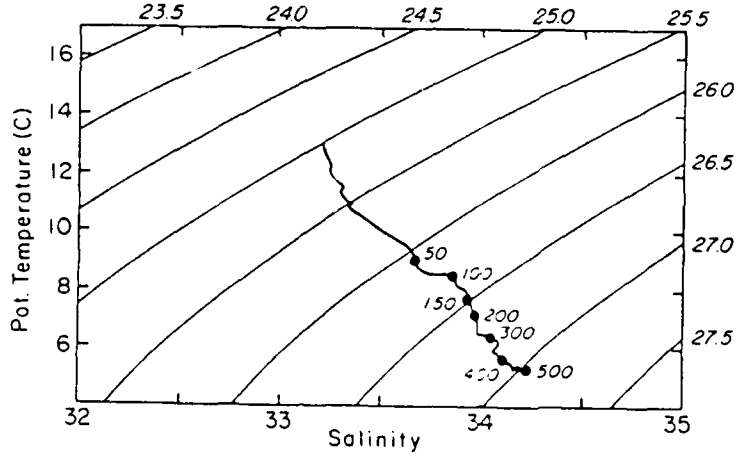
23.5
24.0
24.5
25.0
25.5
26.0
26.5
27.0
27.5
16
14
12
10
8
6
Pot. Temperature (C)
50
100
150
200
300
400
500
32
33
34
35
Salinity

STATION 67

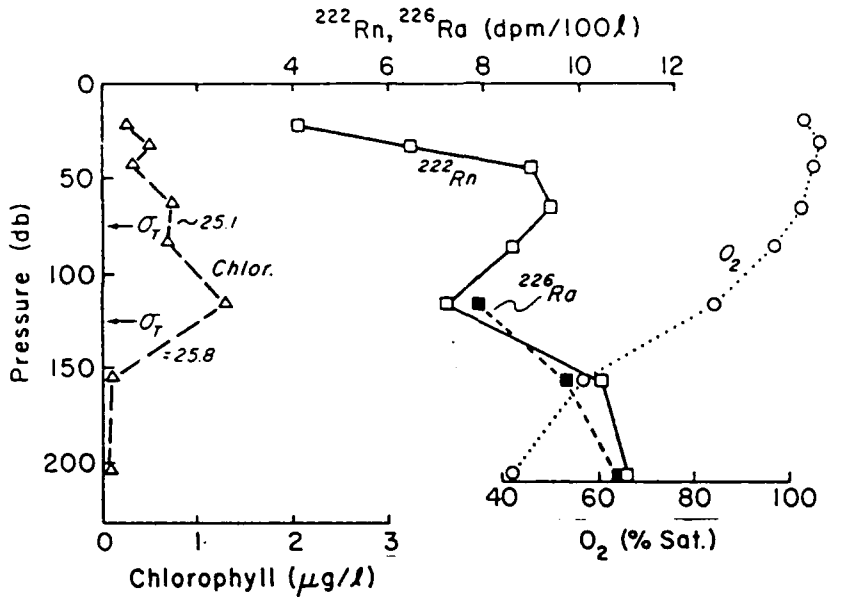
^{222}Rn, ^{226}Ra (dpm/100ℓ)
4
6
8
10
12
0
50
100
150
200
Pressure (db)
σ_T
~25.1
Chlor.
σ_T
=25.8
^{222}Rn
^{226}Ra
O_2
0
1
2
3
Chlorophyll (μg/ℓ)
40
60
80
100
O_2 (% Sat.)

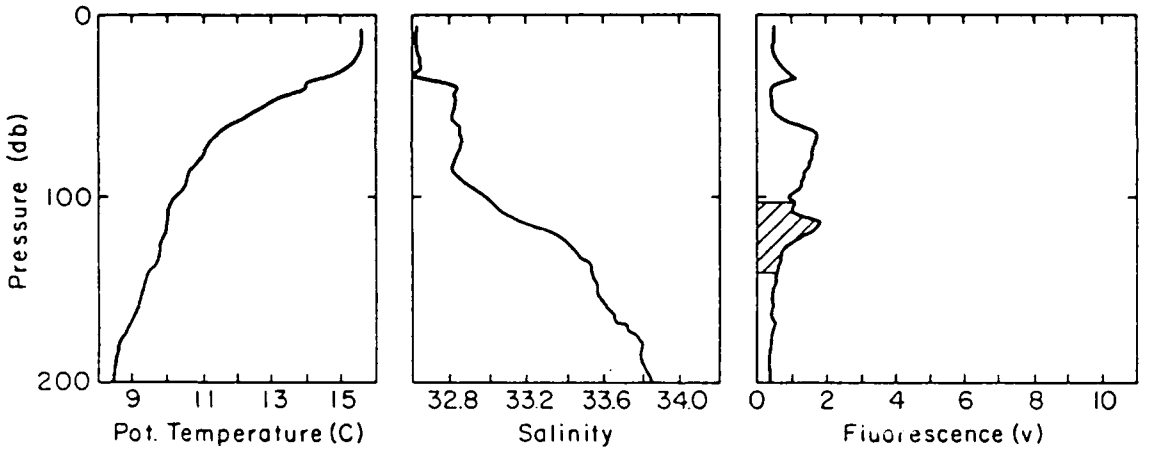
0
100
200
Pressure (db)
9
11
13
15
Pot. Temperature (C)
32.8
33.2
33.6
34.0
Salinity
0
2
4
6
8
10
Fluorescence (v)

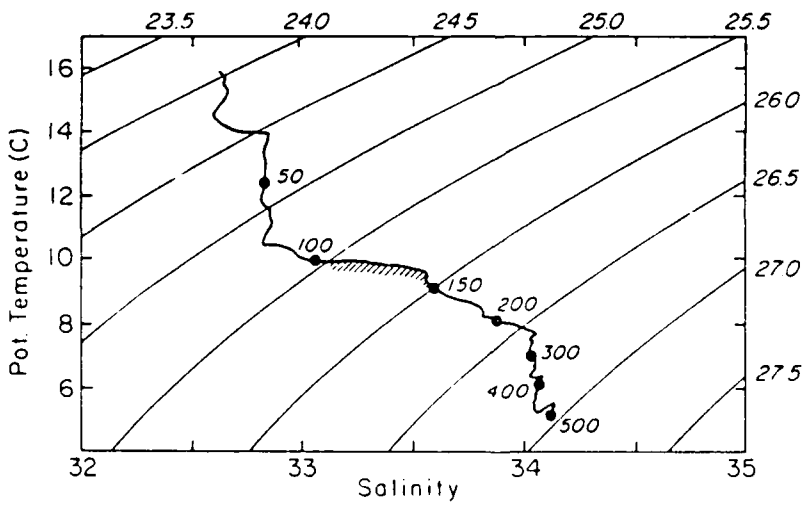
23.5
24.0
24.5
25.0
25.5
16
14
12
10
8
6
Pot. Temperature (C)
26.0
26.5
27.0
27.5
50
100
150
200
300
400
500
32
33
34
35
Salinity

STATION 69

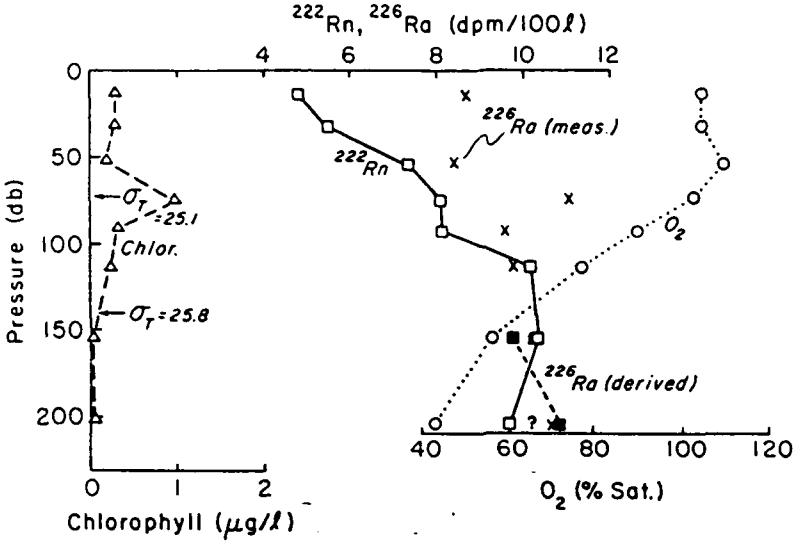
^{222}Rn, ^{226}Ra (dpm/100ℓ)
4 6 8 10 12
0
50
100
150
200
Pressure (db)
σ_T=25.1
Chlor.
σ_T=25.8
^{226}Ra (meas.)
^{222}Rn
O_2
^{226}Ra (derived)
40 60 80 100 120
O_2 (% Sat.)
0 1 2
Chlorophyll (μg/ℓ)

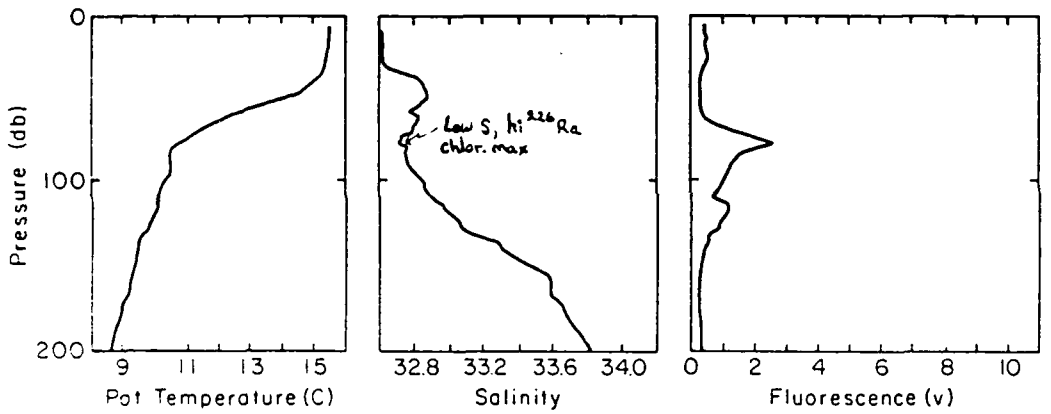
0
100
200
Pressure (db)
9 11 13 15
Pot Temperature (C)
Low S, hi ^{226}Ra
chlor. max
32.8 33.2 33.6 34.0
Salinity
0 2 4 6 8 10
Fluorescence (v)

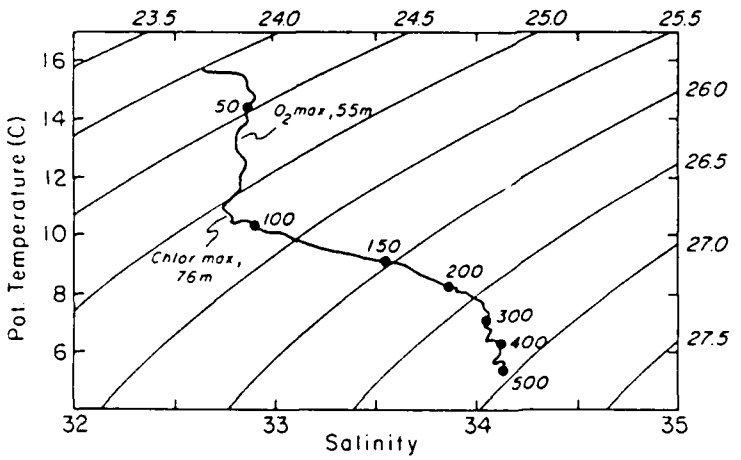
23.5 24.0 24.5 25.0 25.5
16
14
12
10
8
6
Pot. Temperature (C)
50
O_2max, 55m
100
150
200
300
400
500
Chlor max, 76m
26.0
26.5
27.0
27.5
32 33 34 35
Salinity